1969

Microwave propagation through isotropic inhomogeneous photoconductive media

Thomas Van Doren
Missouri University of Science and Technology, vandoren@mst.edu

MICROWAVE PROPAGATION THROUGH ISOTROPIC
INHOMOGENEOUS PHOTOCONDUCTIVE MEDIA

by

THOMAS PAUL VAN DOREN

A DISSERTATION

Presented to the Faculty of the Graduate School of the

UNIVERSITY OF MISSOURI - ROLLA

In Partial Fulfillment of the Requirements for the Degree

DOCTOR OF PHILOSOPHY

in

ELECTRICAL ENGINEERING

1969

G. G. Skitek — Advisor

Norman Dillman

E. C. Bertnolli

Charles Hatfield

William E Hord

J M Rivers

ABSTRACT

The electromagnetic field equations for microwave propagation through a rectangular waveguide filled with a lossy, isotropic, linear, inhomogeneous material are derived in matrix form and solved numerically by computer. The theoretical effects of photo-induced conductivity and dielectric constant variations on microwave attenuation, phase shift, and voltage standing wave ratio are plotted for typical examples in the X-band frequency range. The theoretical calculations indicate that a two order-of-magnitude change in the conductivity can produce a 25 db change in the attenuation or a 100 degree change in the angle of the reflection coefficient. The theoretical predictions are verified qualitatively by experiments performed on photosensitive cadmium sulfide. An unusually strong, room temperature resonance phenomena was observed experimentally in cadmium sulfide. Electron plasma resonance is the suspected explanation, but no definite conclusions are drawn. Several new microwave applications for photoconductive materials are described. Theoretical calculations coupled with experimental measurements produced accurate conductivity measurements of thin (0.05 mm) silicon wafers at X-band frequencies. This technique could be readily adapted to large-scale automatic conductivity measurements. Microwave measurement of the free electron lifetime in photo-excited cadmium sulfide is also reported.

ACKNOWLEDGEMENTS

The author wishes to express his appreciation to Professor G. Skitek and Dr. N. Dillman for their advice and guidance in the preparation of this dissertation. He would also like to acknowledge the many helpful consultations with Dr. J. Adair.

The cadmium sulfide used in this research was supplied by Mr. J. Powderly of the Eagle-Picher Company of Miami, Oklahoma, and the silicon wafers were furnished by the Monsanto Silicon Plant at St. Charles, Missouri. The author is thankful for the assistance provided by the library staff of the University of Missouri - Rolla during the literature review.

Most important, the author is grateful for the patience and assistance of his family, especially the preparation of the manuscript by his wife, Lana.

TABLE OF CONTENTS

LIST OF FIGURES

LIST OF TABLES

LIST OF SYMBOLS

Symbol	Description	Units
$\bar{a}_x$, $\bar{a}_y$, $\bar{a}_z$	unit vectors in rectangular coordinate system	
A	sample cross sectional area	m^2
$\bar{B}$	magnetic flux density	Wb/m^2
c	speed of light in free space	m/sec
d	sample thickness	m
$\bar{D}$	electric flux density	C/m^2
D_n	electron diffusion constant	m^2/sec
D_p	hole diffusion constant	m^2/sec
$\bar{E}$	macroscopic electric field intensity	V/m
$\bar{E}_{ext}$	macroscopic electric field intensity external to a medium	V/m
E_g	energy gap between valence and conduction bands	ev
E_i^+	magnitude of the incident electric field intensity in the ith medium	V/m
E_i^-	magnitude of the reflected electric field intensity in the ith medium	V/m
$\bar{E}_{loc}$	microscopic locally acting electric field intensity	V/m
f_n	frictional damping factor for ion pairs of type n	sec^{-1}
$\bar{f}(\bar{x})$	displacement between electron gas and positive ion lattice	m
f(z)	photo-generation rate of hole-electron pairs	$pairs/m^3\text{-}sec$

h	Plank's constant, 6.62×10^{-34}	J-sec
$\overline{H}$	macroscopic magnetic field intensity	A/m
i	a subscript which designates the ith layer of a multilayer medium	
I_i	incident light intensity	W/m^2
I_o	rate of photon absorption	$(m^3\text{-sec})^{-1}$
j	$(-1)^{\frac{1}{2}}$	
$\overline{J}$	total current density	A/m^2
$\overline{J}_n$	electron current density	A/m^2
$\overline{J}_p$	hole current density	A/m^2
k	wave number	m^{-1}
k_B	Boltzman's constant, 1.38×10^{-23}	$J/^{o}K$
K, K_1	constants	
L	depolarization factor	
L	sample length	m
m^*	effective mass of a particle	kg
m_n	reduced mass of ion pairs of type n	kg
$\overline{M}$	magnetic dipole moment per unit volume	
n	volume density of free electrons	m^{-3}
n_o	volume density of free electrons for non-illuminated conditions	m^{-3}
$n(z)$	spatially varying density of free electrons produced by illumination	m^{-3}
N	volume density of electric dipoles	m^{-3}
N_n	volume density of ion pairs of type n	m^{-3}
$\overline{p}$	microscopic dipole moment	C-m

p	volume density of free holes	m^{-3}
p_o	volume density of free holes for non-illuminated conditions	m^{-3}
$\overline{P}$	total polarization vector	C/m^2
$\overline{P}_b$	polarization produced by bound charge	C/m^2
$\overline{P}_f$	polarization produced by free charge	C/m^2
P_i	incident microwave power	W
$P_t(t)$	time varying transmitted microwave power	W
q	charge on an electron	C
Q_i	rate of photon incidence	quanta/m^2-sec
$\overline{r}$	average separation between the centers of positive and negative charge of an electric dipole	m
R	reflection coefficient	
$R_S(t)$	time varying dc resistance of CdS sample	ohm
$p(z)$	spatially varying density of free holes produced by illumination	m^{-3}
T	absolute temperature	^oK
T	reflection coefficient	
$v_o(t)$	output voltage from dc lifetime measurement	V
V_o	dc reference voltage	V
x, y, z	variables in the rectangular coordinate system	
Y_i	transverse wave admittance of the ith layer	mho
Z_i	transverse wave impedance of the ith layer	mho

Z_{oL}	characteristic impedance of a waveguide load	mho
α	attenuation constant	nep/m
α	polarizability	$C\text{-}m^2/V$
β	quantum efficiency	
β	phase constant	rad/m
β_o	phase constant of air-filled rectangular waveguide	rad/m
γ	propagation constant	m^{-1}
δ	coefficient of light absorption	m^{-1}
ϵ	complex permittivity	F/m
ϵ'	real part of the complex permittivity	F/m
ϵ''	imaginary part of the complex permittivity	F/m
ϵ_b	complex permittivity produced by bound charges	F/m
ϵ_b'	real part of the complex permittivity produced by bound charges	F/m
ϵ_b''	imaginary part of the complex permittivity produced by bound charges	F/m
ϵ_o	permittivity of free space, $8.85\text{x}10^{-12}$	F/m
ϵ_r	relative complex permittivity	F/m
λ	wavelength	m
μ	complex permeability	H/m
μ_o	permeability of free space, $4\pi\text{x}10^{-7}$	H/m
μ_n	electron mobility	$m^2/V\text{-sec}$
μ_p	hole mobility	$m^2/V\text{-sec}$
ρ	volume charge density	C/m^3
ρ	resistivity	ohm-m
σ	complex conductivity	mho/m

σ_f	complex conductivity produced by free charges	mho/m
σ_f'	real part of the complex conductivity produced by free charges	mho/m
σ_f''	imaginary part of the complex conductivity produced by free charges	mho/m
σ_o	conductivity of a non-illuminated sample	mho/m
$\sigma(z)$	spatially varying conductivity produced by illumination	mho/m
τ_c	mean time between collisions of free electrons with the lattice	sec
τ_d	permanent dipole relaxation time	sec
τ_n	free electron lifetime	sec
τ_p	free hole lifetime	
ψ_e	electric susceptibility	
ω	radian frequency	rad/sec
ω_p	plasma resonant frequency	rad/sec
ω_r	resonant frequency in CdS	rad/sec

I. INTRODUCTION

A. Statement of Problem, Purpose, and Scope

The general problem studied was microwave propagation through a linear, isotropic, inhomogeneous, photoconductive media. The purposes of this research were:

1) Review the classical theory for microwave interaction with matter;

2) Derive the electromagnetic field equations for propagation through a section of X-band rectangular waveguide filled with a photoconductive media;

3) Calculate the microwave attenuation, phase shift, and standing wave ratio variations with conductivity, sample thickness, and frequency for several typical cases;

4) Perform qualitative experimental checks on the theoretical calculations;

5) Use the results of the theoretical calculations coupled with additional derived theory to perform microwave measurements of the free electron lifetime in cadmium sulfide and the conductivity of thin silicon wafers;

6) Determine new microwave applications for photoconductive materials.

This research was purposely planned to involve a number of closely related topics. This permitted the author to comprehend the overall problem while simultaneously performing limited original research in several of the areas mentioned above. Little tutorial material and few details of experimental procedures and problems are presented. The reader is assumed to be knowledgeable in solid state physics and electromagnetic field theory.

B. Plan of Development

The purpose of this section is to briefly outline the contents of each chapter. The main body of the dissertation is preceded by a review of the publications related to this research in the areas of photoconductivity, material properties, and microwave propagation through inhomogeneous media. The theoretical development begins in Chapter III with a summary of the relationships between the macroscopic complex permittivity and such microscopic material parameters as the density and mass of free carriers, and the polarizability and type of ions.

The matrix equations relating the incident, reflected, and transmitted electric fields for a section of waveguide filled with an inhomogeneous material are derived in Chapter IV. The results of this derivation are used in Chapter V to perform computer calculations of the microwave properties of X-band rectangular waveguide filled with a lossy dielectric material. The results presented in this chapter form the most important part of the dissertation.

In Chapter VI, the results of several microwave experiments are described. In general, the theoretical predictions from the previous chapter are verified, however, a few surprises are encountered. Chapter VII is devoted to two practical applications of the theory previously presented. Good results are reported for the microwave measurement of the free electron lifetime in CdS and the conductivity of Si wafers.

A few of the microwave devices and applications possible with photoconductive materials are briefly described in Chapter VIII. A summary is contained in the final chapter, along with a list of the original contributions made by the author and suggestions for further research.

With few exceptions, the International System of Units is used in this dissertation.

II. REVIEW OF THE LITERATURE

A. Introduction

The literature review has been subdivided into four general areas; photoconductivity, complex permittivity, wave propagation through inhomogeneous media, and microwave measurement of material parameters. In each area, only the most important articles have been referenced.

B. Photoconductivity

1. General

The early theory of photoconductivity and the experimental measurements performed on twelve chemical elements before 1951 are summarized by Moss (1). More detailed theory and limited experimental work was presented at the Photoconductivity Conference in 1954 (2). Several review articles, rather limited in scope, appeared in the late 1950's (3, 4, 5, 6). Bube (7) has published a thorough review of photoconductivity from its beginning up to 1959. In 1961, Rose (8) summarized the areas still requiring further research, and in 1963 he published a short text (9) which contains typical numerical values for many parameters. Ryvkin (10) and Larach (11) have published two of the latest major works concerned with photoconductivity. Several articles devoted to impurity photoconductivity (12, 13, 14), photoeffects in ZnS (15), and organic photoconductivity (16, 17) deserve recognition.

2. Photoconductive Powders

Methods of preparing Cu-Cl activated photosensitive CdS powders are discussed by Thomsen, et al. (18). Thomsen indicates that the effective mobility for CdS powder is in the range of 10^{-3} cm^2/volt-sec to 10^{-1} cm^2/volt-sec. Nicoll and Kazan (19) have determined that the spectral response for CdS powder is broader than that for single crystal material and is shifted toward longer wavelengths. DeVore (20) discussed the response times and methods of measuring trap distributions in CdS and CdSe powders. Probably the best summary of photoconductive effects in powder material has been presented by Bube (21).

3. Photodielectric Effects

Early explanations (22, 23) of the photodielectric effect were based on an increase in the dielectric constant due to the increased density of easily polarizable trapped carriers. Later work (24, 25, 26, 27, 28) has indicated that in many cases the "apparent" change in dielectric constant is actually the result of changes in the conductivity. Recent work by Kasperovich, et al. (29) has demonstrated changes in the dielectric constant due to charge transfer among impurity centers. All of the above mentioned work was performed at frequencies less than 50 MHz. Very few measurements have been performed in the microwave range. Meilikhov (30) has observed the effect of free carriers on the dielectric constant of Ge at 10 GHz. This effect, known as interfacial polarization, can result in apparent measured values of the dielectric constant of finite size samples that are considerably greater than the bulk value.

C. Complex Permittivity of Materials

1. Use of Complex Permittivity in Electromagnetic Field Equations

The complex permittivity is the link between the macroscopic field quantities and the microscopic material parameters. The use of the complex permittivity is explained in most intermediate field theory texts (31, 32, 33). When deriving expressions for the complex permittivity it is necessary to relate the applied electric field to the actual field acting on a particular molecule. A good discussion of electric fields in dielectric media is given by Schwarz (34).

2. Free Charge Contribution

The classical derivation of the bound charge contribution to the complex permittivity is well understood. However, the same cannot be said for the free carrier contributions. There is still some uncertainity as to whether or not the Lorentz polarization term should be used. Ginzburg (35) and von Hippel (33) have opposing views. There is also disagreement concerning the influence of the lattice dielectric constant on the plasma resonance of the free carriers (36, 37, 38, 39). Depolarization effects and interfacial polarization are normally completely ignored. No derivation has been presented which satisfactorily deals with all of the above mentioned problems. Typical examples of oversimplified derivations are (40, 41, 42).

D. Electromagnetic Wave Propagation Through Inhomogeneous Media

1. Methods of Solution

There have been a variety of techniques developed to solve problems concerned with electromagnetic wave propagation through inhomogeneous media. The same techniques can also be applied to mechanical (i.e. acoustical) waves. Recent books by Wait (43) and Brekhovskikh (44) discuss most of the techniques. Wait (43, 45) derives the exact solution for the special cases of linear and exponential inhomogeneities. Exact solutions for some other cases are available in the form of power series expansions. However, these solutions converge so slow that these techniques are useful only for layers that are thin in comparison with the wavelength.

Numerical integration of the differential equation for the electric or magnetic field intensity using difference equations has been presented by Richmond (46). Approximate solutions obtained by the iterative use of an integral equation are discussed by Heading (47). An example of the use of perturbation and variational methods was presented by Gabriel and Brodwin (48). In those cases where the gradient of the inhomogeneity is small, the Wentzel, Kramers, and Brillouin (WKB) method (49, 50) of approximate solution has been used successfully. Osterberg (51) has reduced the wave equation in inhomogeneous media to a Ricatti differential equation. However, for most cases only an approximate solution can be obtained for the Ricatti equation by numerical integration.

The technique used in this dissertation is an approximate, numerical method known as wave matrices. The derivation presented in Chapter IV is slightly different from the standard approaches (52, 53, 54, 55, 56), however, the end results are equivalent. In the wave matrix approach the inhomogeneity is subdivided into thin homogeneous sections. A matrix relating the incident, reflected, and transmitted waves is determined for each section. The product of all the matrices representing the inhomogeneous media relates the resultant incident, reflected, and transmitted waves. Good approximate solutions for any physically realizable one-dimensional inhomogeneity can be obtained with this method.

2. Calculated Results

Although many of the numerical techniques have been available for over 25 years, it was not until within the past 10 years that computers became available to make such calculations possible. It is surprising to find that during the past 10 years very few calculations regarding wave propagation through homogeneous and inhomogeneous media have been performed. In 1960 Baeumler (58) published results for electromagnetic wave propagation through a single, homogeneous, semi-infinite dielectric slab located in free space. For this special case Baeumler presented several curves of the relative energy transmitted versus the ratio of dielectric conductivity to frequency. Jacobs et al. (58) have performed calculations of the reflection coefficient for infinitely long sections of dielectrically filled rectangular waveguide. Holmes and Feucht (53) have reported calculations of the relative power transmitted versus slab thickness and the magnitude of the reflection coefficient versus angle of incidence for the homogeneous, semi-infinite slab in free space. In 1967, Gunn (59) reported good agreement between calculated and measured values of the propagation constant for a short section of rectangular waveguide loaded longitudinally with a thin strip of semiconducting material. Gunn suggested that the reason his measured values were consistently lower than the calculated values was the effect of the insulating barrier between the semiconducting material and the waveguide wall. The author noted a similar effect on the conductivity measurements of silicon wafers. Also in 1967, Jacobs et al. (60) reported calculated and experimental results for the reflection coefficient of a short section of semiconductor filled rectangular waveguide at 70 GHz. Only homogeneous media were considered in all of the above research. The computer calculations for homogeneous media contained in Chapter V are broader in scope and more detailed than any results published to date. Limited calculations for inhomogeneous media are also presented in Chapter V.

E. Microwave Measurement of Material Parameters

1. Lifetime Measurement

A detailed discussion of all the standard methods of performing dc lifetime measurements was presented by Ryvkin (10). Additional special techniques are discussed by Stevenson and Keyes (61), Watters and Ludwig (62), and Blakemore (63).

Theoretical derivations relating the time constant of the transmitted microwave power to the lifetime of the excess free carriers were presented by Nag and Das (64) and Atwater (65). Both of these authors neglect the effects of reflections from the test material. A more detailed derivation is presented in Appendix E. All derivations indicate that a necessary condition for accurate lifetime measurements is $\sigma \ll \omega\epsilon$.

Various methods of performing microwave lifetime measurements are indicated by Ramsa et al. (66), Jacobs et al. (67), and Deb and Nag (68). In each of these cases measurements were performed on Ge with a conductivity of 30 mhos/m to 50 mhos/m. Since $\omega\epsilon \approx 10$ for Ge at 10 GHz, the conductivity in each case was not less than $\omega\epsilon$. Hence, the reported lifetime measurements are of doubtful accuracy. Similar measurements have been performed on Si, but to date no such measurements have been reported for CdS.

2. Complex Permittivity Measurement

Jacobs et al. (69, 70, 58) performed some of the earliest microwave measurements of the conductivity of thick (5 mm) samples of Ge and Si. Their technique consisted of completely filling a short section of X-band waveguide with the sample, and then, determining the conductivity indirectly from measurements of either the reflection or transmission coefficient. Nag and Roy (71) used a similar procedure. In 1963, Nag and Roy (72, 73, 74, 75) reported measurements of conductivity and dielectric constant of thin Si samples placed longitudinally in the waveguide and backed by a short.

Lindmayer and Kutsko (76) have reported measurements of the conductivity of Si at 25 GHz. In 1968, Sheikh and Gunn (77) presented theoretically calculated curves of variation in propagation constant with conductivity and dielectric constant. They considered the case of thin slabs of either Si or Ge placed longitudinally in the waveguide. No experimental work was performed.

III. FORMULATION OF THE COMPLEX PERMITTIVITY IN TERMS OF MICROSCOPIC MATERIAL PARAMETERS

A. Introduction

In order to fully discuss the interaction of electromagnetic radiation with matter, the macroscopic theory of Maxwell must be combined with the detailed microscopic theory of Lorentz. To do this rigoriously and in detail is a statistical quantum mechanical problem well beyond the purpose of this chapter. The standard classical formulation of the complex permittivity in terms of the polarization of bound and free charges is adequate. In the classical approach the basic relationships between the macroscopic and microscopic material parameters are clearly evident, whereas, in a quantum mechanical approach they are usually hidden by the mathematical complexity.

The macroscopic electromagnetic properties of any material (32, 33, 78) can be completely specified by <u>any two</u> of the complex constitutive parameters known as permeability (μ), permittivity (ϵ), and conductivity (σ). Normally μ and ϵ are the two parameter sets used, where the effects of free carrier conduction (σ) are included in the complex permittivity. For the most general anisotropic material both μ and ϵ are second rank tensors or dyadics. Throughout this dissertation only linear, isotropic, nonmagnetic materials will be considered. Hence, μ is considered to be constant and equal to the permeability of free space; and, ϵ is considered to be a complex, time independent, spatially varying scalar which includes the conductivity as explained in the next section.

B. <u>Discussion of the Basic Electromagnetic Field Equations Involving Material Parameters</u>

Maxwell's equations for a macroscopic medium are,

$$\nabla \cdot \overline{D} = \rho, \tag{3.1}$$

$$\nabla \cdot \overline{B} = 0, \tag{3.2}$$

$$\nabla x \overline{E} = - \partial \overline{B}/\partial t, \tag{3.3}$$

$$\nabla x \overline{H} = \overline{J} + \partial \overline{D}/\partial t, \tag{3.4}$$

where ρ is the volume density of unneutralized charge, $\overline{J}$ is a combination of the conduction and convection current densities, and $\partial \overline{D}/\partial t$ is the displacement current density. All of these macroscopic parameters are assumed to be averaged over a volume at least as large as a unit cell (79). Additional auxiliary equations required are,

$$\nabla \cdot \overline{J} = - \partial \rho/\partial t \tag{3.5}$$

$$\overline{D} = \epsilon_b \overline{E} = \epsilon_o \overline{E} + \overline{P} \tag{3.6}$$

$$\overline{B} = \mu \overline{H} = \mu_o (\overline{H} + \overline{M}) \tag{3.7}$$

$$\overline{J} = \sigma_f \overline{E} \tag{3.8}$$

where $\overline{P}$ is the polarization (net electric dipole moment per unit volume) and $\overline{M}$ is the magnetization (net magnetic dipole moment per unit volume). Since only nonmagnetic materials are considered, $\overline{M} = 0$. As discussed later, $\overline{P}$ and $\overline{E}$ are related by

$$\overline{P} = \psi_e \epsilon_o \overline{E}, \tag{3.9}$$

where ψ_e is a characteristic of the material known as the electric susceptibility.

Assuming harmonic time variation of the form $\exp(+j\omega t)$, equation (3.4) reduces to,

$$\nabla \times \overline{H} = (\sigma_f + j\omega\epsilon_b)\overline{E}. \tag{3.10}$$

At this point it is necessary to clearly define what the symbols σ_f and ϵ_b represent, because there are a variety of different, acceptable definitions in common use (33). σ_f accounts for <u>all</u> the phenomena associated with <u>free charges.</u>

$$\sigma_f = \sigma_f' - j\sigma_f'', \tag{3.11}$$

where σ_f' represents conversion by free carriers of electromagnetic energy into other forms of energy, such as heat, and, σ_f'' represents storage of electromagnetic energy by the free carriers in a manner analogous to electric dipole polarization. In fact, σ_f'' will actually be treated as one component of the real part of the total complex permittivity. ϵ_b accounts for <u>all</u> the phenomena associated with <u>bound charges</u>.

$$\epsilon_b = \epsilon_b' - j\epsilon_b'', \tag{3.12}$$

where ϵ_b' represents the lattice contribution to the real part of the total complex permittivity; and, ϵ_b'' represents conversion by bound charges of electromagnetic energy into other forms of energy, such as the heat produced by dielectric hysteresis.

Using equations (3.10), (3.11), and (3.12), the total complex permittivity, ϵ, is defined by,

$$\epsilon = \left[(\sigma_f' - j\sigma_f'') + j\omega(\epsilon_b' - j\epsilon_b'')\right]/(j\omega). \tag{3.13}$$

Then,

$$\epsilon = \epsilon' - j\epsilon''$$

$$\epsilon = (\epsilon_b' - \sigma_f''/\omega) - j(\epsilon_b'' + \sigma_f'/\omega), \quad (3.14)$$

where,

$$\epsilon' = \epsilon_b' - \sigma_f''/\omega \quad (3.15)$$

$$\epsilon'' = \epsilon_b'' + \sigma_f'/\omega. \quad (3.16)$$

Frequently, the complex relative dielectric constant, ϵ_r, is used.

$$\epsilon_r = \epsilon_r' - j\epsilon_r'', \quad (3.17)$$

where

$$\epsilon_r' = \epsilon_b'/\epsilon_o - \sigma_f''/\omega\epsilon_o \quad (3.18)$$

$$\epsilon_r'' = \epsilon_b''/\epsilon_o + \sigma_f'/\omega\epsilon_o \quad (3.19)$$

Note that equation (3.18) indicates that free carriers may contribute to the real part of ϵ_r. This phenomena is developed more fully in Section D.

C. Contribution of Bound Charge to the Complex Permittivity

For dielectric media, the link between the macroscopic and microscopic theories occurs through the polarization, $\overline{P}$. Some of the most common expressions involving $\overline{P}$ are;

$$\overline{P} = \psi_e \epsilon_o \overline{E}, \quad (3.9)$$

$$\overline{P} = \overline{D} - \epsilon_o \overline{E}, \quad (3.6)$$

$$\overline{P} = N\overline{p} = Nq\overline{r}, \quad (3.20)$$

$$\overline{P} = N\alpha\overline{E}_{loc} = N\alpha(\overline{E} + \overline{P}/3\epsilon_o), \quad (3.21)$$

where $\overline{E}$ is the resultant macroscopic electric field intensity, $\overline{p}$ is the microscopic dipole moment, N is the volume density of dipoles, r is the average separation between the centers of positive and negative charges which produce $\overline{p}$, α is the average polarizability of the dipoles, $\overline{E}_{loc}$ is the locally acting field at the dipole, and $\overline{P}/3\epsilon_o$ is the Lorentz polarization field. (See Appendix A for a summary of the relationships between the various electric fields associated with a dielectric material.) Normally, equation (3.21) is considered to be the most fundamental because it relates $\overline{P}$ to the microscopic parameters N, α, and $\overline{E}_{loc}$. The permittivity is related to the polarization by

$$\epsilon_b = \epsilon_o + \overline{P}/\overline{E}, \tag{3.22}$$

where the ratio $\overline{P}/\overline{E}$ is a complex, frequency and space dependent scalar for the linear, inhomogeneous, isotropic material considered in this dissertation. Once the complete relationship between $\overline{P}$ and $\overline{E}$ is specified, then, ϵ_b is specified.

The total polarization can be subdivided into four basic components: orientational (or dipolar), ionic (or atomic), electronic, and interfacial polarization. The orientational polarization is caused by the alignment of permanent dipole moments. The electronic and ionic polarizations are the result of dipole moments induced by the displacement of the electron cloud with respect to the nucleus and by the displacement of positive and negative ions, respectively. In heterogeneous materials there is also the possibility of an interfacial polarization arising from the accumulation of charge at potential barriers such as structural interfaces or grain boundaries. This component is usually important only for material samples of small dimensions, such as crystalline powder. The reciprocal of the relaxation time of each polarization component determines the frequency about which anomalous dispersion and resonance absorption will occur. For orientational, ionic, and electronic polarization these frequencies fall in the microwave, infrared, and visible portions of the spectrum, respectively.

The manner in which the microscopic parameters determine the orientational and ionic polarizations is briefly described next. Interfacial polarization, which is caused by the motion of free charge, is discussed in Section D.

1. Orientational Polarization

Kittel's (79) summary of Debye's detailed theory of dielectric relaxation of polar molecules results in the following relationship between $\overline{P}$ and $\overline{E}_{loc}$ for harmonic fields,

$$\overline{P} = - \frac{N(\overline{p}\cdot\overline{p})\overline{E}_{loc}}{3k_B T(1 + j\omega\tau_d)} \qquad (3.23)$$

where $\overline{p}$ is the permanent dipole moment, k_B is Boltzmann's constant, T is the absolute temperature, and τ_d is the relaxation time of the dipoles. The relaxation time is defined as the time required for the dipoles to orient in such a way that the polarization reduces to 1/e of its original value after the exciting field has been removed.

Water at room temperature has a relaxation frequency

($f = 1/\tau_d$) of about 30 GHz, and ice at 253°K (-20°C) has a relaxation frequency of about 1 KHz. OH^- ions substituted for Cl^- ions in a KCl crystal have a relaxation frequency of about 10 GHz at 1°K. Also, the NH_3 molecule has a broad absorption spectrum centered about 23.8 GHz. There are many additional examples of dielectric relaxation occuring in the microwave region.

2. Ionic Polarization

A classical analysis (33, 80, 81) of the steady-state response of singly ionized ions in a crystal to a harmonic field $\bar{E}_{int}$ inside the crystal results in

$$\bar{P} = \sum_n \frac{(N_n q^2/m_n)\bar{E}_{int}}{\left[\omega_n^2 - N_n q^2/(3m_n \epsilon_o) - \omega^2\right] + j2\omega f_n} \tag{3.24}$$

where n is summed over the various types of ion pairs, and for a particular type N_n is the volume density of ion pairs, m_n is the reduced mass of an ion pair, ω_n is the natural resonant frequency of the ion pairs, and f_n is a frictional damping factor. From equations (3.22) and (3.24),

$$\begin{aligned} \epsilon_b &= \epsilon_b' - j\epsilon_b'' \\ &= \epsilon_o + \sum_n \frac{N_n q^2/m_n}{\left[\omega_n^2 - N_n q^2/(3m_n \epsilon_o) - \omega^2\right] + j2\omega f_n} \end{aligned} \tag{3.25}$$

Equation (3.25) could be used to plot the standard anomalous dispersion curve associated with ϵ_b' and the resonance absorption curve associated with ϵ_b''. Results similar in form to equations (3.24) and (3.25) are obtained for electronic polarization.

In general, once either $\epsilon_b'(\omega)$ or $\epsilon_b''(\omega)$ is known for all ω, then the Kramers-Kronig relation may be used to find the unknown part of $\epsilon_b(\omega)$. This is analogous to synthesizing a positive real impedance function from either a magnitude or a phase function.

D. <u>Contribution of Free Charge to the Complex Permittivity</u>

A rigorous derivation (35, 38, 82, 83) of the complex conductivity σ_f requires a statistical, quantum mechanical solution of the Boltzmann transport equation. Fortunately, such detail is not required in this work. A classical description of the phenomenon is adequate provided a sufficiently detailed model is used. Most derivations are based on a sample of infinite dimensions. If a finite size sample is assumed, then the important phenomenon of interfacial polarization must be included. This leads to plasma resonance and depolarization effects.

The one-dimensional equation of motion for an electron "gas" of volume density n in a finite size sample is

$$m^* \frac{d^2\overline{f}(\overline{x})}{dt^2} + (m^*/\tau_c)\frac{d\overline{f}(\overline{x})}{dt} = -q\overline{E}_{loc}, \qquad (3.26)$$

where m* is the effective mass of the electron in the conduction band, τ_c is the mean time between "collisions" of the electrons with the lattice, and $\overline{f}(\overline{x})$ is the x displacement of the electron "gas" relative to the stationary lattice caused by the locally acting electric field intensity

$\overline{E}_{loc}$. τ_c has not been rigorously specified. This is one of the parameters that would require considerable attention if a detailed derivation were given. This simplified model assumes that each electron losses all of its momentum each time it "collides" with the lattice, and it also assumes that τ_c is independent of the electron velocity. Neither of these assumptions seriously affects the plasma resonance or depolarization effects, which are the main concern here. After modifying the results of Appendix A for the case of a conducting media, the local field may be expressed as

$$\overline{E}_{loc} = \overline{E}_{ext} - L\overline{P}_b/\epsilon_o + \overline{P}_b/(3\epsilon_o) - L\overline{P}_f/\epsilon_o, \qquad (3.27)$$

where $\overline{P}_b$ and $\overline{P}_f$ refer to the polarization of the bound and free charges, respectively, $\overline{P}_b/(3\epsilon_o)$ is the Lorentz polarization term, and L is the depolarization factor. The polarization of the free charges, $\overline{P}_f$, was previously defined in the section on bound charges as interfacial polarization. $\overline{P}_f$ is also called macrostructural polarization. This component of the polarization is frequently overlooked by many authors. In the final expression for the complex conductivity it will be seen that this term has a very significant effect. There is considerable controversy in the literature (33, 35) as to whether or not the Lorentz term should be included. The present consensus appears to be that when considering effects on a macroscopic scale the Lorentz term should not be included. Hence, the scalar equation of motion becomes

$$\frac{d^2 f(x)}{dt^2} + (1/\tau_c)\frac{df(x)}{dt} + \frac{Lnq^2 f(x)}{m^* \epsilon_o} = -(q/m^*)E_{int}, \qquad (3.28)$$

since

$$\overline{P}_f = -nq\overline{f}(\overline{x}). \tag{3.29}$$

Let

$$\omega_p^2 = nq^2/(\epsilon_o m^*) \tag{3.30}$$

and

$$E_{int} = E_o \exp(j\omega t), \tag{3.31}$$

then the steady state solution of equation (3.28) is

$$f(x) = \frac{-(q/m^*)E_o \exp(j\omega t)}{(L\omega_p^2 - \omega^2) + j\omega/\tau_c}. \tag{3.32}$$

Since

$$J = -nq\,\frac{df(x)}{dt} = \sigma_f E_o, \tag{3.33}$$

$$\sigma_f = \frac{j\omega\,\omega_p^2\,\epsilon_o}{(L\omega_p^2 - \omega^2)^2 + (\omega/\tau_c)^2}\left[(L\omega_p^2 - \omega^2) - j(\omega/\tau_c)\right]. \tag{3.34}$$

Since

$$\sigma_f = \sigma_f' - j\sigma_f'', \tag{3.35}$$

$$\sigma_f' = \frac{(\omega^2\omega_p^2\,\epsilon_o)/\tau_c}{(L\omega_p^2 - \omega^2)^2 + (\omega/\tau_c)^2} \tag{3.36}$$

$$\sigma_f'' = \frac{-\omega\,\omega_p^2\,\epsilon_o(L\omega_p^2 - \omega^2)}{(L\omega_p^2 - \omega^2)^2 + (\omega/\tau_c)^2}. \tag{3.37}$$

The quantity $(L\omega_p^2)$ results from the interfacial polarization, P_f. If L is set equal to zero, then σ_f' and σ_f'' reduce to the <u>oversimplified</u> expressions used by most authors. Note that for $L \neq 0$, σ_f'' can be either positive or negative depending upon ω, and hence, the free carrier contribution to the real part of the dielectric constant can be either positive or negative as verified by Meilikhov (30) with Ge at 10 GHz. For a finite size sample with perfect contacts $P_f = 0$, because the infinite supply of electrons at the electrodes prevents the formation of any interfacial polarization. Note that if $P_f \neq 0$, then equation (3.36) indicates that $\sigma_f' = 0$ at $\omega = 0$. This does not mean that the bulk conductivity is zero, but rather that the effective conductivity that one would measure is zero because any applied dc electric field would be reduced to zero inside the material by the interfacial polarization.

E. Photoconductivity

Photoconductivity is the process by which the density of free carriers in a material is changed by the absorption of photons. Practically all of the theory used in this dissertation is also valid for any other mechanism which changes the density of free carriers. Examples of other such mechanisms are carrier injection or extraction at a junction, temperature changes, and electron bombardment.

If the complex permittivity of a photoconductor is known for both dark and light conditions, then the characteristics of an electromagnetic wave propagating through this material can be determined. Since the imaginary part of the conductivity, σ_f'', is usually negligible except for special conditions of temperature and frequency, this component will be neglected in the following discussion. The conductivity is assumed to be time independent but spatially varying. Hence, for a material with a one-dimensional variation

$$\sigma_f' = \sigma(z) = \sigma_o + \Delta\sigma(z), \tag{3.38}$$

where σ_o is the dark conductivity which is assumed to be constant throughout the material, and $\Delta\sigma(z)$ is the conductivity variation produced by photon absorption (or some other mechanism).

$$\sigma_o = q\mu_{no}n_o + q\mu_{po}p_o, \tag{3.39}$$

where μ_{no} and μ_{po} are the electron and hole mobilities, respectively, and n_o and p_o are the electron and hole densities, respectively, for the condition of termal equilibrium and zero incident light intensity.

$$\sigma(z) = q\left[\mu_{no} + \Delta\mu_n(z)\right]\left[n_o + \Delta n(z)\right] + q\left[\mu_{po} + \Delta\mu_p(z)\right]\left[p_o + \Delta p(z)\right] \tag{3.40}$$

where, the quantities prefixed by Δ are the variations produced by light absorption. From equation (3.38) and (3.40) it is seen that

$$\sigma(z) = q\left[\mu_{no}\Delta n(z) + \Delta\mu_n(z)n_o + \Delta\mu_n(z)\Delta n(z)\right] + q\left[\mu_{po}\Delta p(z) + \Delta\mu_p(z)p_o + \Delta\mu_p(z)\Delta p(z)\right]. \tag{3.41}$$

For most materials, the changes in electron and hole mobilities are negligible if the total electron and hole densities are less than about 10^{22} carriers/m^3 (10^{16} carriers/cm^3) and the electric field strength is less than 10^4V/m. Hence,

$$\Delta\sigma(z) = q\left[\mu_{no}\Delta n(z) + \mu_{po}\Delta p(z)\right]. \tag{3.42}$$

If expressions can be found for $\Delta n(z)$ and $\Delta p(z)$ and ϵ_b is known, then, the complete expression for the complex permittivity of the photoconductor is known. $\Delta n(z)$ and $\Delta p(z)$ are determined primarily by the generation rate and lifetime of the free carriers. The generation rate is derived in Appendix A for a one-dimensional case and is given by

$$f(z) = I_o \exp(-\delta z); \qquad 0 \leq z \leq d \tag{3.43}$$

where I_o has units of (electron-hole pairs)/m^3-sec, and δ is the coefficient of light absorption. The diffusion of charge carriers because of inhomogeneous illumination also affects $\Delta n(z)$ and $\Delta p(z)$. The derivation of the general equations involving $\Delta n(z)$ and $\Delta p(z)$, including diffusion, are presented in Appendix B. Solution of the resulting three coupled partial differential equations for a photoconductive layer of finite thickness can usually be accomplished only by numerical techniques. Since a precise quantitative knowledge of $\Delta n(z)$ and $\Delta p(z)$ is not actually required for this work, the standard simplifying assumptions are made, which yield

$$\Delta n(z) = \tau_n f(z) \tag{3.44}$$

$$\Delta p(z) = \tau_p f(z) \tag{3.45}$$

where τ_n and τ_p are the <u>free</u> lifetimes of the electrons and holes, respectively. This results in the following expression for the conductivity,

$$\sigma(z) = \sigma_o + q(\mu_{no}\tau_n + \mu_{po}\tau_p) I_o \exp(-\delta z). \tag{3.46}$$

F. Photodielectric Effect

In Chapter V it will be shown that changes as small as 10% in the dielectric constant can produce changes as large as 100% in the transmitted microwave power. Although the conductivity is usually the parameter most affected at microwave frequencies, the real part of the complex permittivity can be changed in the following ways by photoexcitation:

1) Increase in dielectric constant due to the increased density of easily polarizable trapped electrons. The relaxation time of this mechanism is typically 10^{-7} sec (23), but may vary by two orders of magnitude.

2) Decrease in dielectric constant due to the increased density of free carriers. This is indicated in equation (3.37).

3) Increase in dielectric constant due to interfacial polarization. Meilikhov (30) has reported increases in the dielectric constant of Ge at 10 GHz because of this mechanism. Equation (3.37) is in agreement with Meilikhov's observed results.

4) Recently Kasperovich, et al. (20) have reported changes in the dielectric constant as a result of "jump" conductivity. "Jump" conductivity can be caused by optically stimulated charge transfer among impurities.

G. General Expression for the Complex Permittivity

Neglecting the Lorentz polarization term in all cases and combining the results of sections C and D, the general expression for the total relative complex permittivity is

$$\epsilon_r = 1 + \sum_k \frac{N_k p_k^2}{3\epsilon_o k_B T(1 + j\omega\tau_{dk})} + \sum_l \frac{N_l q^2/(\epsilon_o m_l)}{(\omega_l^2 - \omega^2) + j2\omega f_l} + \sum_m \frac{N_m q^2/(\epsilon_o m_m)}{(\omega_m^2 - \omega^2) + j2\omega f_m} + \sum_n \frac{-jN_n q^2/(\epsilon_o m_n^*)}{(L\,\omega_{pn}^2 - \omega^2) + j\omega/\tau_{cn}}. \tag{3.47}$$

The summations over k, l, m, and n represent the contributions from the various types of dipoles, ions, atoms, and free charges, respectively. The first three contributions correspond to the orientational, ionic, and electronic polarizations of the lattice and the fourth term corresponds to the inertia of the free carriers and the interfacial polarization. For most of the work in this dissertation, the complex permittivity may be satisfactorily approximated by

$$\epsilon = \epsilon_b' - j\sigma_f'/\omega. \tag{3.48}$$

However, explanations for some of the experimental results requires the use of a more detailed theory such as that given in equation (3.47).

IV. DERIVATION OF THE ELECTROMAGNETIC FIELD EQUATIONS FOR PROPAGATION THROUGH RECTANGULAR WAVEGUIDE FILLED WITH AN ISOTROPIC INHOMOGENEOUS MEDIA

A. Introduction

Most electromagnetic field problems involving inhomogeneous media cannot be solved in closed form (43, 44). If the inhomogeneity is of a special form, such as linear or exponential, or if the media deviates only slightly from a homogeneous material, then either closed form solutions or good approximate solutions are possible. The approximate method (52, 53, 57, 84) of solution used in this dissertation is a very powerful technique applicable to any type of inhomogeneity along the waveguide axis. The only restriction to the use of this technique is that normally a computer is required. The technique is analogous to the ABCD-parameter approach used for transmission lines in circuit theory.

B. Derivation

Figure 4.1 depicts a section of rectangular waveguide filled with an isotropic, inhomogeneous medium. The medium is subdivided into thin transverse sections which completely fill the cross section of the waveguide. Each thin section is assumed to be homogeneous. In reality then, the problem of one inhomogeneous medium is exchanged for a series of problems each involving a homogeneous medium. Any or all of

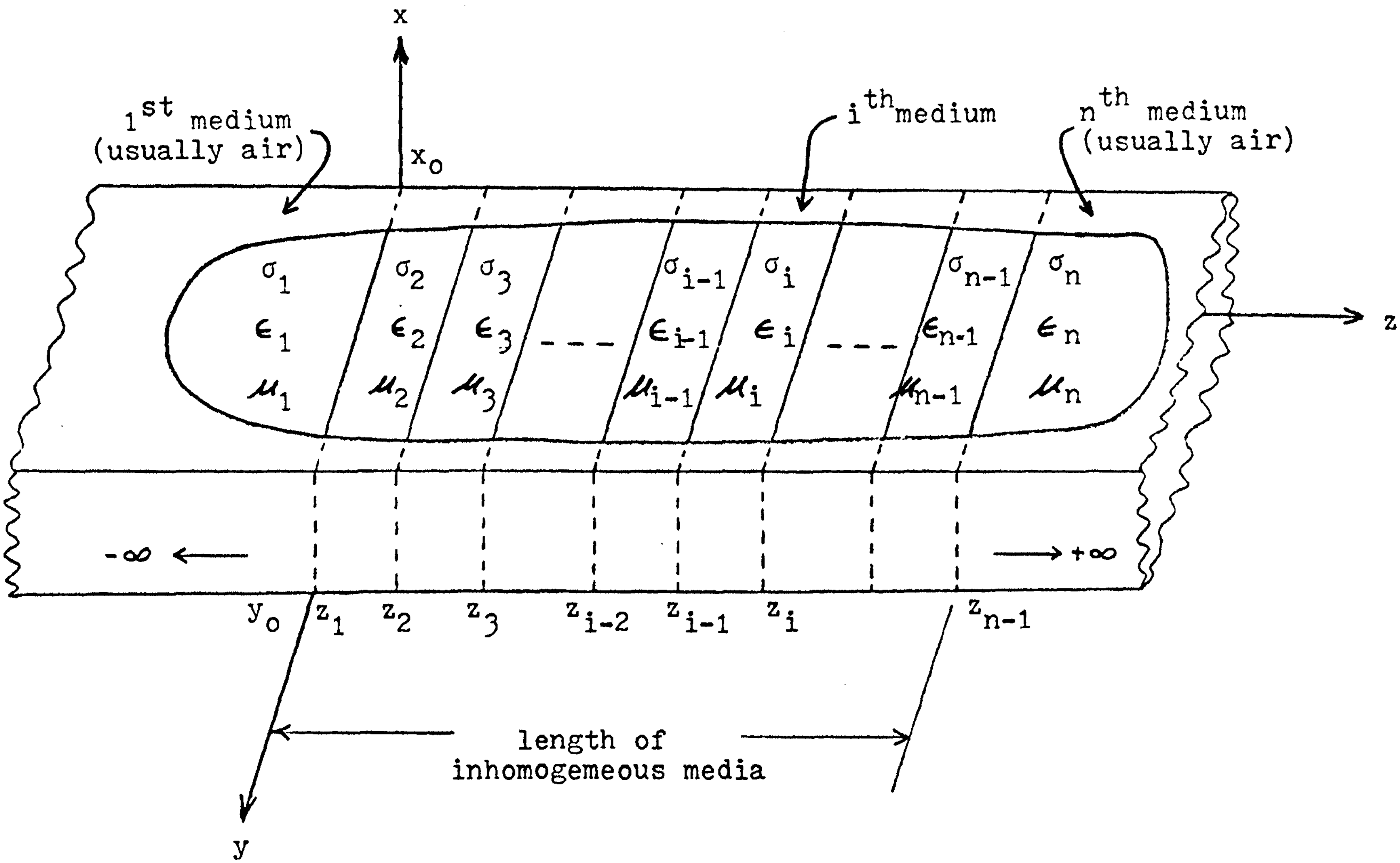

FIGURE 4.1. An inhomogeneously filled waveguide subdivided into homogeneous transverse sections

the parameters σ, ϵ, and μ may be inhomogeneous. However, only variations along the waveguide axis (z axis) are permitted. Note that $\sigma = \sigma_f$ and $\epsilon = \epsilon_b$. The subscripts "f" and "b" have been dropped, since another subscript, "i", has been added to designate the medium.

Only TE_{m0} (transverse electric) modes are considered. Results for TE_{mn} and TM_{mn} (transverse magnetic) modes may be found from a simple extension of the derivation presented here. (For example, the solution for TM_{mn} modes can be immediately obtained from the solution for TE_{mn} modes by using the duality conditions.) Harmonic time variation is assumed. It is understood that in order to obtain the actual expression for a physically measurable field quantity, either the real part or the imaginary part of the corresponding time harmonic function must be used. The solution for the electromagnetic fields in the i^{th} medium begins with Maxwell's equations:

$$\nabla \times \overline{E}_i = - j\omega\mu_i \overline{H}_i \tag{4.1}$$

$$\nabla \times \overline{H}_i = (\sigma_i + j\omega\epsilon_i)\overline{E}_i \tag{4.2}$$

$$\nabla \cdot \mu_i \overline{H}_i = 0 \tag{4.3}$$

$$\nabla \cdot \epsilon_i \overline{E}_i = \rho_i = 0. \tag{4.4}$$

Note that equation (4.4) indicates that space charge effects are not included in this derivation. Taking the curl of equation (4.1) and then making use of equation (4.2) yeilds,

$$\begin{aligned} \nabla \times \nabla \times \overline{E}_i &= - j\omega\mu_i(\nabla \times \overline{H}_i) \\ &= - j\omega\mu_i(\sigma_i + j\omega\epsilon_i)\overline{E}_i. \end{aligned} \tag{4.5}$$

Using the vector identity

$$\nabla \times \nabla \times \overline{E}_i = \nabla(\nabla \cdot \overline{E}_i) - \nabla^2 \overline{E}_i, \tag{4.6}$$

equation (4.5) reduces to

$$\nabla^2 \overline{E}_i + k_i^2 E_i = 0. \tag{4.7}$$

where

$$k_i^2 = -\, j\omega\mu_i(\sigma_i + j\omega\epsilon_i). \tag{4.8}$$

Note that k_i must be that root of k_i^2 which has a negative imaginary part.

Assuming a TE_{mo} mode,

$$\overline{E}_i = E_{ix}(y, z)\overline{a}_x = Y(y)Z(z)\overline{a}_x. \tag{4.9}$$

Using the standard separation of variables method of solution:

$$\frac{\partial^2 E_{ix}}{\partial x^2} + \frac{\partial^2 E_{ix}}{\partial y^2} + \frac{\partial^2 E_{ix}}{\partial z^2} + k_i^2 E_{ix} = 0 \tag{4.10}$$

simplifies to

$$Y''/Y = -\, Z''/Z - k_i^2 = -\, k_{i1}^2 \tag{4.11}$$

where, k_{i1} is an unknown constant. Solving equation (4.11) subject to the waveguide boundary conditions yields,

$$Y(y) = C_1 \sin(k_{i1} y) \tag{4.12}$$

where,

$$k_{i1} = m\pi/y_o; \qquad m = 0, \pm 1, \pm 2, \ldots \tag{4.13}$$

and,

$$Z(z) = C_2 \exp\left[j(k_i^2 - k_{i1}^2)^{\frac{1}{2}}(z - z_{i-1})\right] + C_3 \exp\left[-\, j(k_i^2 - k_{i1}^2)^{\frac{1}{2}}(z - z_{i-1})\right]; \quad z_{i-1} \leq z \leq z_i. \tag{4.14}$$

Hence,

$$\overline{E}_{ix}(y, z) = \Big\{E_i^+\exp\big[-\gamma_i(z - z_{i-1})\big] + E_i^-\exp\big[\gamma_i(z - z_{i-1})\big]\Big\} \sin(m\pi y/y_o)\ \overline{a}_x;$$

$$z_{i-1} \leq z \leq z_i, \tag{4.15}$$

where

$$E_i^+ = C_1C_3$$

$$E_i^- = C_1C_2$$

$$\gamma_i = \alpha_i + j\beta_i = j(k_i^2 - k_{i1}^2)^{\frac{1}{2}}$$

$$= \left[(m\pi/y_o)^2 - \omega^2\mu_i\epsilon_i + j\omega\mu_i\sigma_i\right]^{\frac{1}{2}}. \tag{4.16}$$

From here on, all equations involving the i^{th} medium are assumed to have z restricted to the range, $z_{i-1} \leq z \leq z_i$. E_i^+ and E_i^- are the complex amplitudes of the incident and reflected electric field intensities, respectively, at a point z_{i-1}^- just to the right of the boundary between the $(i-1)^{th}$ and i^{th} media (Figure 4.2).

Because of the definition of E_i^+ and E_i^-, the sign of some of the exponentials in the final result differs from the signs in the "standard" solution. In the "standard" approach, E_i^+ and E_i^- are defined at the right hand extreme of the i^{th} layer.

The magnetic field intensity can be found from $\overline{E}_{ix}$ by use of equation (4.1),

$$\overline{H}_i = \frac{\nabla \times \overline{E}_i}{-j\omega\mu_i} = \left[\frac{\partial E_{ix}}{\partial z}\overline{a}_y - \frac{\partial E_{ix}}{\partial y}\overline{a}_z\right]/(-j\omega\mu_i) \tag{4.17}$$

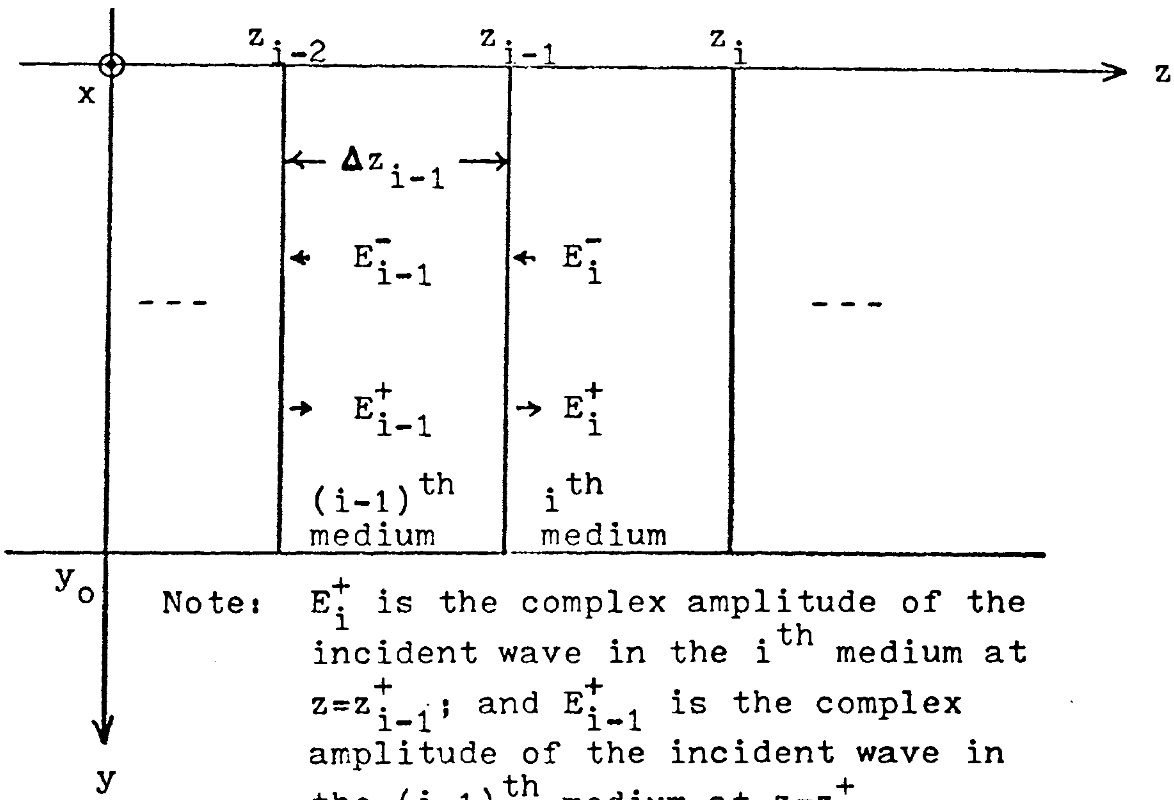

Note: E^+_i is the complex amplitude of the incident wave in the i^{th} medium at $z=z^+_{i-1}$; and E^+_{i-1} is the complex amplitude of the incident wave in the $(i-1)^{th}$ medium at $z=z^+_{i-2}$. (See Figure 4.1.)

FIGURE 4.2. Notation for electric field intensity boundary conditions at $z=z_{i-1}$

Hence,

$$\overline{H}_{iy} = \frac{\gamma_i}{(-j\omega\mu_i)}\Big\{-E_i^+\exp\left[-\gamma_i(z - z_{i-1})\right]$$

$$+E_i^-\exp\left[\gamma_i(z - z_{i-1})\right]\Big\} \cos(m\pi y/y_o)\ \overline{a}_y \qquad (4.18)$$

and,

$$\overline{H}_{iz} = \frac{-(m\pi/y_o)}{-j\omega\mu_i}\Big\{E_i^+\exp\left[-\gamma_i(z - z_{i-1})\right]$$

$$+E_i^-\exp\left[\gamma_i(z - z_{i-1})\right]\Big\} \cos(m\pi y/y_o)\ \overline{a}_z. \qquad (4.19)$$

The transverse impedance of the waveguide for the i^{th} medium, Z_i, is defined as

$$Z_i = E_{ix}^+/H_{iy}^+ = E_{ix}^-/(-H_{iy}^-) = j\omega\mu_i/\gamma_i = 1/Y_i. \qquad (4.20)$$

Hence,

$$\overline{H}_{iy} = \Big\{Y_i E_i^+\exp\left[-\gamma_i(z - z_{i-1})\right]$$

$$- Y_i E_i^-\exp\left[\gamma_i(z - z_{i-1})\right]\Big\} \sin(m\pi y/y_o)\ \overline{a}_y. \qquad (4.21)$$

For the $(i-1)^{th}$ medium, the transverse electric and magnetic field intensities are

$$\overline{E}_{(i-1)x} = \Big\{E_{i-1}^+\exp\left[-\gamma_{i-1}(z - z_{i-2})\right]$$

$$+ E_{i-1}^-\exp\left[\gamma_{i-1}(z - z_{i-2})\right]\Big\} \sin(m\pi y/y_o)\ \overline{a}_x \qquad (4.22)$$

$$\overline{H}_{(i-1)y} = \Big\{Y_{i-1}E_{i-1}^+\exp\left[-\gamma_{i-1}(z - z_{i-2})\right]$$

$$- Y_{i-1}E_{i-1}^-\exp\left[\gamma_{i-1}(z - z_{i-2})\right]\Big\} \sin(m\pi y/y_o)\ \overline{a}_y, \qquad (4.23)$$

where, now z is restricted to the range, $z_{i-2} \leq z \leq z_{i-1}$.

Since the tangential electric field intensity must be continuous across a boundary (Figure 4.2),

$$\overline{E}_{(i-1)x} = \overline{E}_{ix} \text{ at } z = z_{i-1} \qquad (4.24)$$

requires that

$$E_{i-1}^{+}\exp\left[-\gamma_{i-1}(z_{i-1} - z_{i-2})\right] + E_{i-1}^{-}\exp\left[\gamma_{i-1}(z_{i-1} - z_{i-2})\right] = E_i^{+} + E_i^{-}. \qquad (4.25)$$

Since the magnetic field intensity must be continuous across a boundary on which no surface current flows,

$$\overline{H}_{(i-1)x} = \overline{H}_{ix} \text{ at } z = z_{i-1} \qquad (4.26)$$

requires that,

$$Y_{i-1}E_{i-1}^{+}\exp\left[-\gamma_{i-1}(z_{i-1} - z_{i-2})\right] - Y_{i-1}E_{i-1}^{-}\exp\left[\gamma_{i-1}(z_{i-1} - z_{i-2})\right] = Y_iE_i^{+} - Y_iE_i^{-}. \qquad (4.27)$$

Let

$$\Delta z_{i-1} = (z_{i-1} - z_{i-2}) \qquad (4.28)$$

where z_{i-1} is the thickness, in meters, of the $(i-1)^{th}$ medium. It is not necessary that the inhomogeneous region be subdivided into sections of equal thickness, however, this is usually the easiest method of subdivision.

Solving equations (4.25) and (4.27) simultaneously yields

$$E_{i-1}^{+} = (1 + Y_i/Y_{i-1})\exp(\gamma_{i-1}\,\Delta z_{i-1})E_i^{+}/2 + (1 - Y_i/Y_{i-1})\exp(\gamma_{i-1}\,\Delta z_{i-1})E_i^{-}/2 \qquad (4.29)$$

$$E_{i-1}^{-} = (1 - Y_i/Y_{i-1})\exp(-\gamma_{i-1}\,\Delta z_{i-1})E_i^{+}/2 + (1 + Y_i/Y_{i-1})\exp(-\gamma_{i-1}\,\Delta z_{i-1})E_i^{-}/2 \qquad (4.30)$$

The transmission and reflection coefficients, T_i and R_i, at the boundary between the $(i-1)^{th}$ and i^{th} media are given by

$$T_i = \frac{2Y_{i-1}}{Y_{i-1} + Y_i} = \frac{2Z_i}{Z_{i-1} + Z_i} \tag{4.31}$$

$$R_i = \frac{Y_{i-1} - Y_i}{Y_{i-1} + Y_i} = \frac{Z_i - Z_{i-1}}{Z_i + Z_{i-1}} . \tag{4.32}$$

Then equations (4.29) and (4.30) simplify to

$$E^+_{i-1} = (1/T_i)\Big[\exp(\gamma_{i-1}\Delta z_{i-1})E^+_i + R_i\exp(\gamma_{i-1}\Delta z_{i-1})E^-_i\Big] \tag{4.33}$$

$$E^-_{i-1} = (1/T_i)\Big[R_i\exp(\gamma_{i-1}\Delta z_{i-1})E^+_i + \exp(-\gamma_{i-1}\Delta z_{i-1})E^-_i\Big]. \tag{4.34}$$

Using Figure 4.2, it can be seen that equations (4.33) and (4.34) determine the incident and reflected components of $\overline{E}_{i-1}$ at $z = z^+_{i-2}$ in terms of the incident and reflected components of $\overline{E}_i$ at $z = z^+_{i-1}$. Using this procedure repeatedly for each of the (n-2) layers, the electric field intensity in the first medium may be related to the field in the n^{th} medium by the matrix equation,

$$\begin{bmatrix} E^+_1 \\ E^-_1 \end{bmatrix} = \begin{bmatrix} 1/T_2 & R_2/T_2 \\ R_2/T_2 & 1/T_2 \end{bmatrix} \times \left\{ \prod_{i=3}^{n} \begin{bmatrix} \exp(\gamma_{i-1}\Delta z_{i-1})/T_i & R_i\exp(\gamma_{i-1}\Delta z_{i-1})/T_i \\ R_i\exp(-\gamma_{i-1}\Delta z_{i-1})/T_i & \exp(-\gamma_{i-1}\Delta z_{i-1})/T_i \end{bmatrix} \right\} \begin{bmatrix} E^+_n \\ E^-_n \end{bmatrix} \tag{4.35}$$

The next chapter is concerned with the numerical solution of equation (4.35) for various types of inhomogeneities.

For the special case of a homogeneously filled waveguide, only one layer (n=3) is required. Assuming that there is no reflected wave in the third medium, $E_3^- = 0$, and equation (4.35) reduces to

$$\begin{bmatrix} E_1^+ \\ E_1^- \end{bmatrix} = \begin{bmatrix} 1/T_2 & R_2/T_2 \\ R_2/T_2 & 1/T_2 \end{bmatrix}$$
$$\begin{bmatrix} \exp(\gamma_2\,\Delta z_2)/T_3 & R_3\exp(\gamma_2\,\Delta z_2)/T_3 \\ R_3\exp(-\gamma_2\,\Delta z_2)/T_3 & \exp(-\gamma_2\,\Delta z_2)/T_3 \end{bmatrix} \begin{bmatrix} E_3^+ \\ 0 \end{bmatrix} . \quad (4.36)$$

V. NUMERICAL SOLUTION OF THE ELECTROMAGNETIC FIELD EQUATIONS FOR VARIOUS TYPES OF HOMOGENEOUS AND INHOMOGENEOUS CONDUCTIVITY VARIATIONS

A. Introduction

The examples discussed in this chapter are concerned either with propagation inside a lossy, dielectrically filled X-band (8.2 GHz to 12.4 GHz) rectangular waveguide or propagation through a semi-infinite, lossy, dielectric slab in free space. In each of the above cases, both homogeneous and inhomogeneous media are considered. Particular emphasis is given to propagation through a homogeneously filled waveguide, since for this case, experiments can be easily conducted to test the theoretical predictions. The following assumptions were made in calculating the results presented:

(1) $\mu = \mu_0$;

(2) Only TEM mode for free space examples;

(3) Only TE_{10} mode for waveguide examples.

The above assumptions were made for the sake of convenience only, so that the important results would not be confused with additional unnecessary variables. It must be emphasized that although conductivity variations are the main concern in this chapter, the mathematical techniques and computer programs developed by the author are capable of solving problems with arbitrary, simultaneous variations in μ, ϵ_b, and σ_f. The computer programs used in calculating and plotting the results are contained in Appendix D.

B. Homogeneous Media

One of the purposes of this research was to determine the range over which the conductivity of a lossy dielectric must be varied in order to produce a significant change in the reflected and transmitted microwave power. The results of this and related research efforts are discussed in the following three sections.

1. VSWR Versus Conductivity

In this section variations in reflected power, transmitted power, power absorbed, voltage standing wave ratio, attenuation (insertion loss), and angle of reflection and transmission coefficients versus conductivity are presented.

Figures 5.1a through 5.1g illustrate the results of a typical waveguide example. Large variations in reflected, transmitted, and absorbed powers occur only over a two order-of-magnitude variation in the conductivity. However, this range of conductivity variation is different for the reflected, absorbed, and transmitted powers. Using the 10 GHz curve, the reflected power variation occurs over a range of 1.0 mhos/m to 100 mhos/m, whereas, the transmitted power variation occurs over a range of 0.1 mhos/m to 10 mhos/m. The absorbed power variation overlaps portions of the above two ranges, and is centered about 2.0 mhos/m. This indicates that the transmitted and reflected powers may be modulated independently. The value of conductivity

Waveguide Program No. 25

$\epsilon_r = 10.0$ Thickness = 48.8, 4.88, 0.488 mm

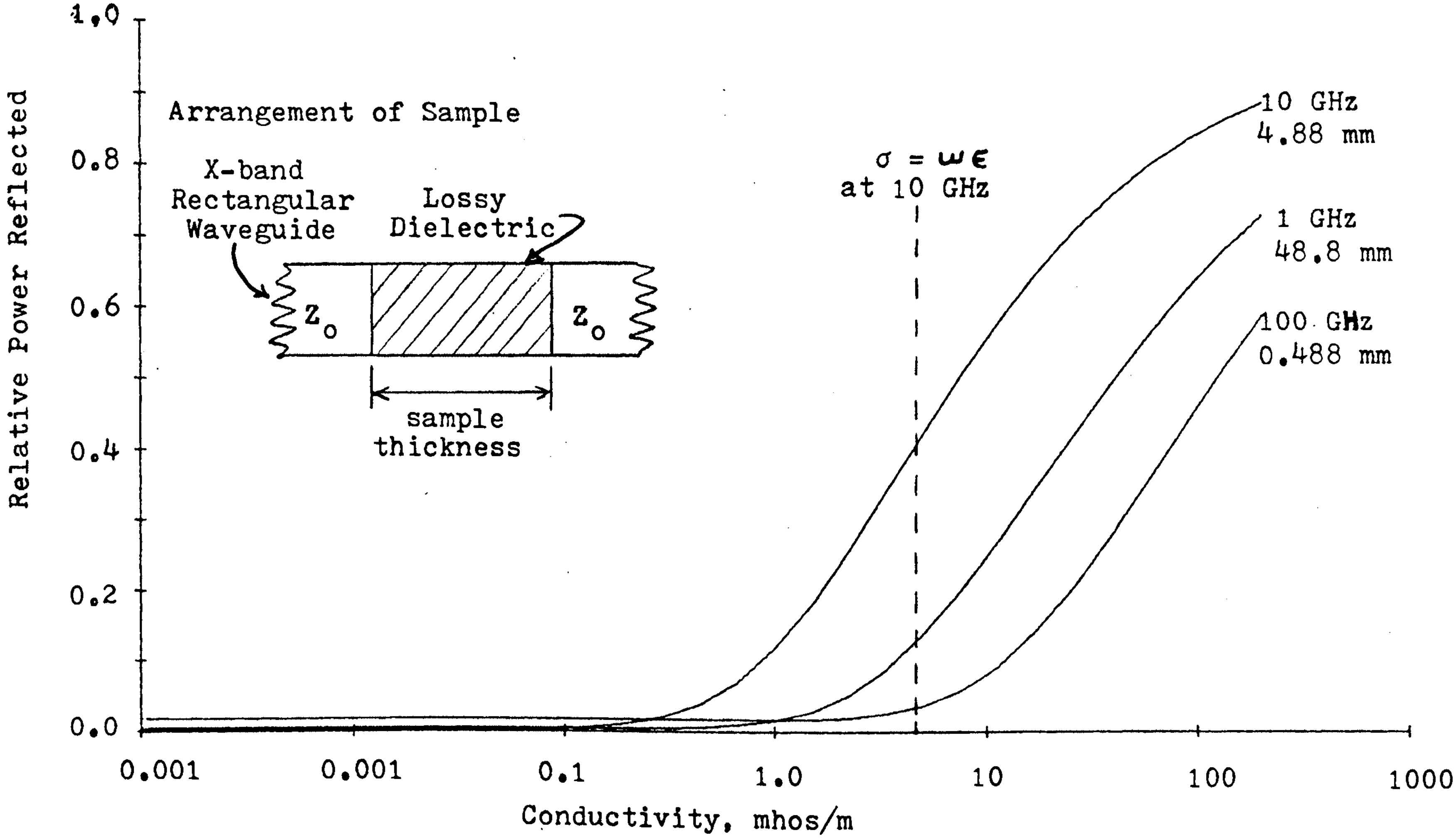

FIGURE 5.1a. Relative power reflected versus conductivity for short section of dielectrically filled waveguide

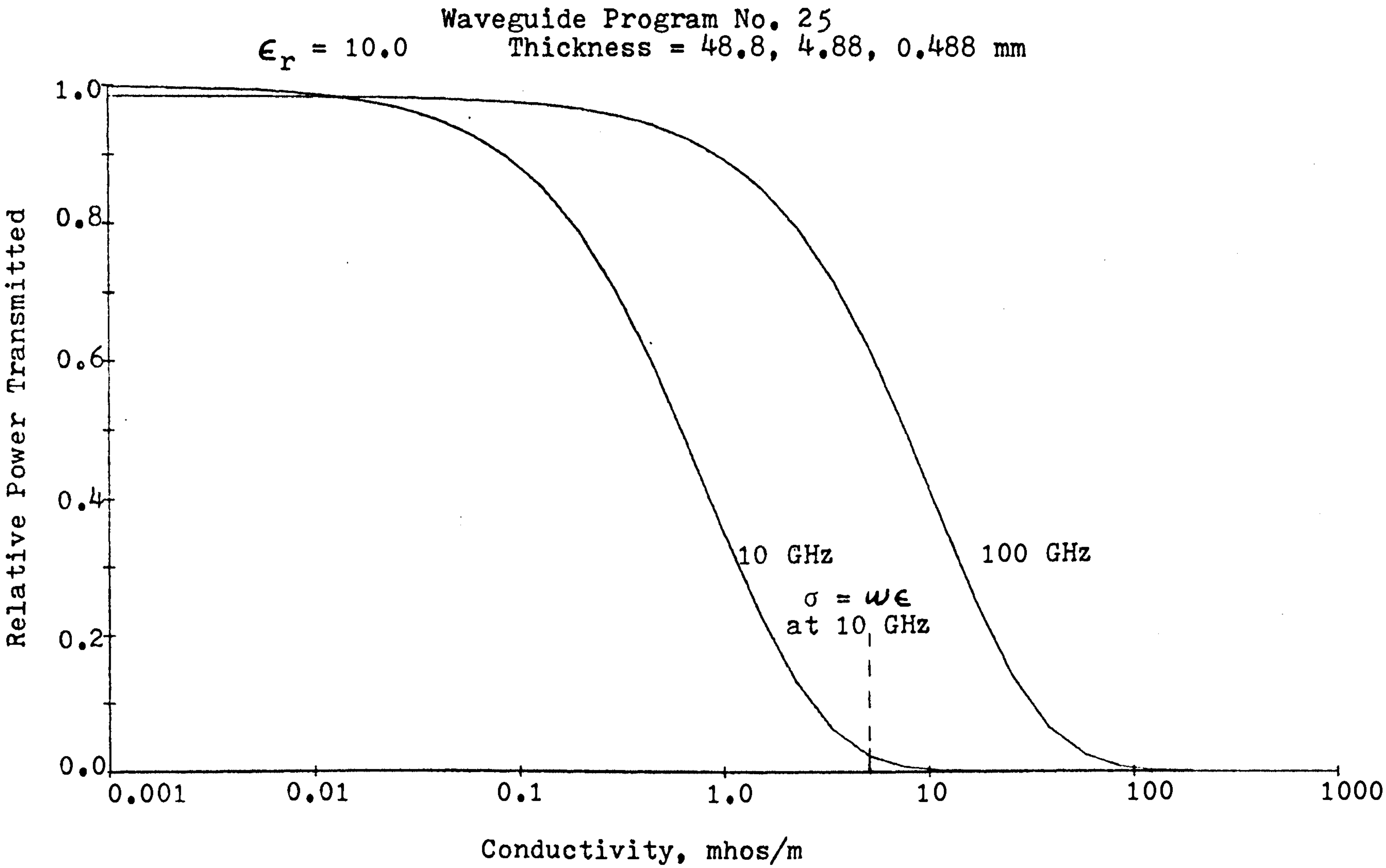

FIGURE 5.1b. Relative power transmitted versus conductivity for a dielectrically filled waveguide

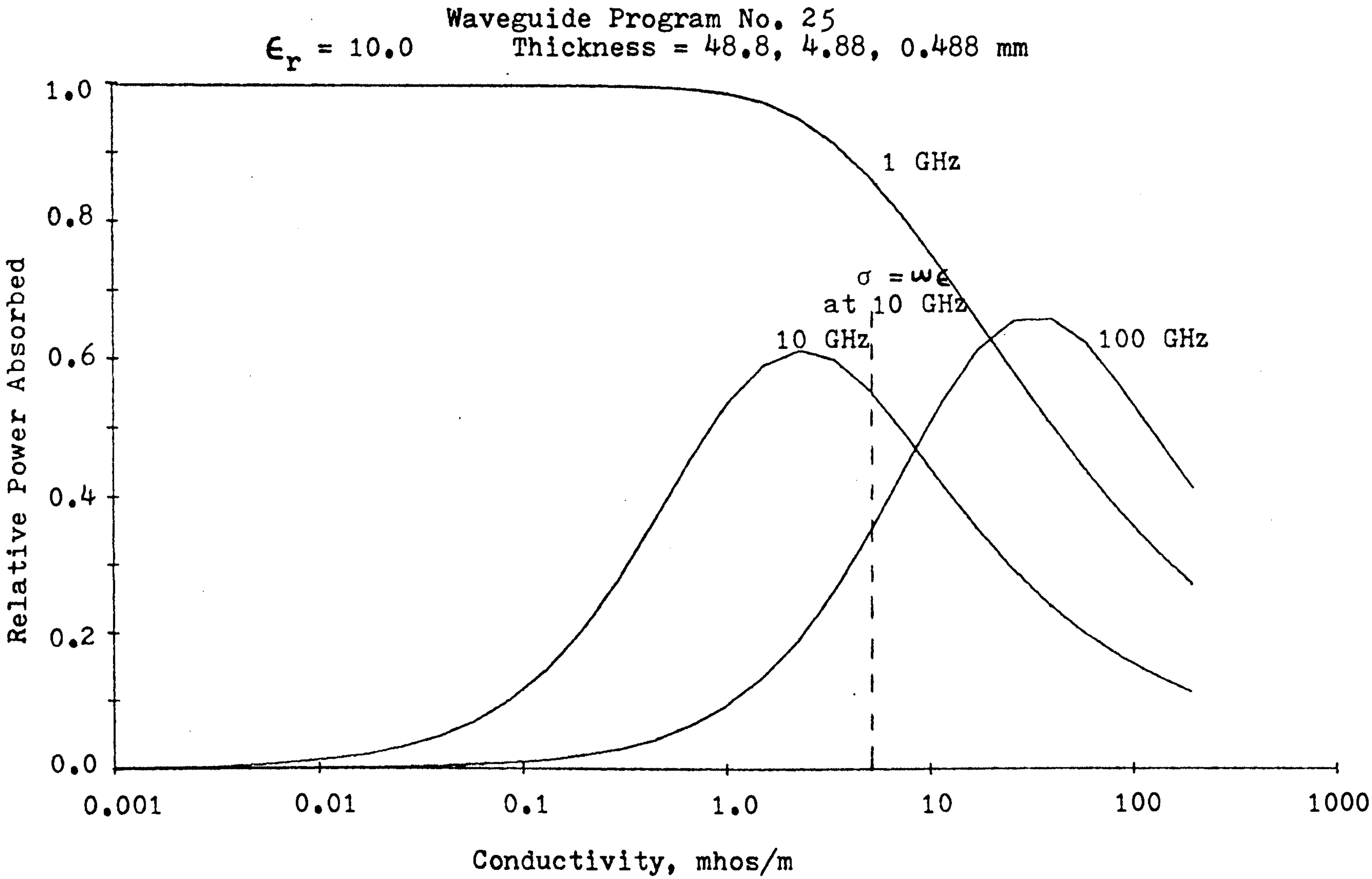

FIGURE 5.1c. Relative power absorbed versus conductivity for a dielectrically filled waveguide

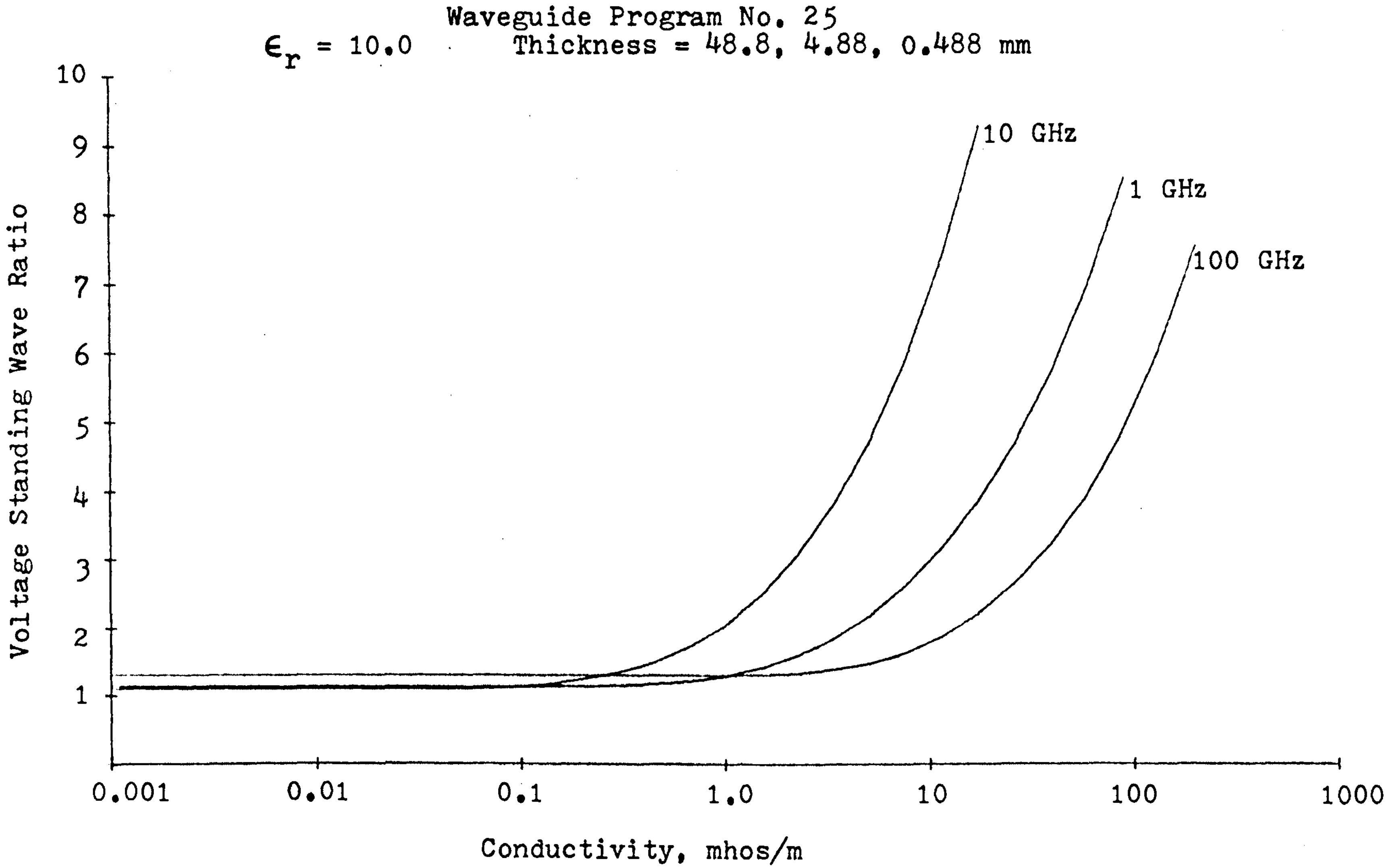

FIGURE 5.1d. Voltage standing wave ratio versus conductivity for a dielectrically filled waveguide

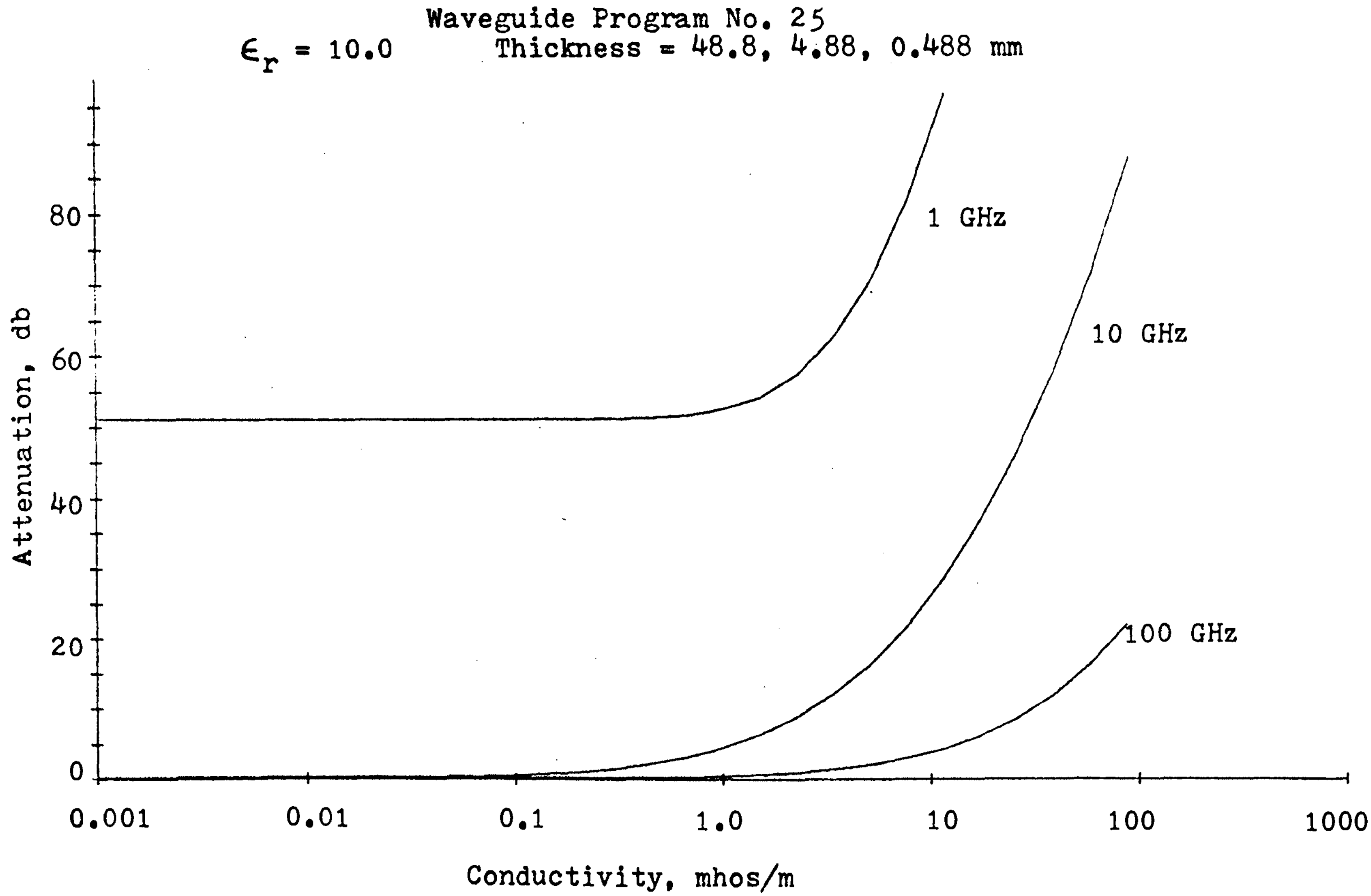

FIGURE 5.1e. Attenuation of transmitted wave versus conductivity for a dielectrically filled waveguide

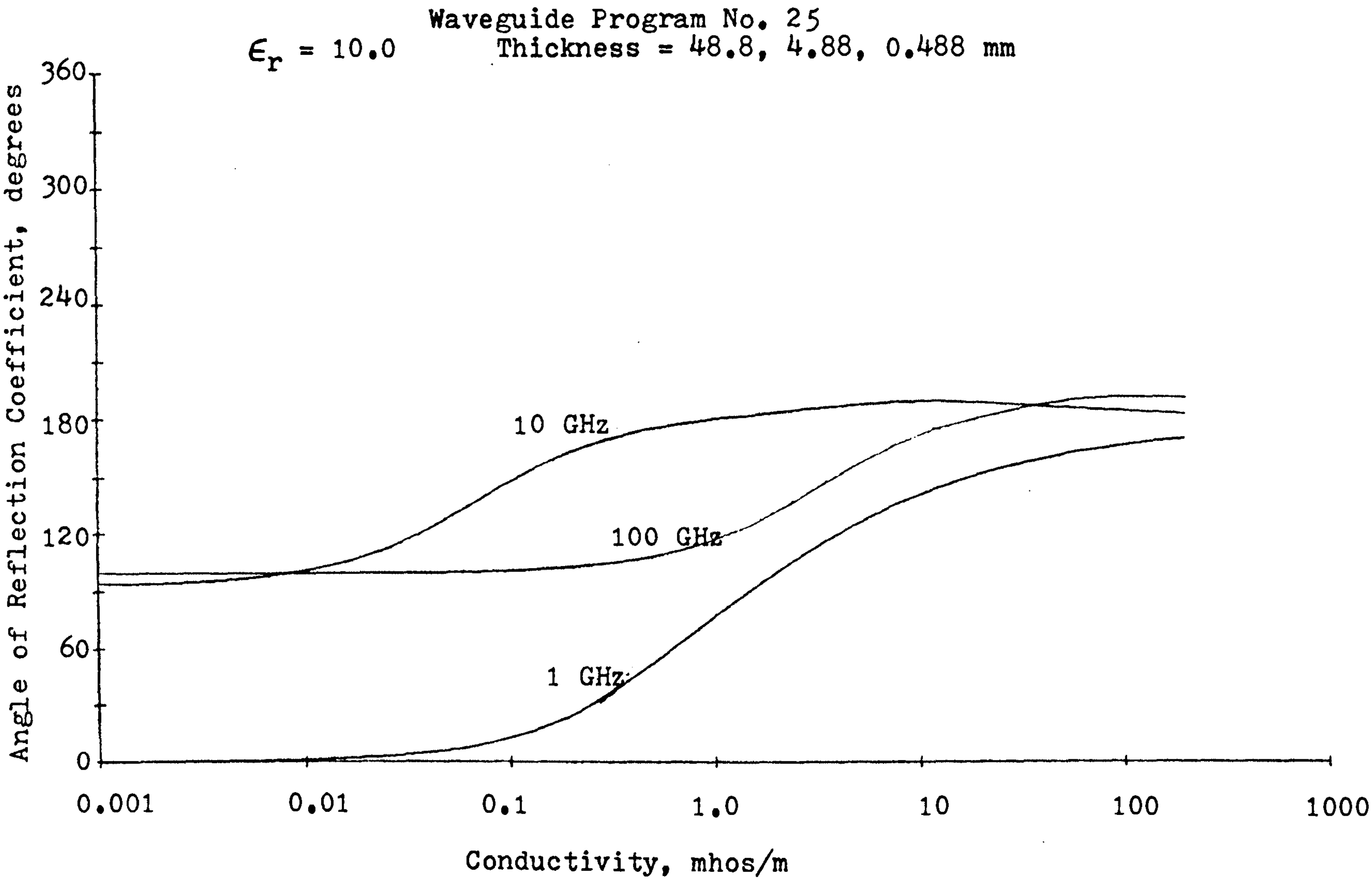

FIGURE 5.1f. Angle of reflection coefficient versus conductivity for a dielectrically filled waveguide

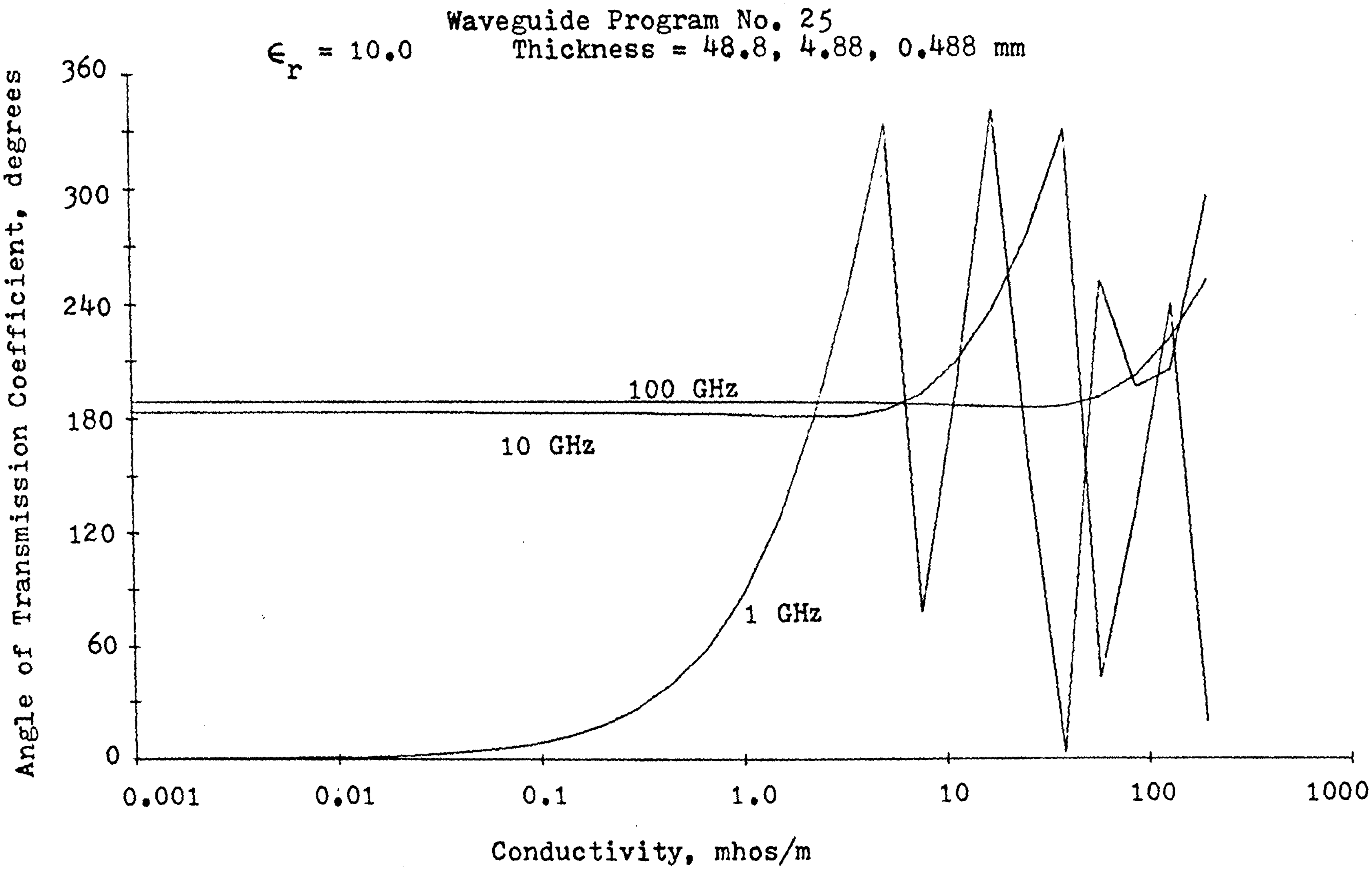

FIGURE 5.1g. Angle of transmission coefficient versus conductivity for a dielectrically filled waveguide

corresponding to $\sigma = \omega\epsilon$ determines the center of the conductivity range about which the different power variations occur. The important point to note is that very little change in microwave power is produced unless the conductivity is varied over a specific, limited range. This range varies with frequency, dielectric constant, sample thickness, and guide dimensions. The possibility of limited phase modulation is indicated in Figures 5.1f and 5.1g. The 1 GHz curve does not follow the normal pattern because this frequency is below the cutoff frequency of the dielectrically filled guide ($f_c = 2.08$ GHz). For frequencies well above cutoff ($f > 2f_c$), the curves shift to the left as the frequency is reduced. As the cutoff frequency is approached the curves shift back to the right as shown in Figure 5.2. The peculiar shape of the 2 GHz and 4 GHz curves is caused by the variation in impedance matching with changing conductivity. These curves illustrate an important practical point. The range of conductivity that can be measured by a test setup consisting of one size of waveguide can be greatly increased by operating the sample filled portion of the waveguide both above and below cutoff, while always operating the remainder of the waveguide above cutoff. This would require that the waveguide be filled with a lossless dielectric of higher dielectric constant than that of the sample. For example, to measure conductivities near 100 mhos/m, dielectrically filled K-band (18.0 GHz to 26.5 GHz) waveguide operating around 3 GHz could be used instead

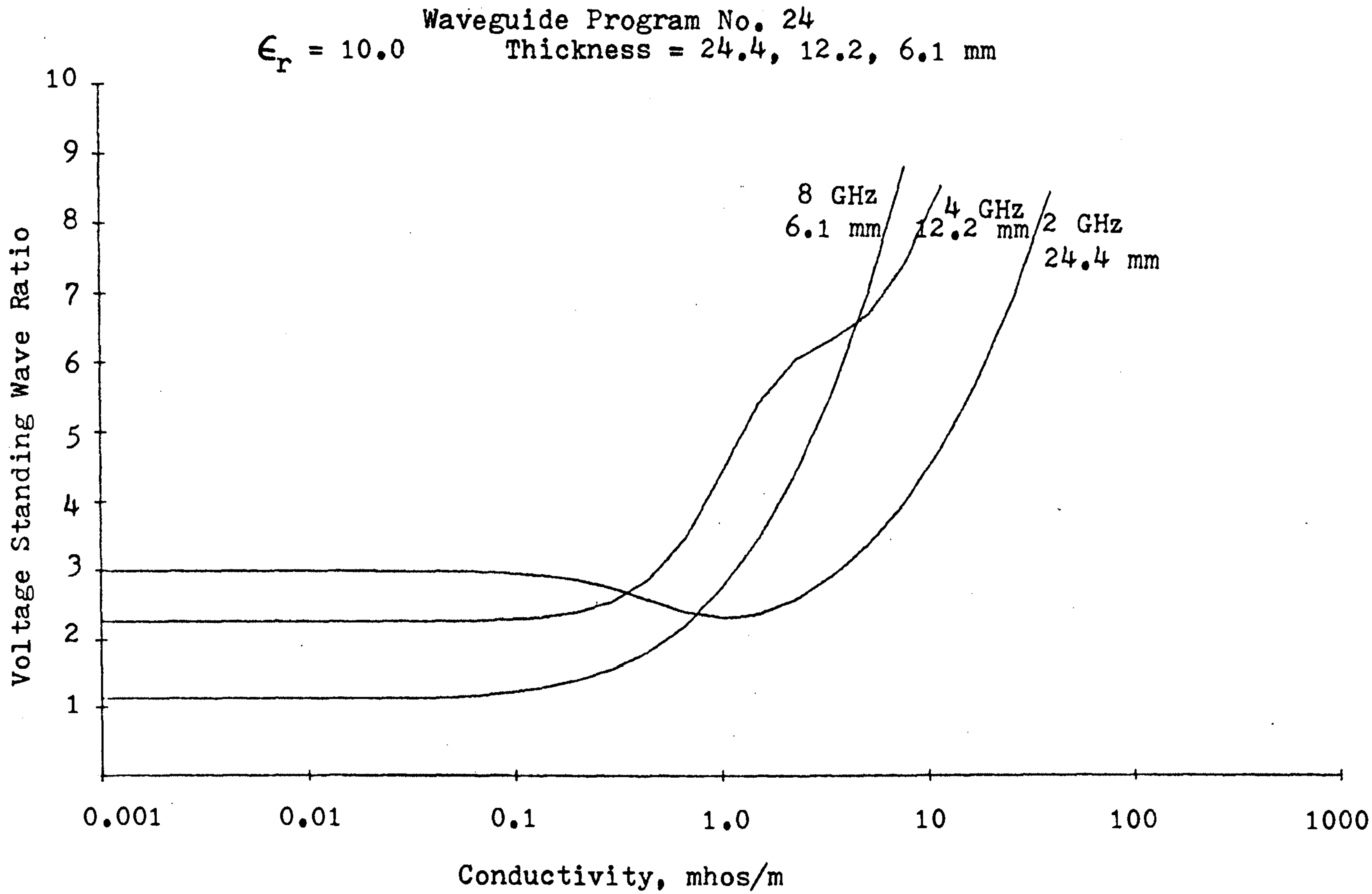

FIGURE 5.2. Voltage standing wave ratio versus conductivity for a dielectrically filled waveguide.

of the extremely small air filled waveguide required at 100 GHz.

Part of the results for microwave propagation through a lossy, semi-infinite slab in free space is shown in Figures 5.3a through 5.3d. The 10 GHz and 100 GHz curves correspond almost exactly to the curves from the waveguide example. This is as expected since in the waveguide example both frequencies are well above cutoff and the dielectric constant is high, hence, the size of the waveguide has only a minor influence on the curves. The difference in the position of the 1 GHz curve for the free space and waveguide examples is also evident. For TE polarization, the effect of increasing the angle of incidence shifts all curves in Figure 5.3 slightly to the left.

Figures 5.4a and 5.4b illustrate the variation in VSWR and attenuation with conductivity for a thin Si wafer placed transverse to the direction of propagation in rectangular, X-band waveguide. The use of such calculated data in conjunction with experimental VSWR measurements has resulted in the accurate determination of the conductivity of various Si samples by the author. This measurement technique could be easily adapted to large scale, automatic operation. This subject is discussed in more detail in Chapter VII.

2. VSWR Versus Sample Thickness

Figures 5.5a through 5.5f show the effect of varying

Single Layer Program No. 7 $\epsilon_r = 10.0$
Angle of Incidence = 0° Thickness = 47.5, 4.75, 0.475 mm

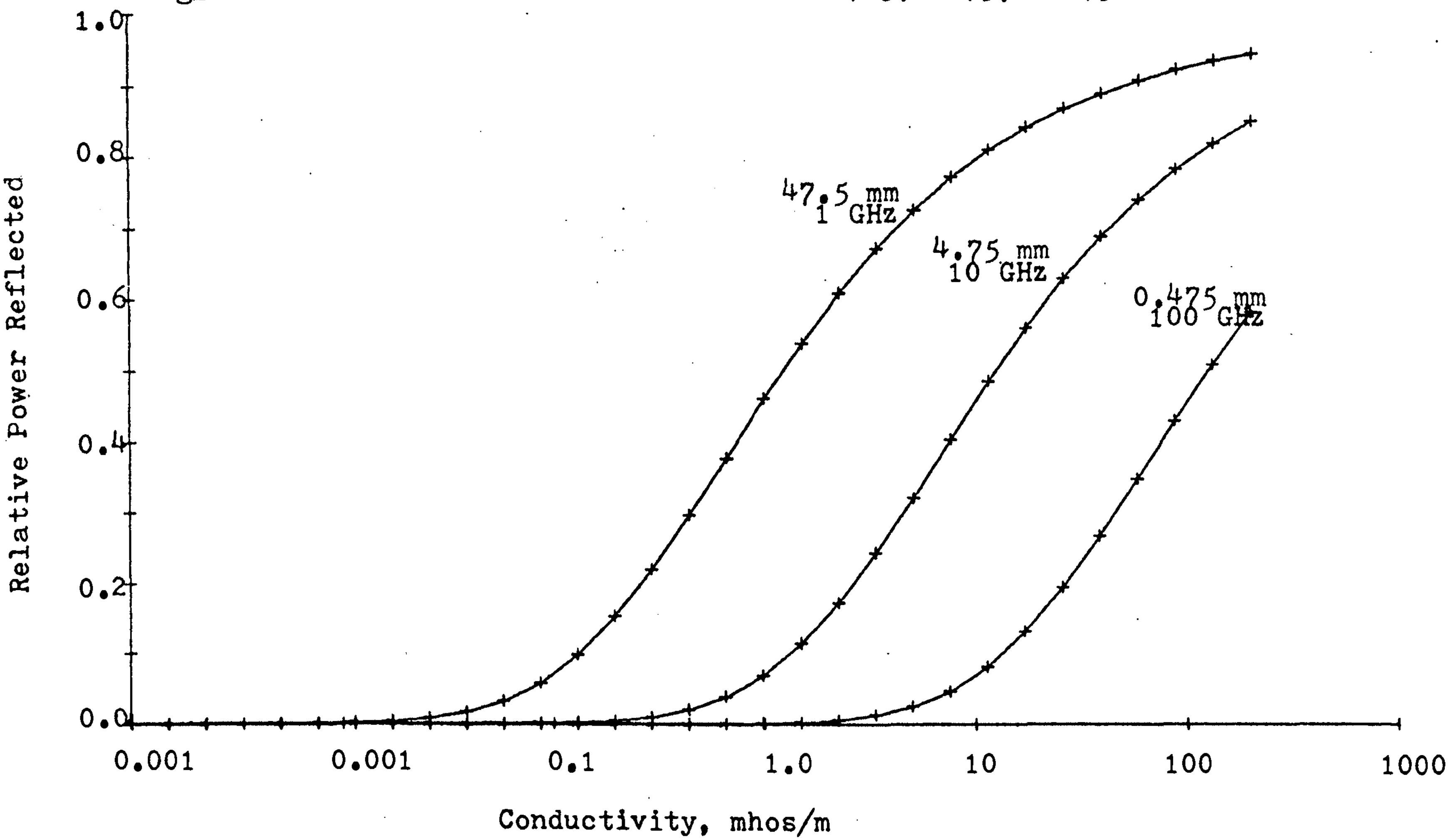

FIGURE 5.3a. Relative power reflected versus conductivity for a semi-infinite slab in free space

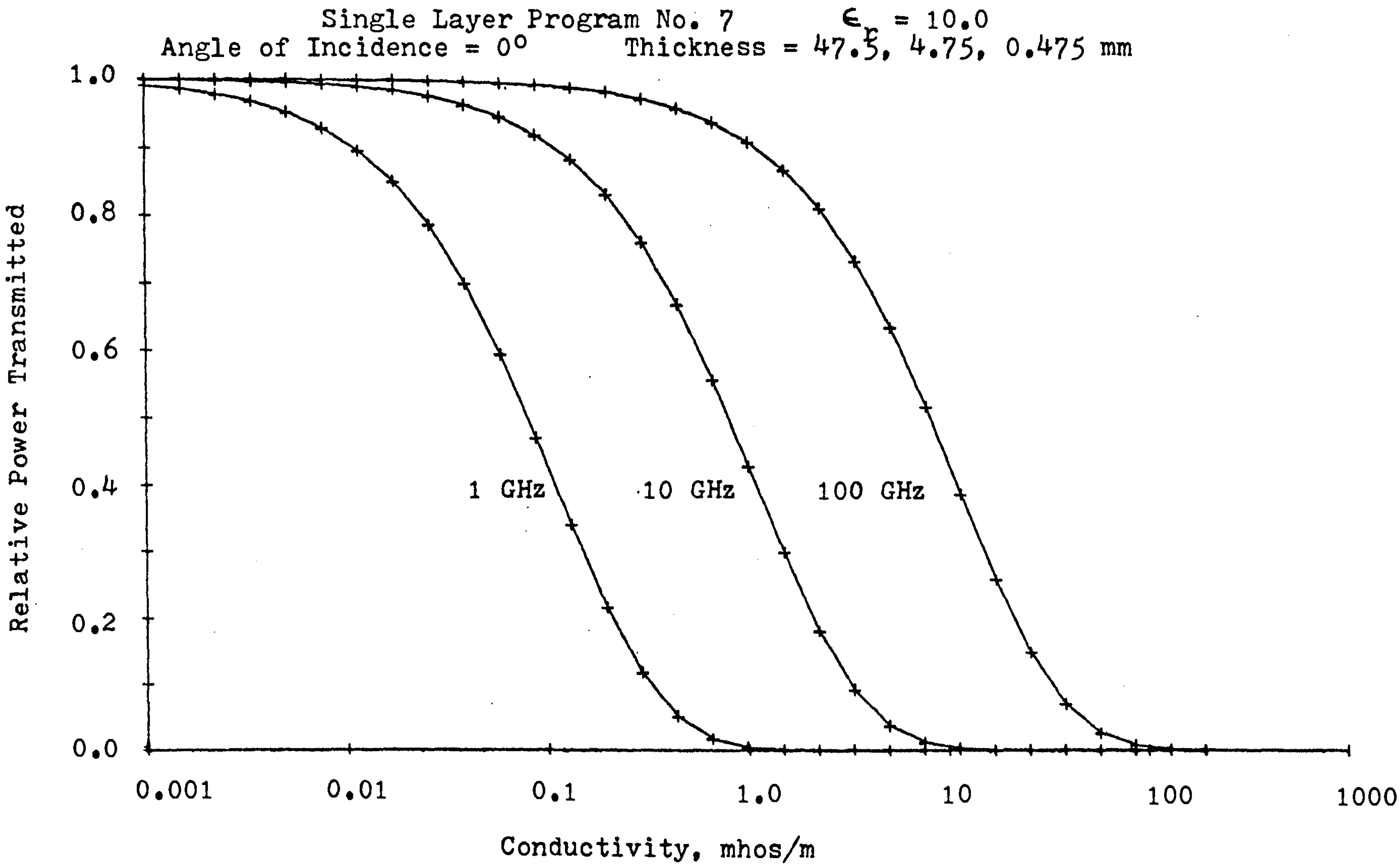

FIGURE 5.3b. Relative power transmitted versus conductivity for a semi-infinite slab in free space

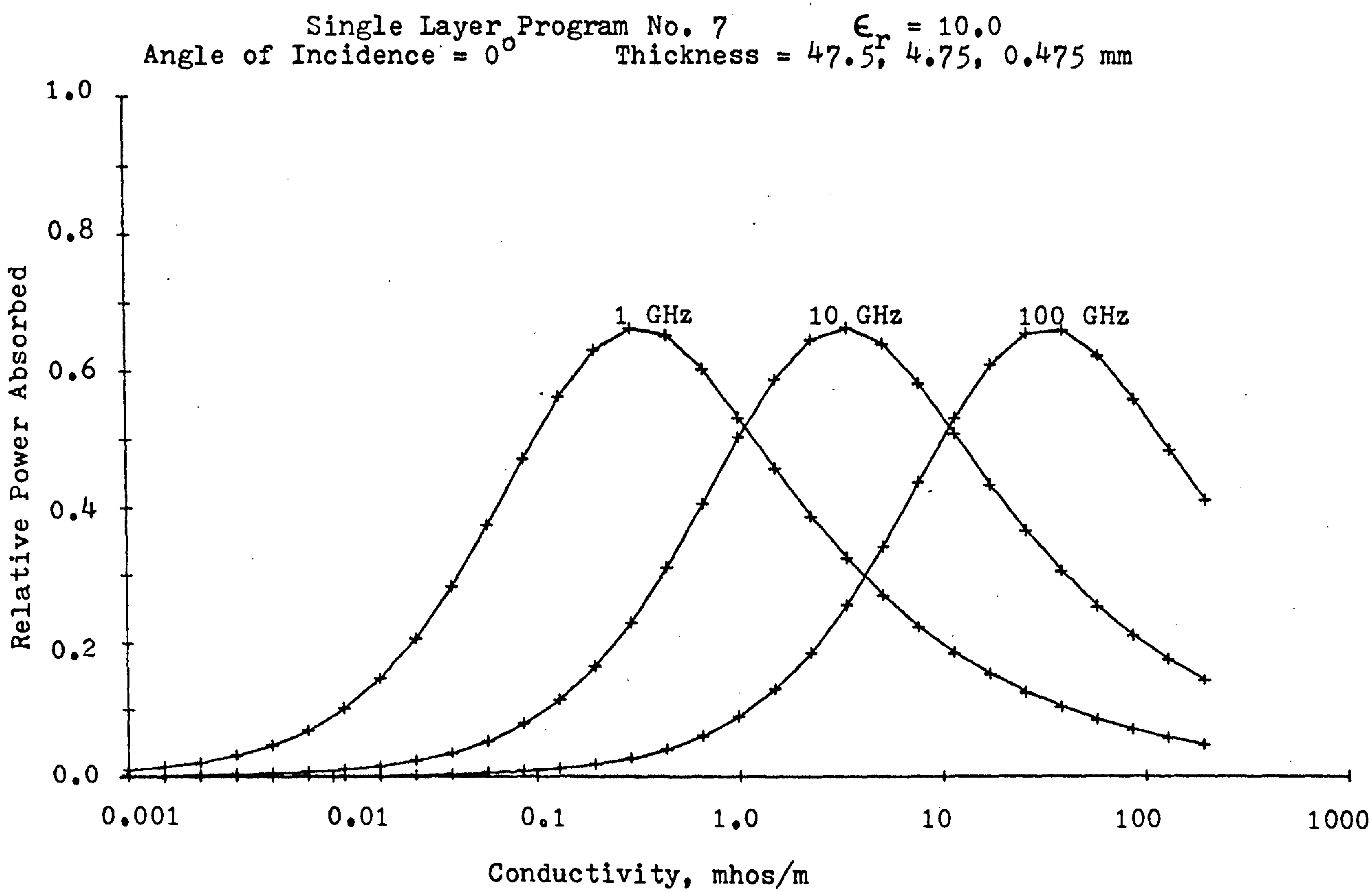

FIGURE 5.3c. Relative power absorbed versus conductivity for a semi-infinite slab in free space

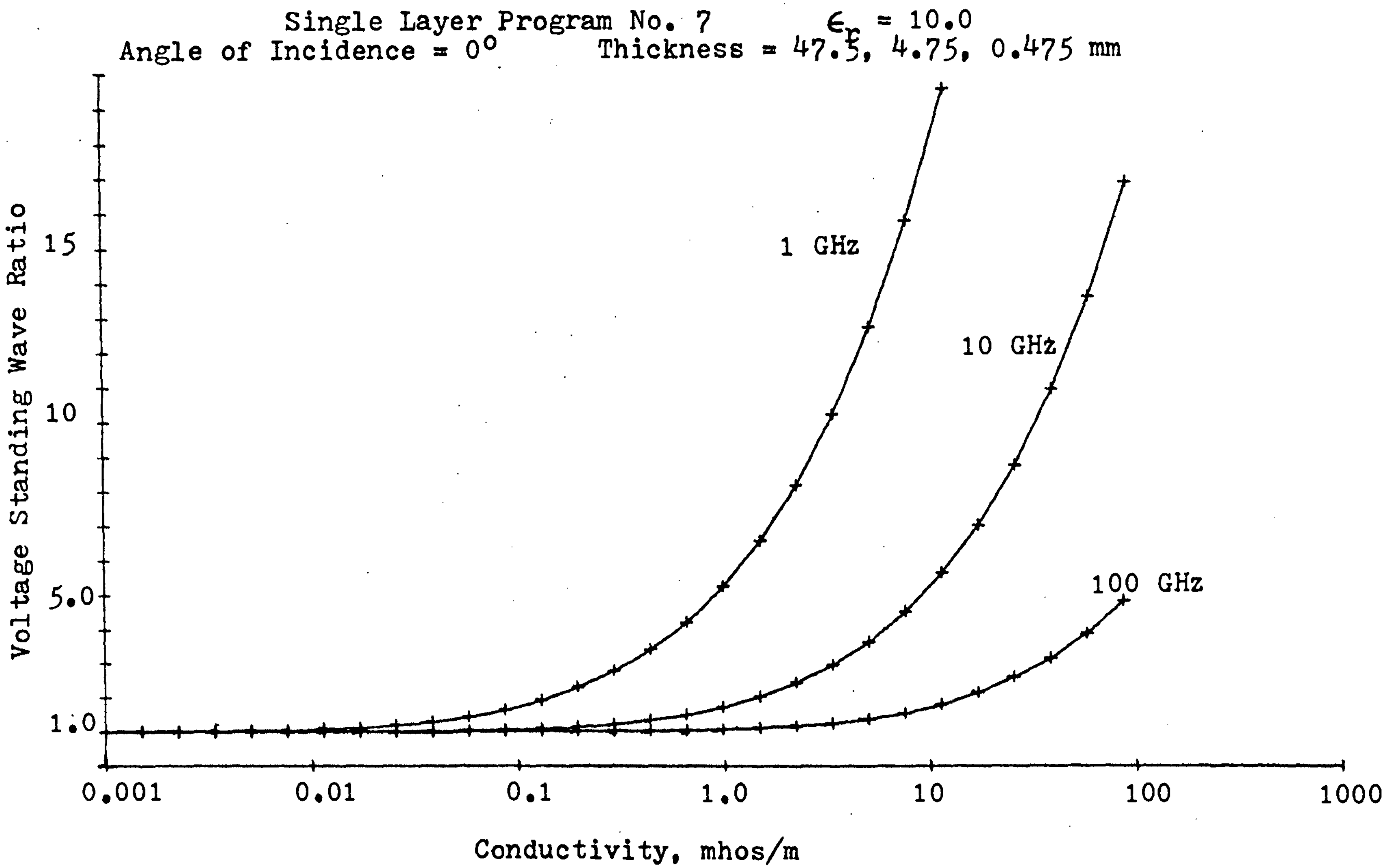

FIGURE 5.3d. Voltage standing wave ratio versus conductivity for a semi-infinite slab in free space

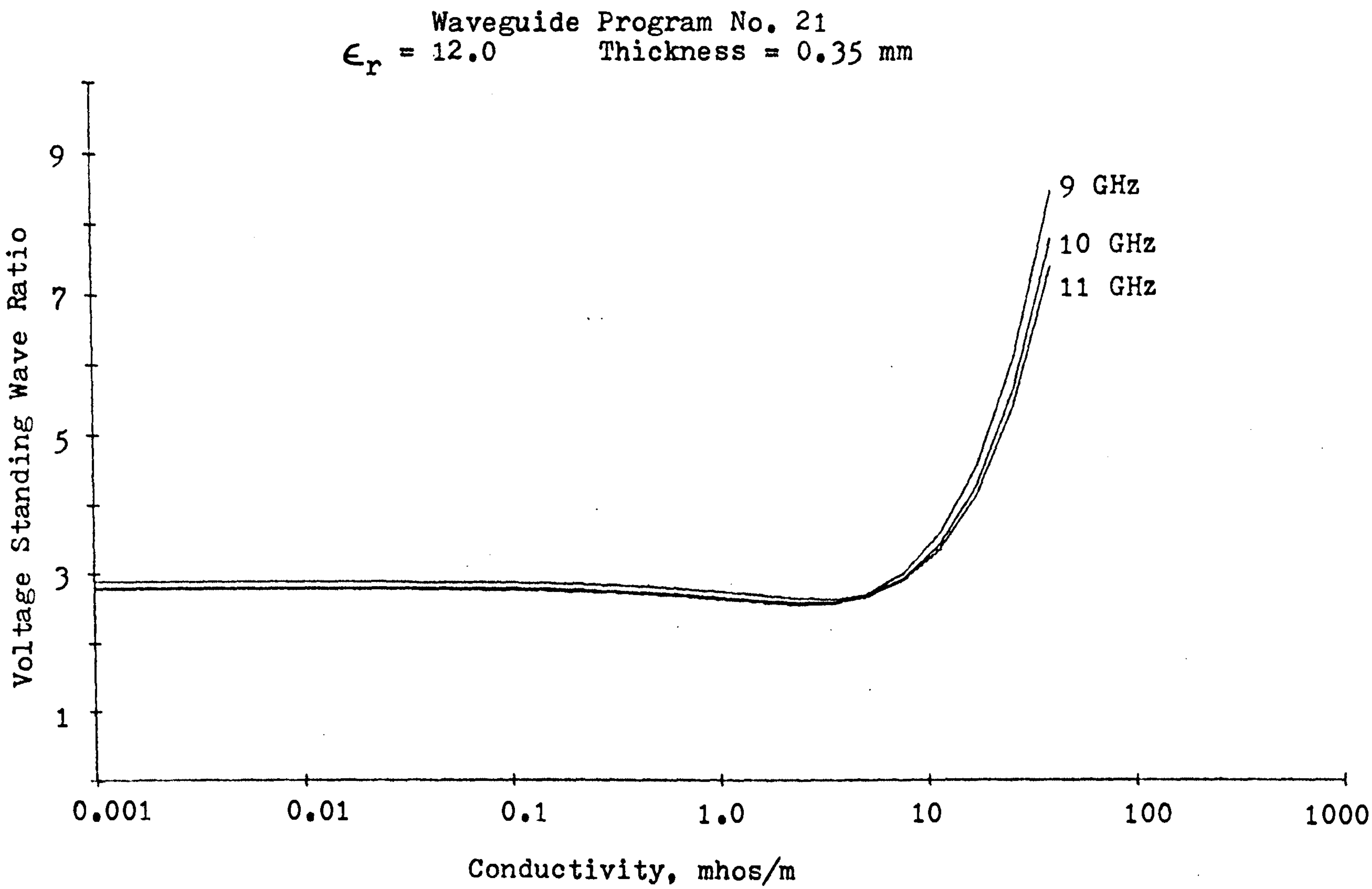

FIGURE 5.4a. Voltage standing wave ratio versus conductivity for a thin Si wafer inside a waveguide

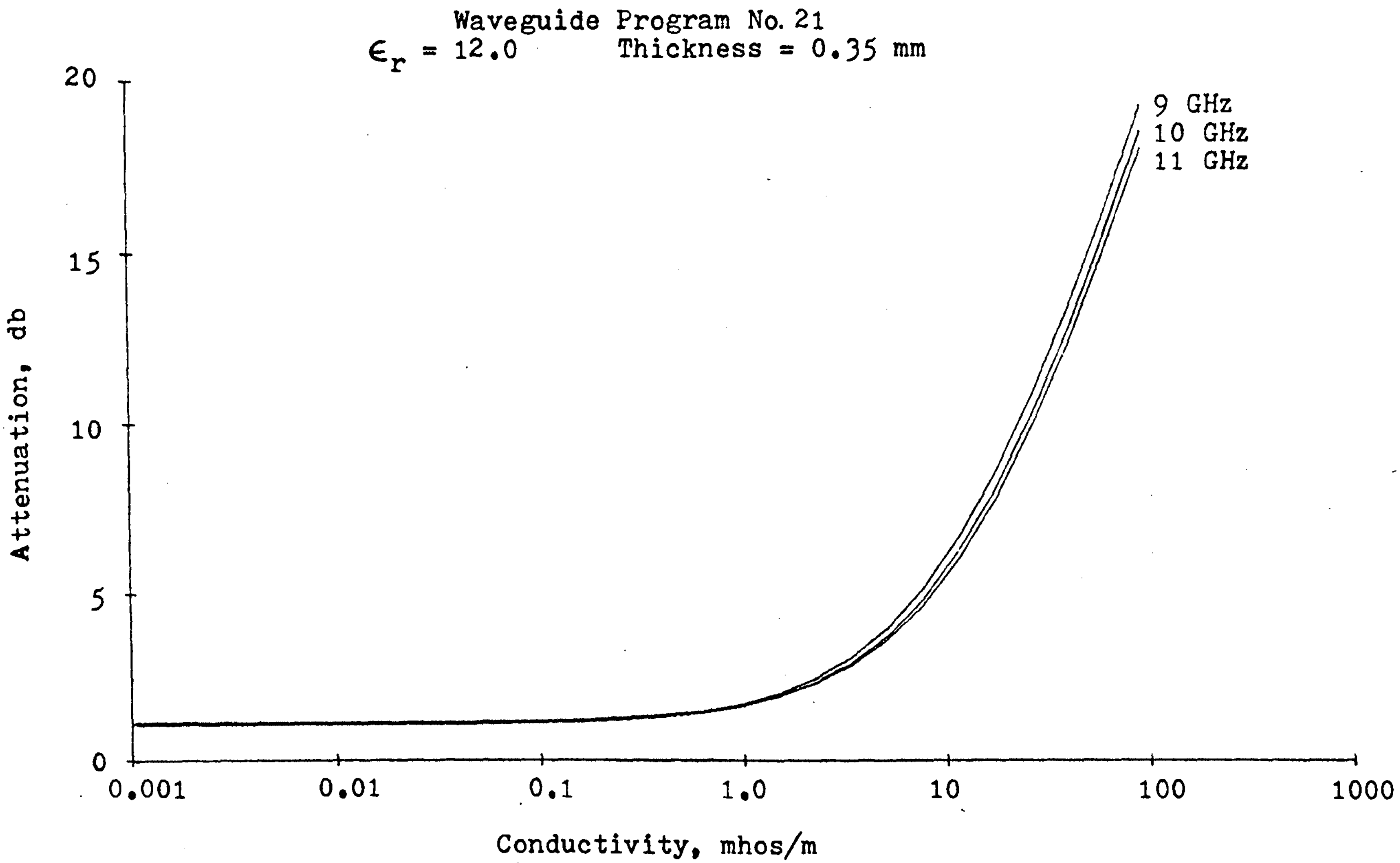

FIGURE 5.4b. Attenuation versus conductivity for a thin Si wafer inside a waveguide

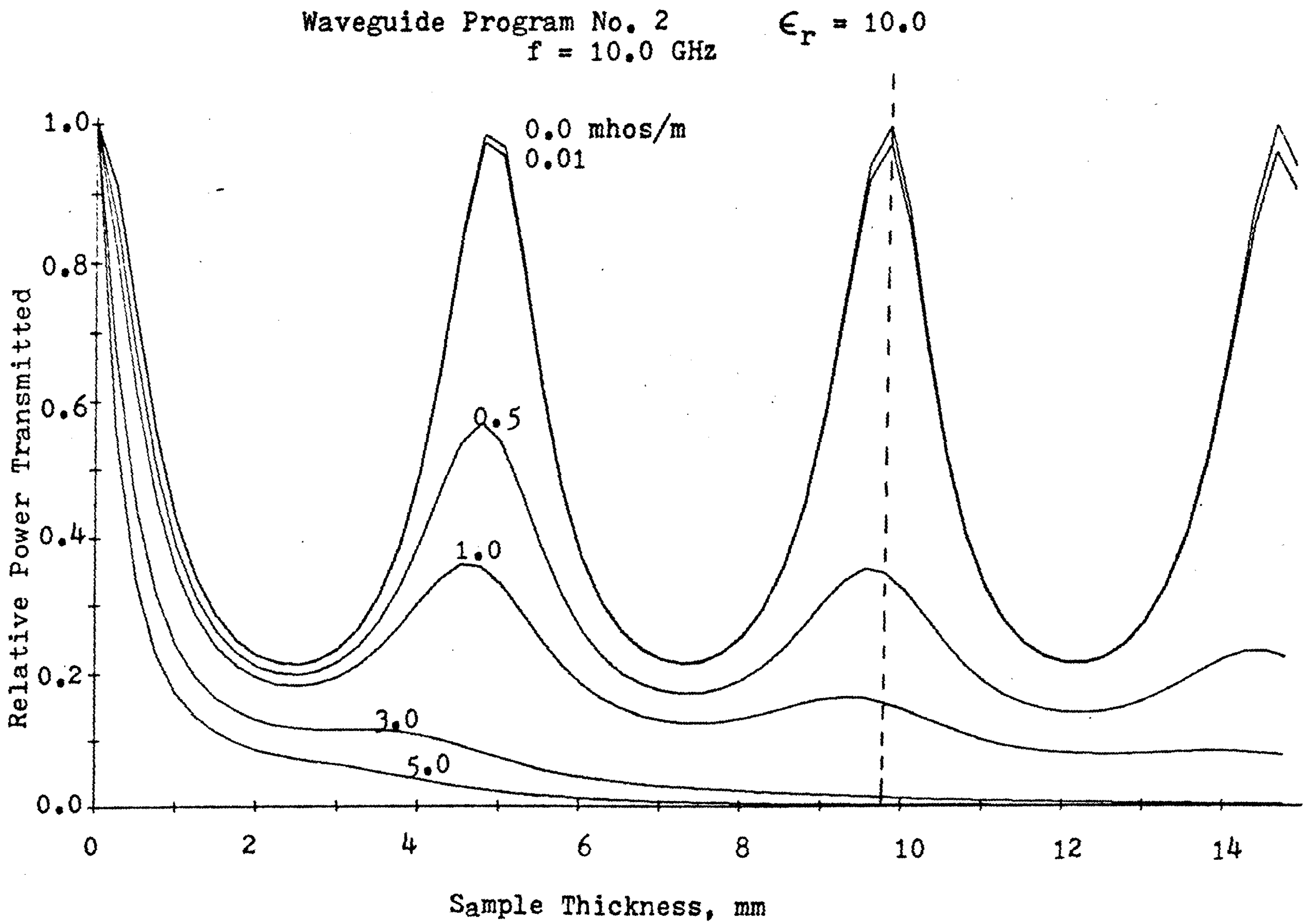

FIGURE 5.5a. Relative power transmitted versus sample thickness for a dielectrically filled waveguide

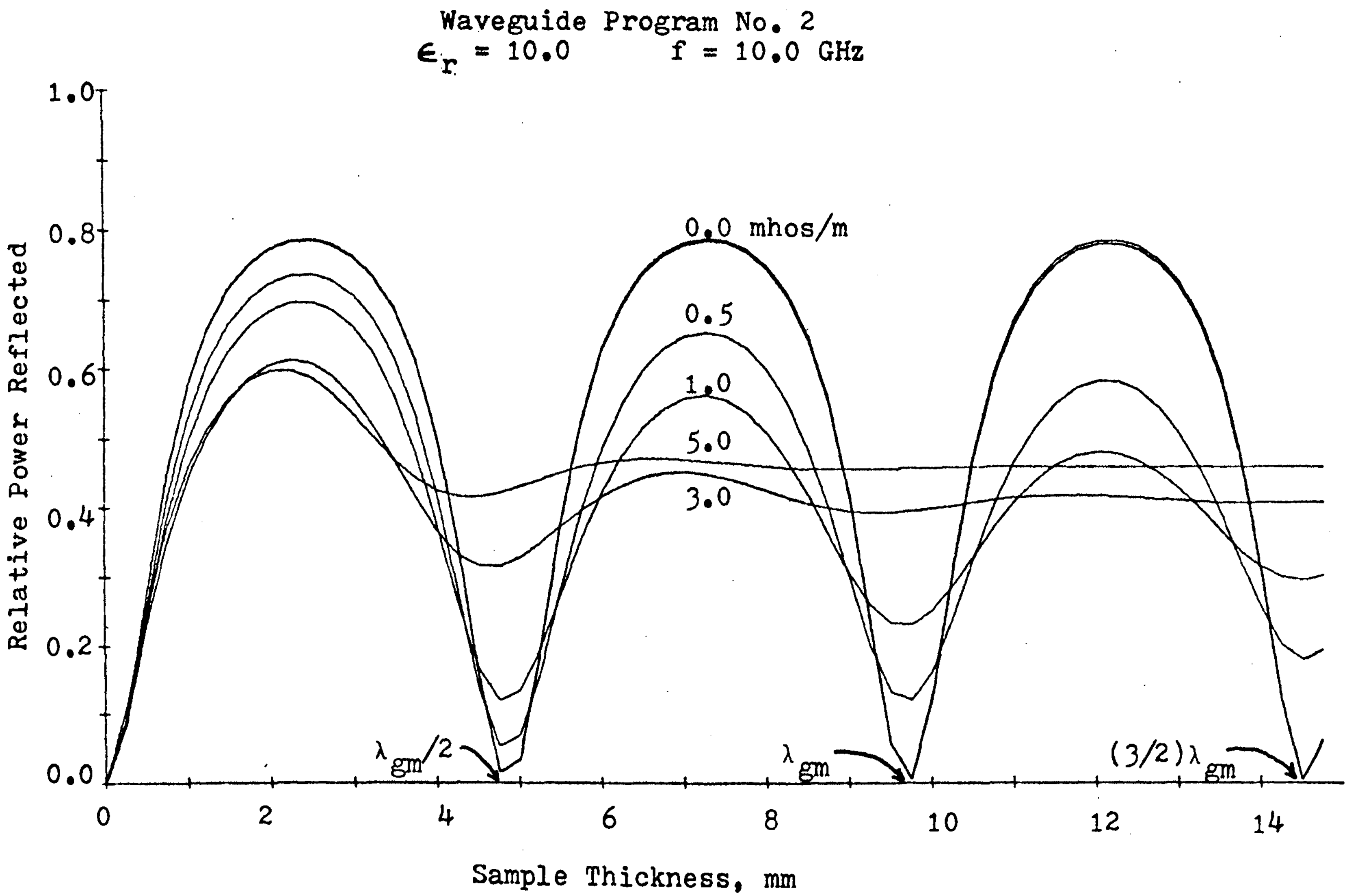

FIGURE 5.5b. Relative power reflected versus sample thickness for a dielectrically filled waveguide

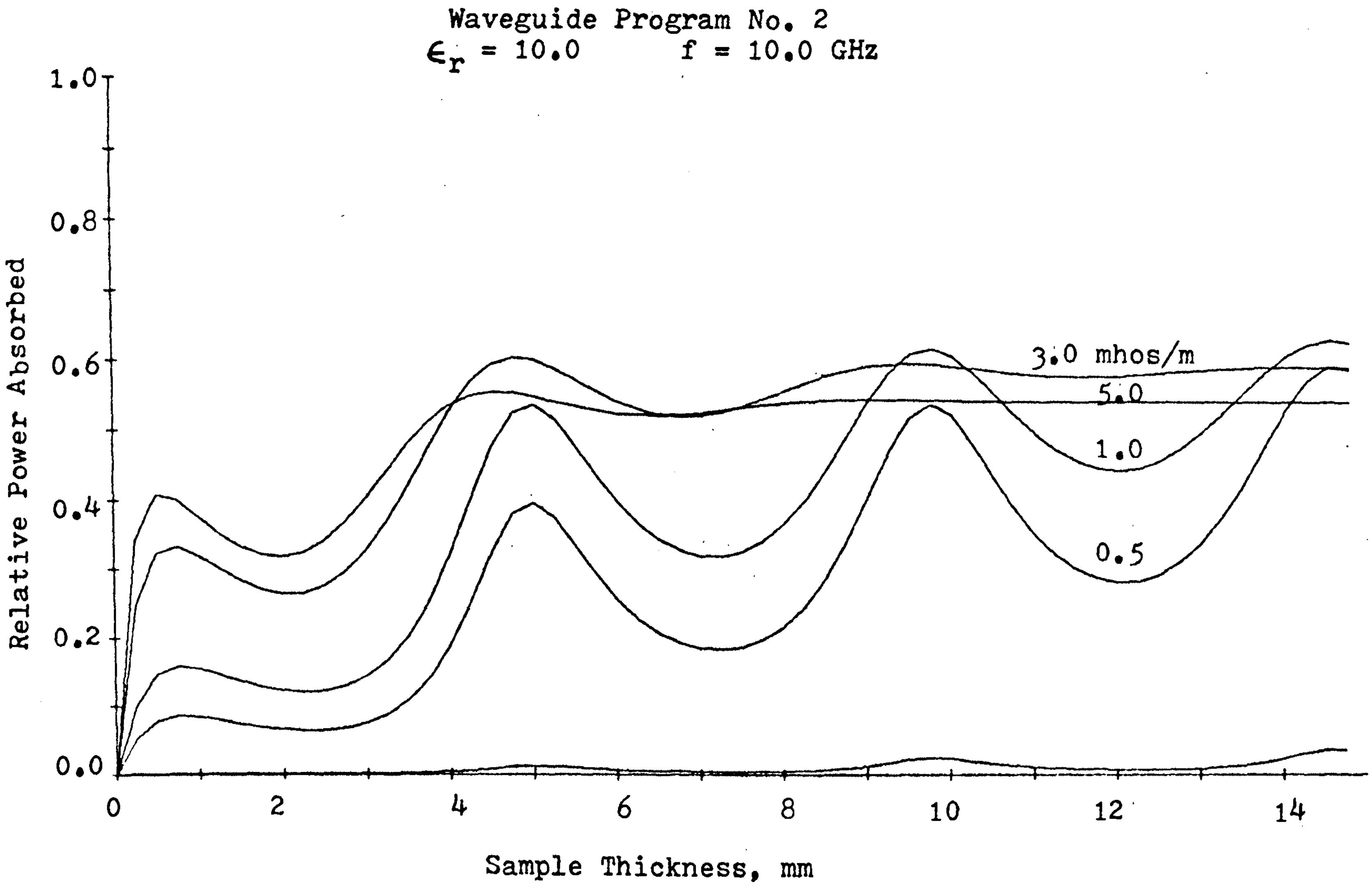

FIGURE 5.5c. Relative power absorbed versus sample thickness for a dielectrically filled waveguide

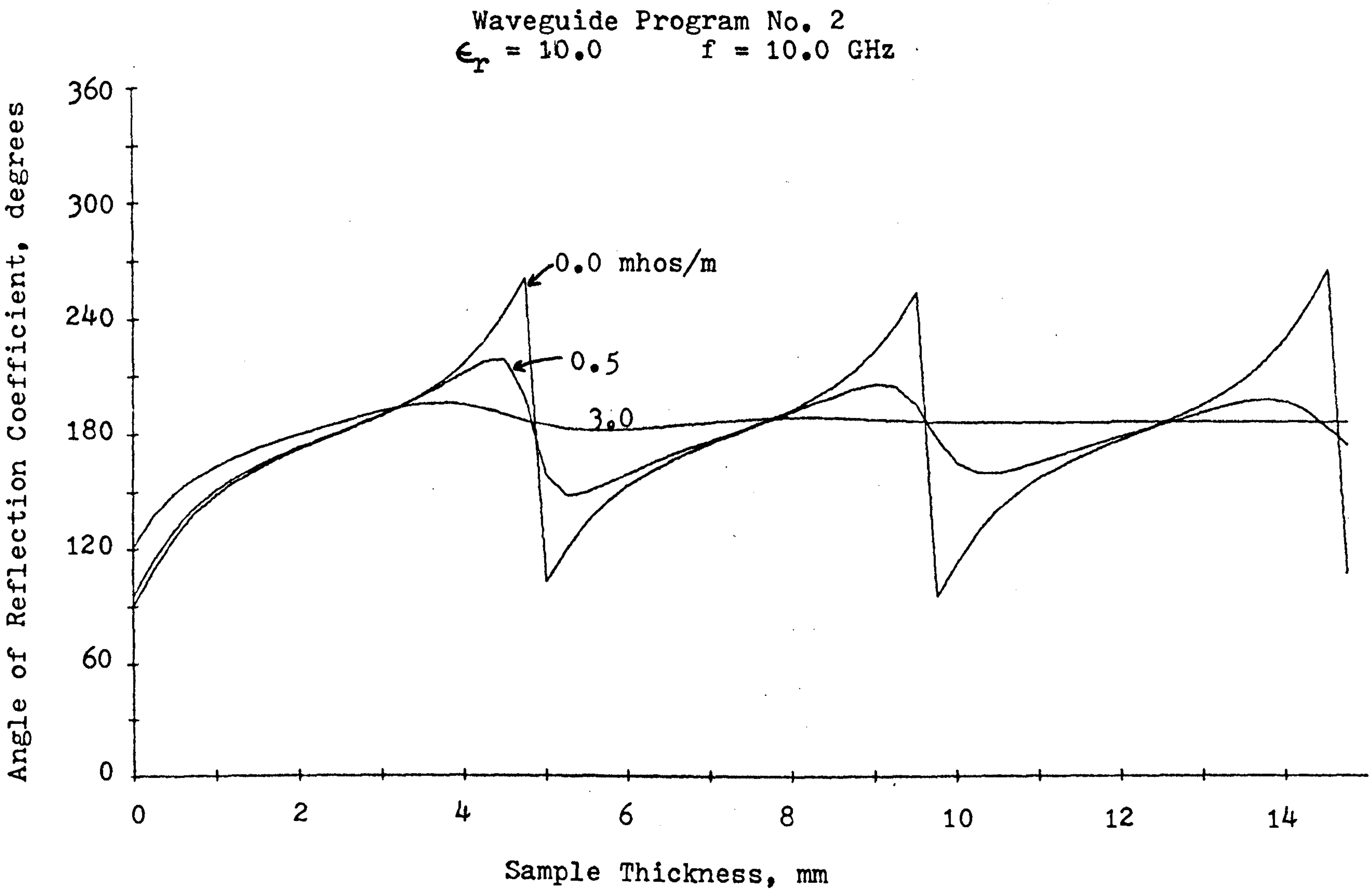

FIGURE 5.5d. Angle of reflection coefficient versus sample thickness for a dielectrically filled waveguide

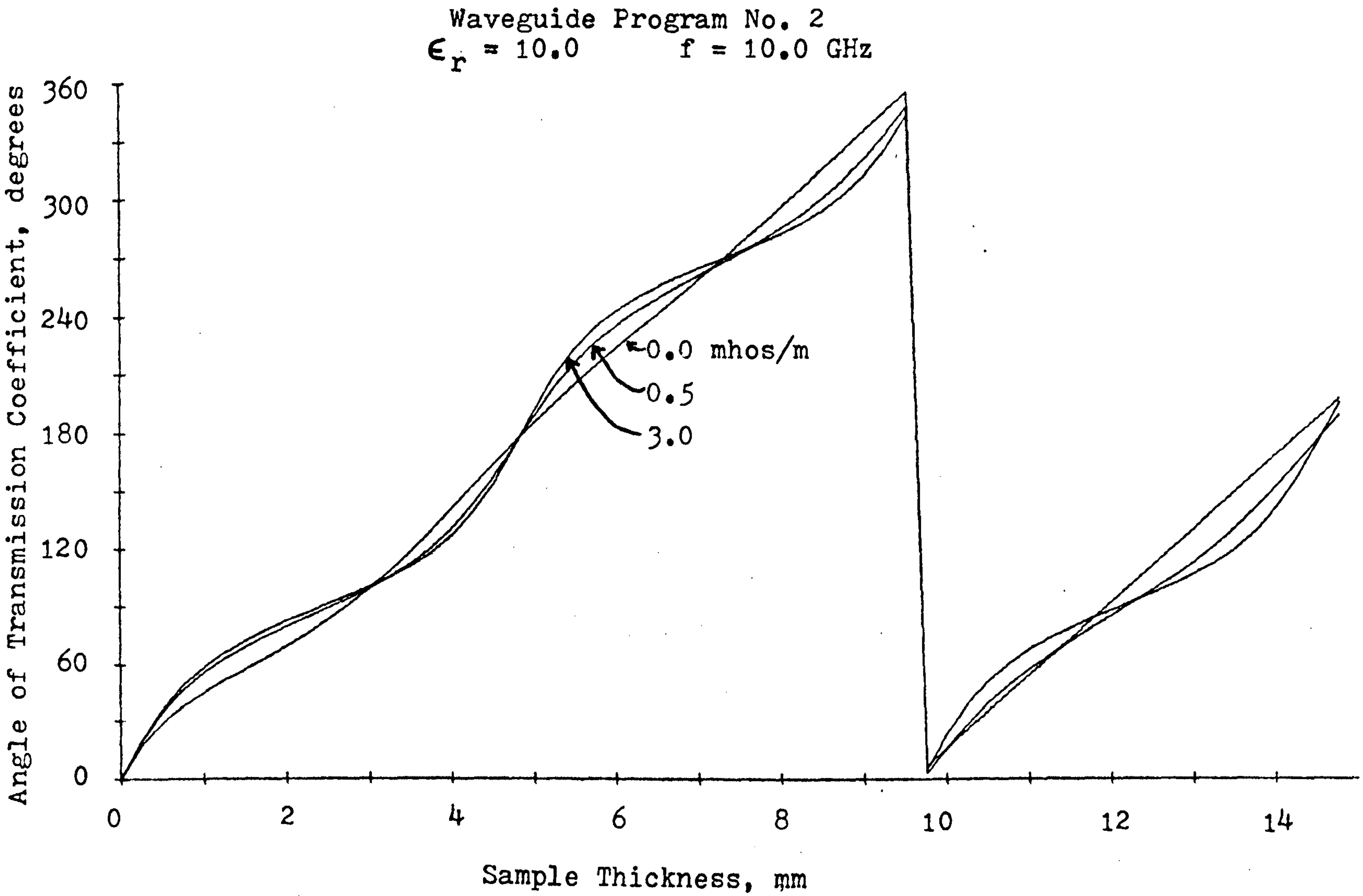

FIGURE 5.5e. Angle of transmission coefficient versus sample thickness for a dielectrically filled waveguide

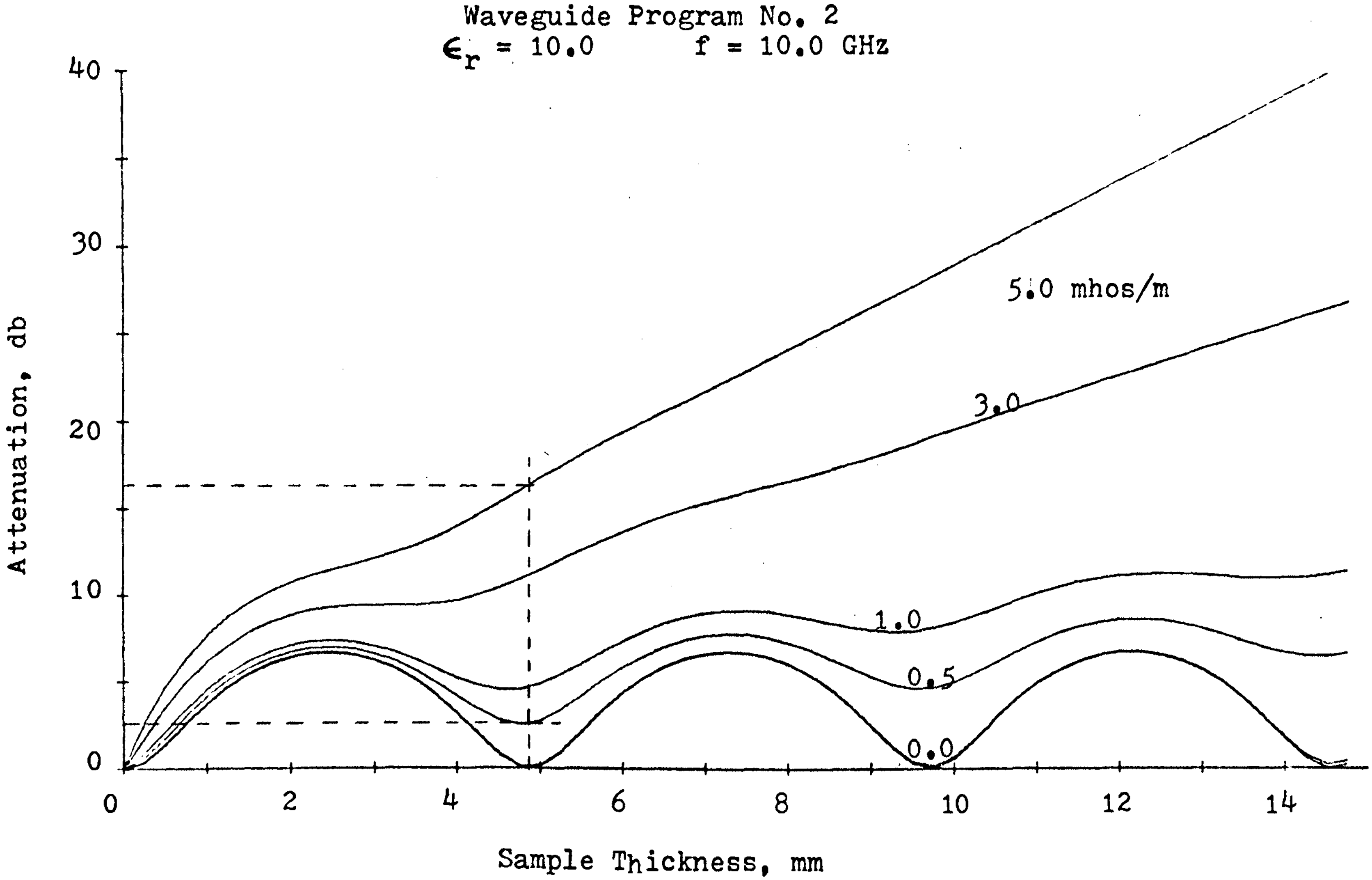

FIGURE 5.5f. Attenuation versus sample thickness for a dielectrically filled waveguide

sample thickness for different values of conductivity of a dielectrically filled waveguide. The $\sigma = 0.0$ mhos/m curve was compared with hand calculated results. This was one of several checks used to test the validity of the computer calculated data. Figure 5.5a indicates a slight shift of the transmitted power peaks to smaller sample thicknesses for increasing conductivity. Figure 5.5b indicates that the reflected power, and hence the VSWR, may either increase or decrease with increasing conductivity depending upon the sample thickness. Figures 5.5d and 5.5e can be used to determine the sample thicknesses at which changes in the angle of the reflection coefficient or the angle of the transmission coefficient with conductivity are a maximum. Finally, Figure 5.5f verifies the intuitive suspicion that changes in transmitted power with conductivity have a relative maximum at each sample thickness corresponding to approximately $N\lambda_{gm}/2$, where λ_{gm} is the guide wavelength in the lossless dielectric. For example, with a sample thickness of 4.88 mm and dark conductivity of 0.5 mhos/m the insertion loss is 2.5 db. For many photoconductive materials the conductivity can be easily increased by at least one order-of-magnitude. Assuming the conductivity is increased to 5.0 mhos/m, the insertion loss would increase to 17 db with a net change in transmitted power of 14.5 db.

Further theoretical investigation, stimulated by experimental observation, indicated that changes in the real part of the permittivity can also be a very effective means of modulating the reflected and transmitted powers as shown in Figures 5.6a through 5.6e. It was observed experimentally that in some cases the transmitted power increased with increasing light intensity. This can be explained either by a negative photoconductivity effect or a change in the dielectric constant. The possibility of negative photoconductivity was eliminated when it was found that for a given sample the transmitted power increased for some values of sample thickness and decreased for others, with increasing light intensity. Figures 5.6a and 5.6b easily explain such experimental observations. Assuming a small (10-20%) change in dielectric constant, the transmitted power may increase or decrease by as much as approximately 6 db depending upon the sample thickness. Figures 5.6d and 5.6e also indicate that more effective phase modulation can be produced by changes in dielectric constant than by changes in conductivity. Unfortunately, for most materials at microwave frequencies it is easier to change the conductivity by an order-of-magnitude than it is to change the dielectric constant by 10%. Note in Figure 5.6a that the effect of small changes in dielectric constant could be eliminated by the use of a 3.0 mm thick sample.

Figure 5.7 illustrates the change in power transmitted through a short section of dielectrically filled waveguide

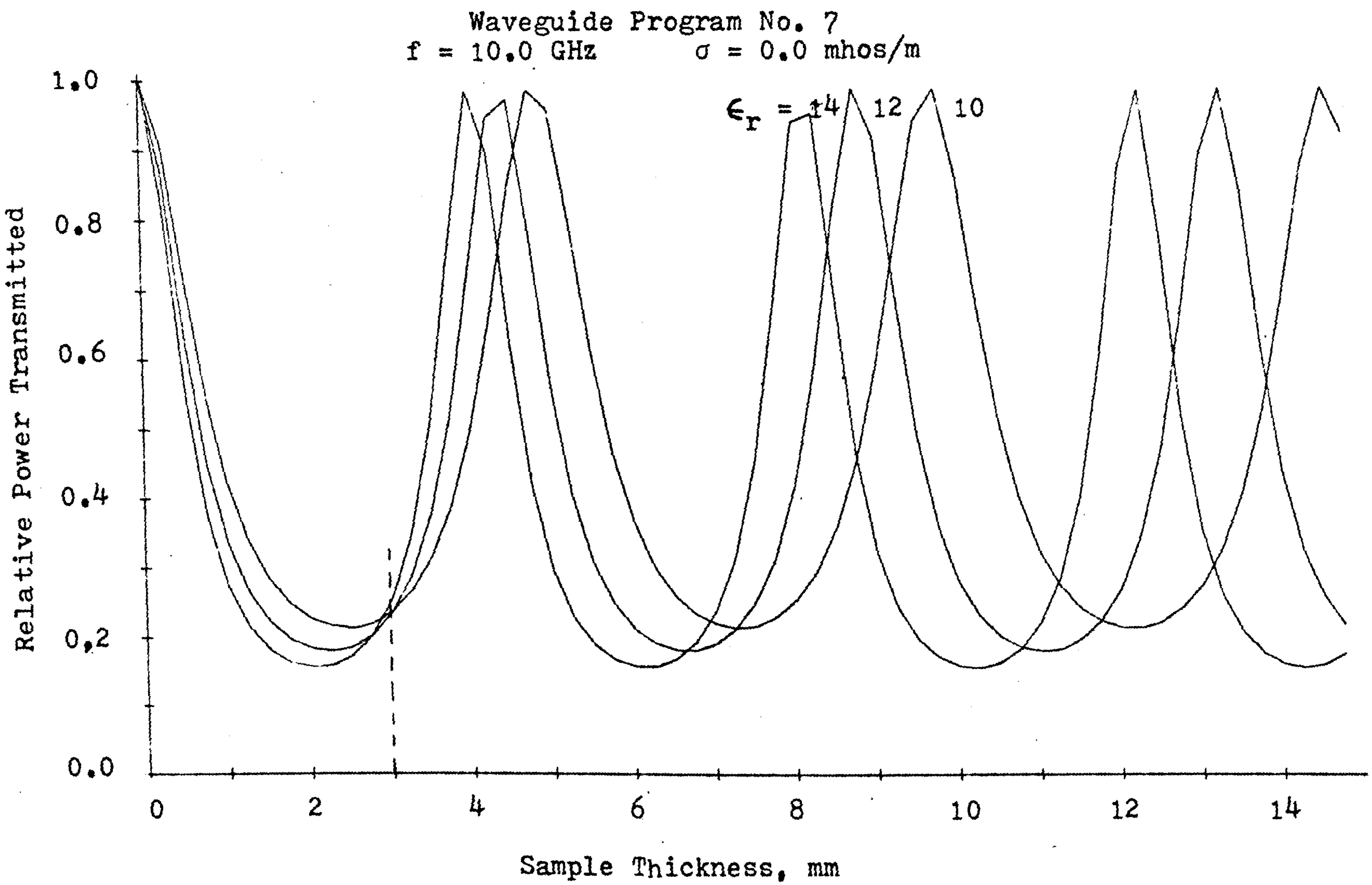

FIGURE 5.6a. Relative power transmitted versus sample thickness for a dielectrically filled waveguide

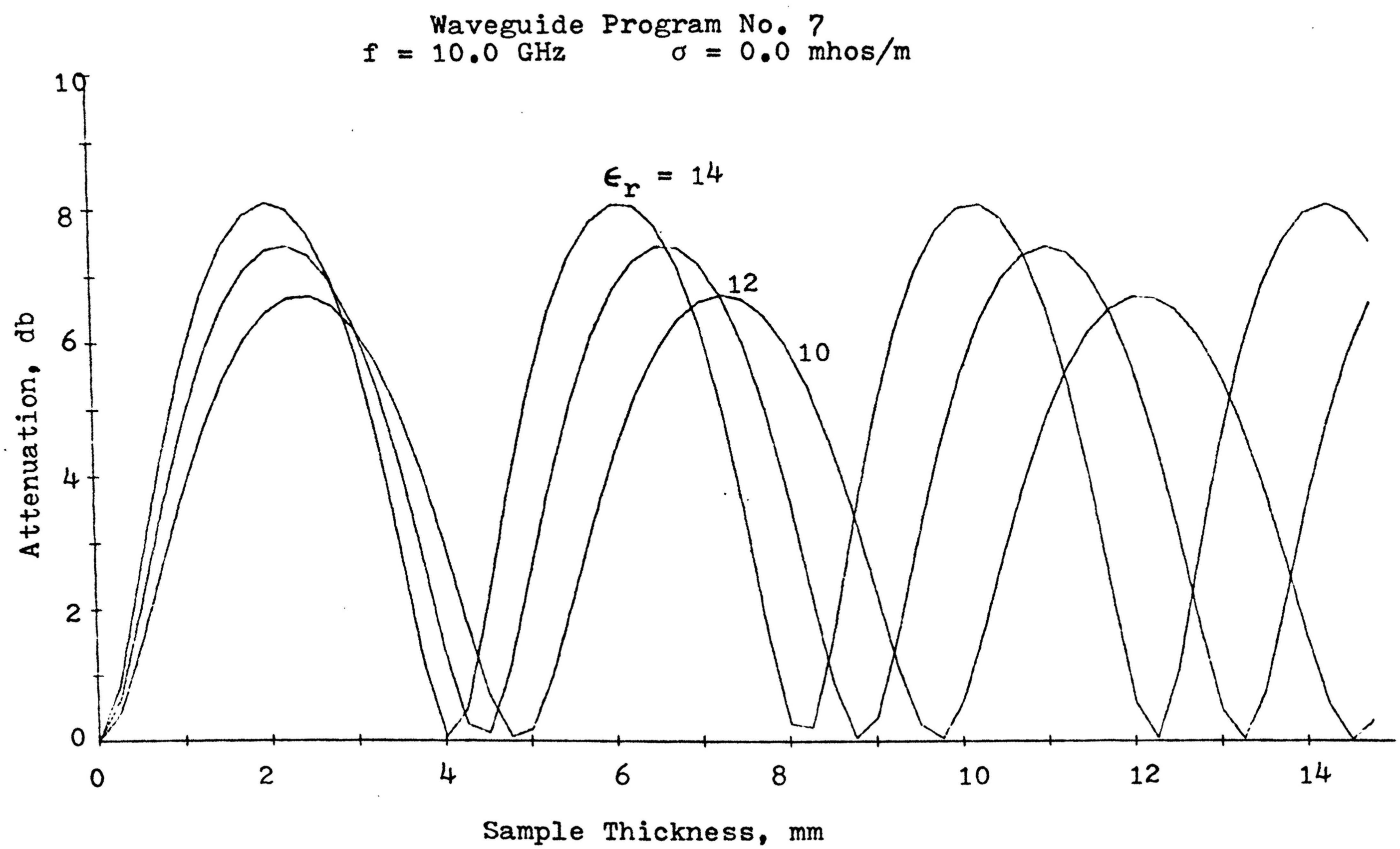

FIGURE 5.6b. Attenuation versus sample thickness for a dielectrically filled waveguide

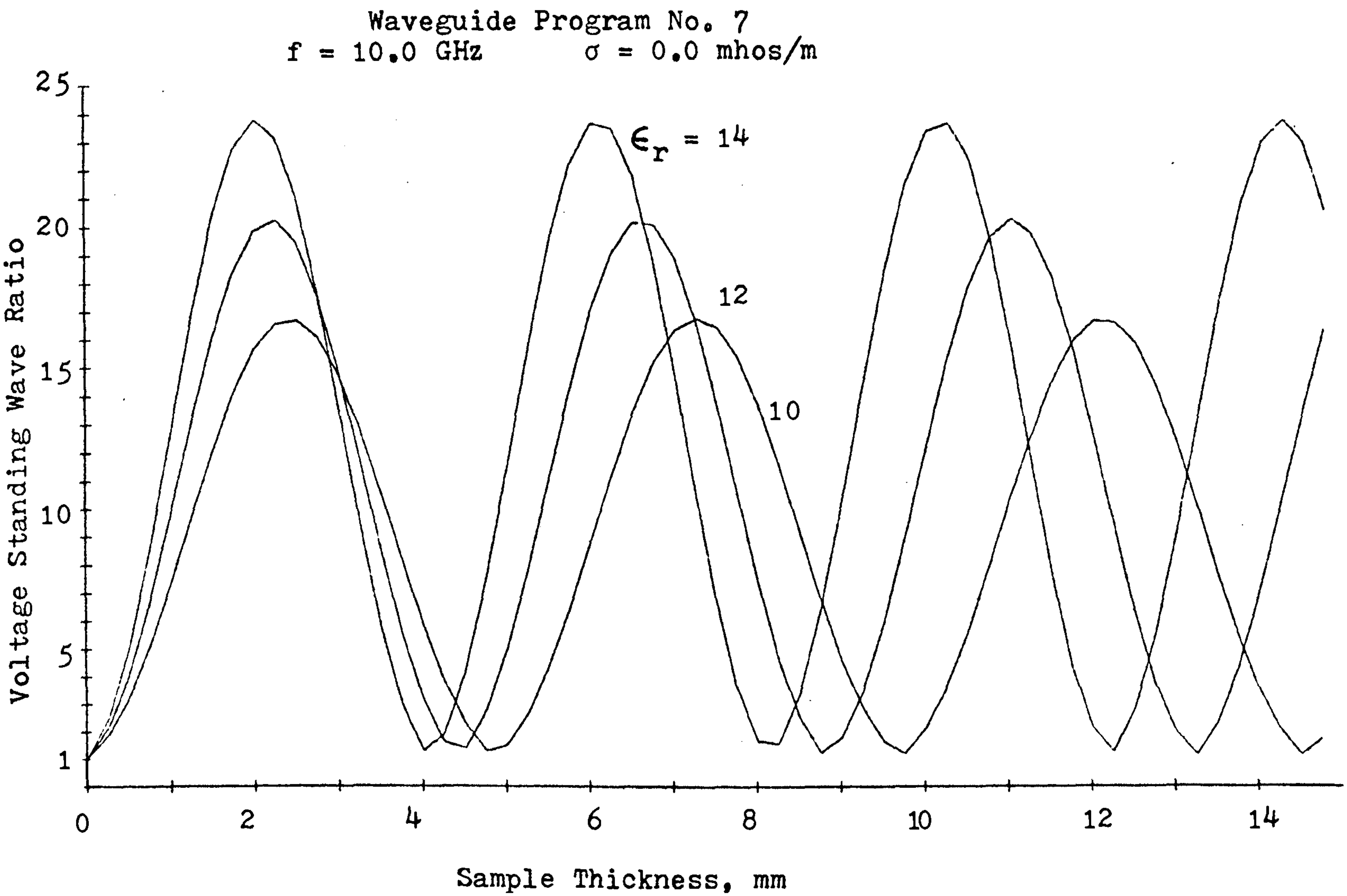

FIGURE 5.6c. Voltage standing wave ratio versus sample thickness for a dielectrically filled waveguide

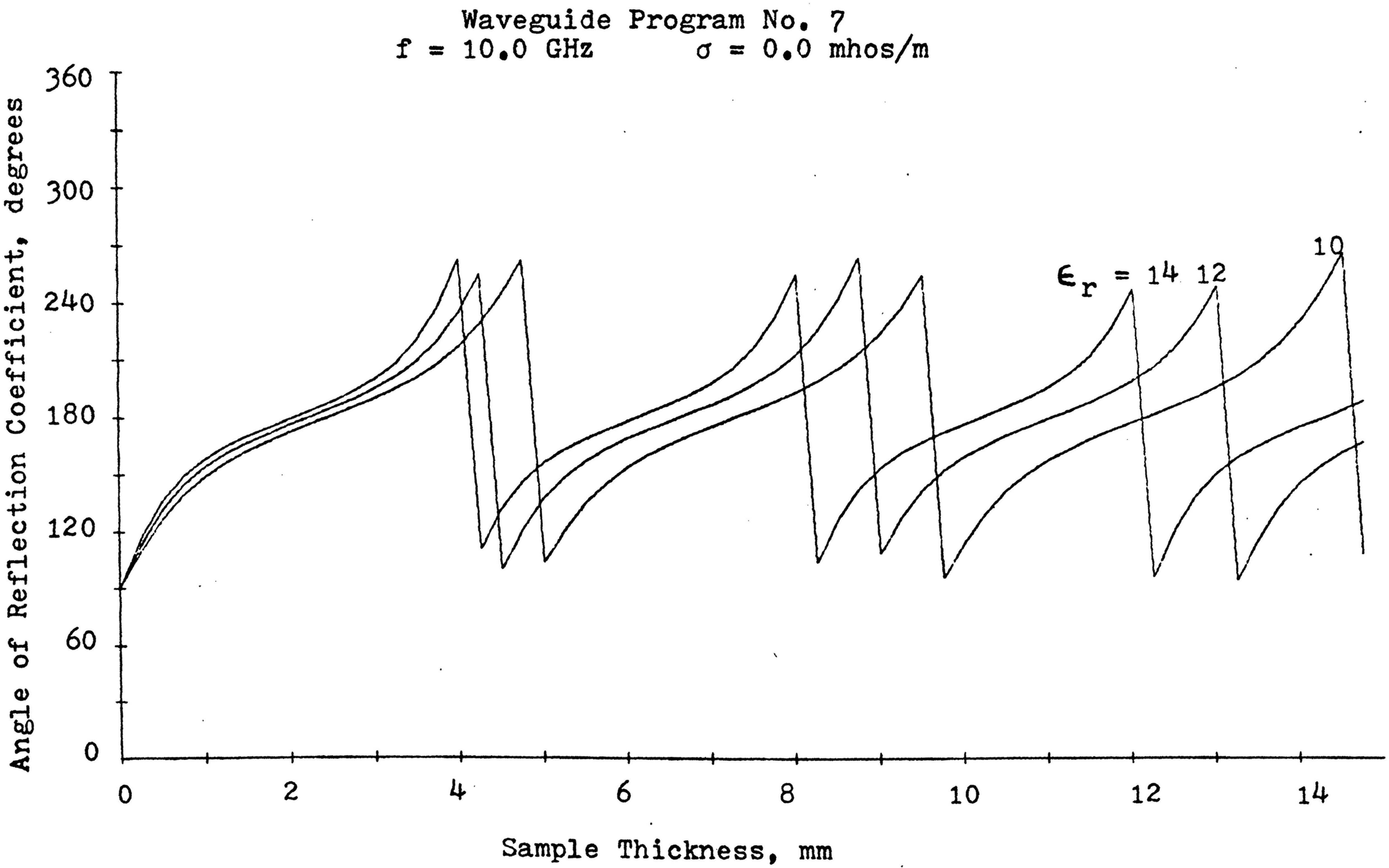

FIGURE 5.6d. Angle of reflection coefficient versus sample thickness for a dielectrically filled waveguide

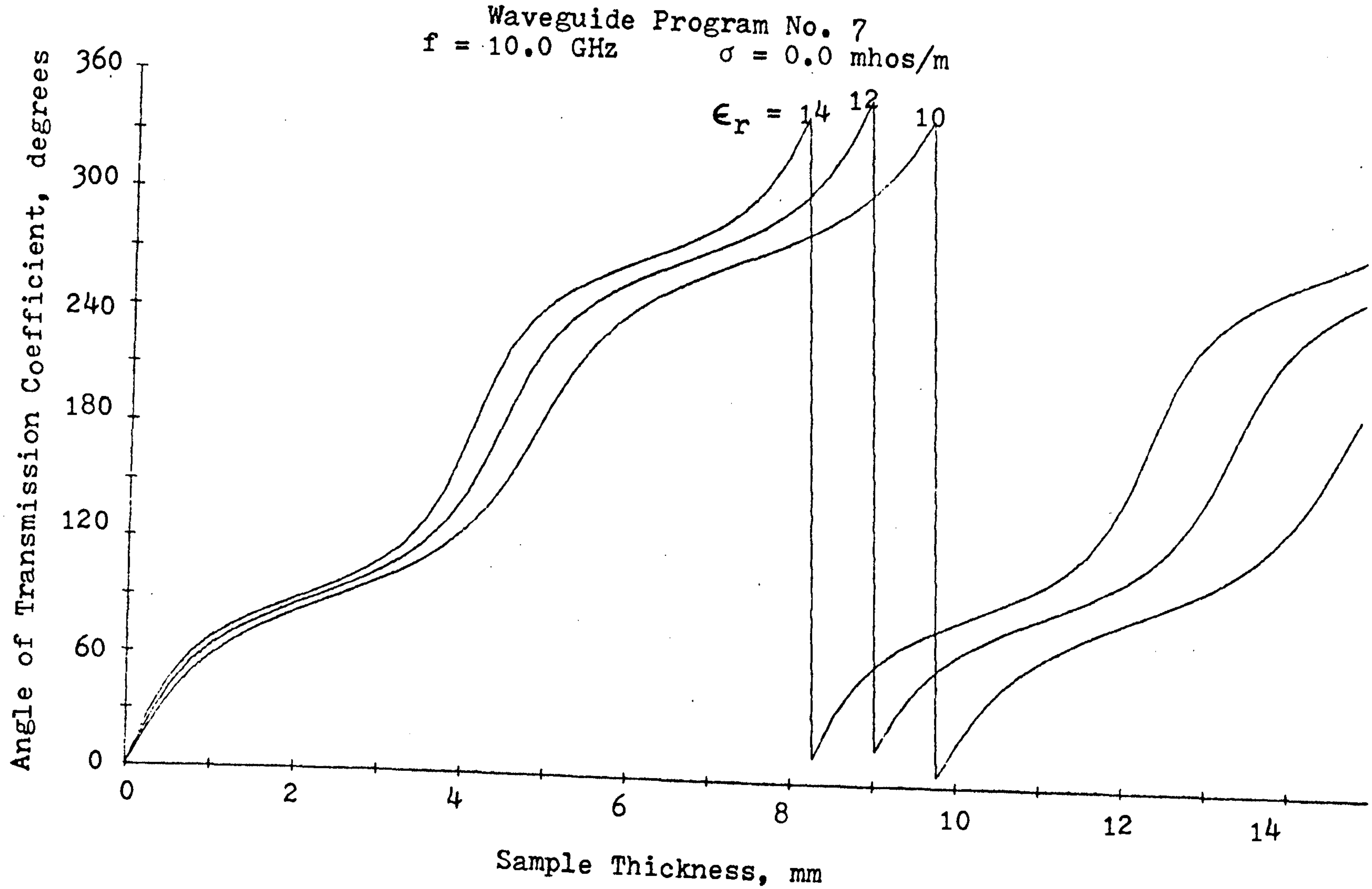

FIGURE 5.6e. Angle of transmission coefficient versus sample thickness for a dielectrically filled waveguide

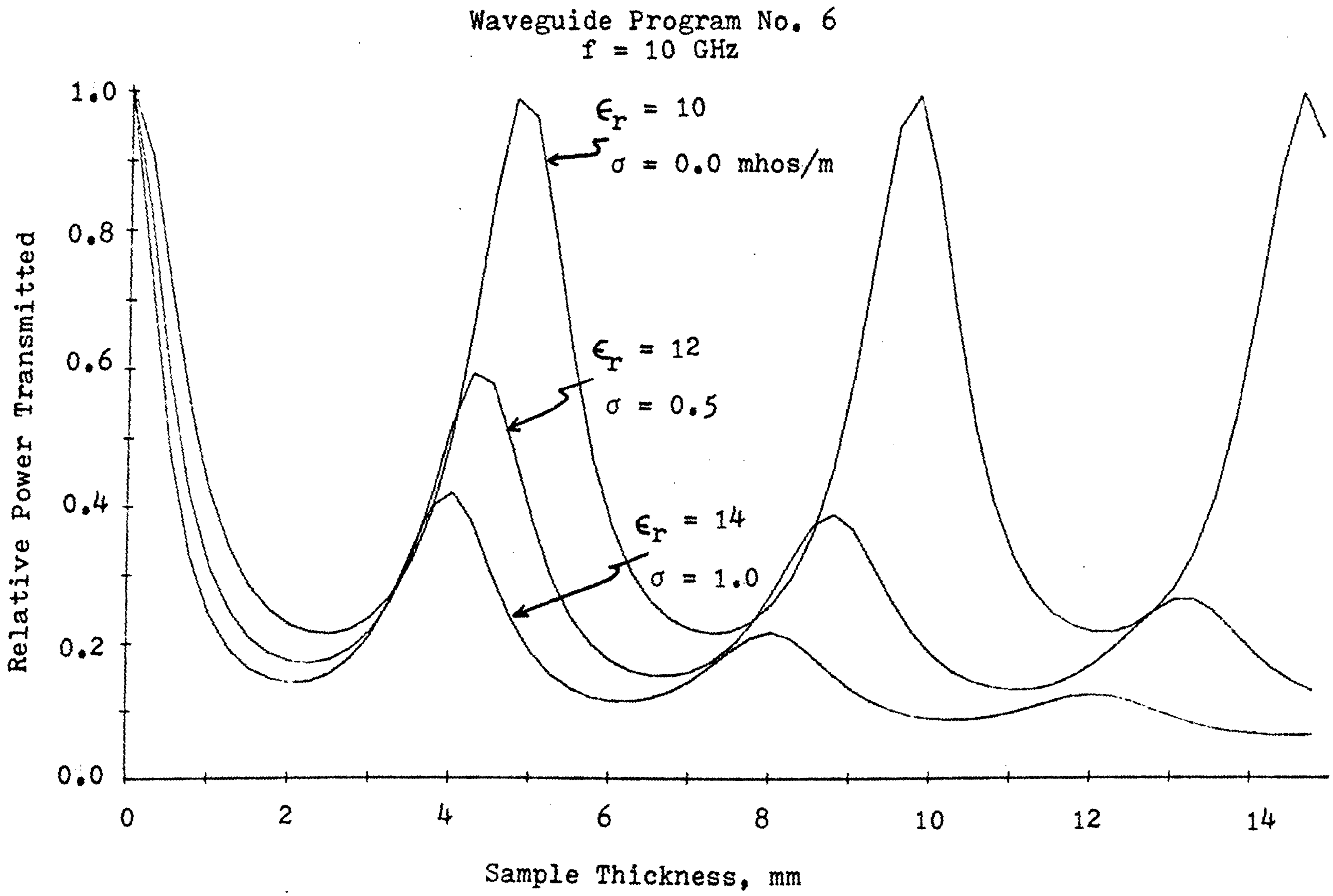

FIGURE 5.7. Relative transmitted power versus sample thickness for a dielectrically filled waveguide

for simultaneous increases in the conductivity and dielectric constant of the material.

3. VSWR Versus Frequency

It was observed experimentally that, for a given sample and fixed conductivity variation, the attenuation and VSWR produced varied radically with the operating microwave frequency. This necessitated a theoretical investigation of photoconductivity effects over the entire X-band range. Figures 5.8a through 5.8e illustrate the results for a typical example. Figures 5.8a and 5.8e indicate that for a particular sample thickness there are certain frequency ranges over which the attenuation changes are a maximum. The frequencies at which maximum change occur correspond approximately to wavelengths that are an integral multiple of twice the sample thickness. This was demonstrated previously in Figure 5.5a. Figures 5.8b and 5.8d predict that with increasing conductivity the VSWR may either increase or decrease depending upon the operating frequency. This result was verified experimentally. These same two figures also indicate the frequencies at which variations in reflected power and VSWR are minimized. This information was helpful while performing the free carrier lifetime measurements, since changes in the reflected power due to increased conductivity had to be made negligible.

For the examples investigated, the conductivity was assumed to be independent of frequency. The resonance phenomena observed experimentally and discussed in the next

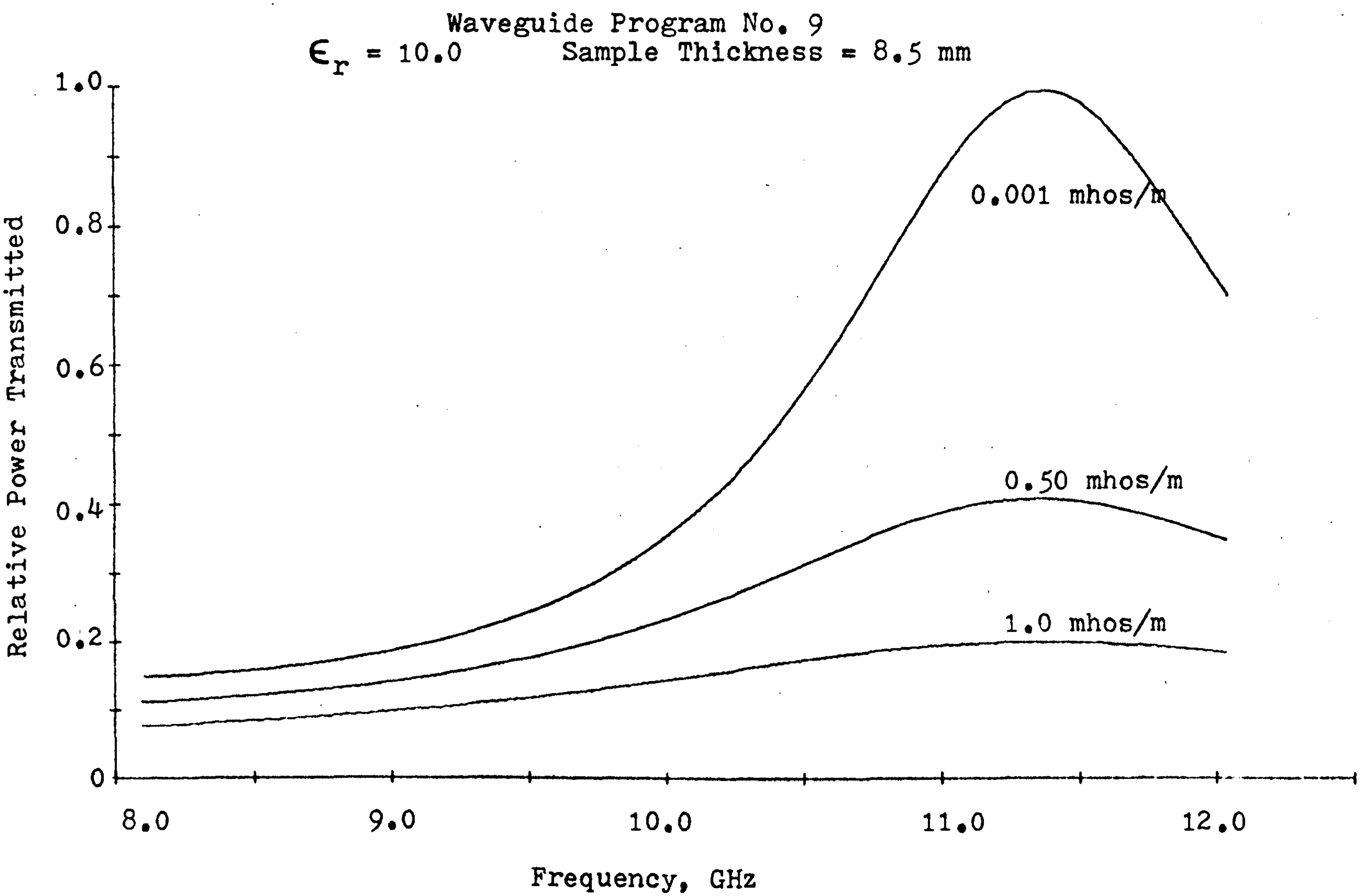

FIGURE 5.8a. Relative power transmitted versus frequency for a dielectrically filled waveguide.

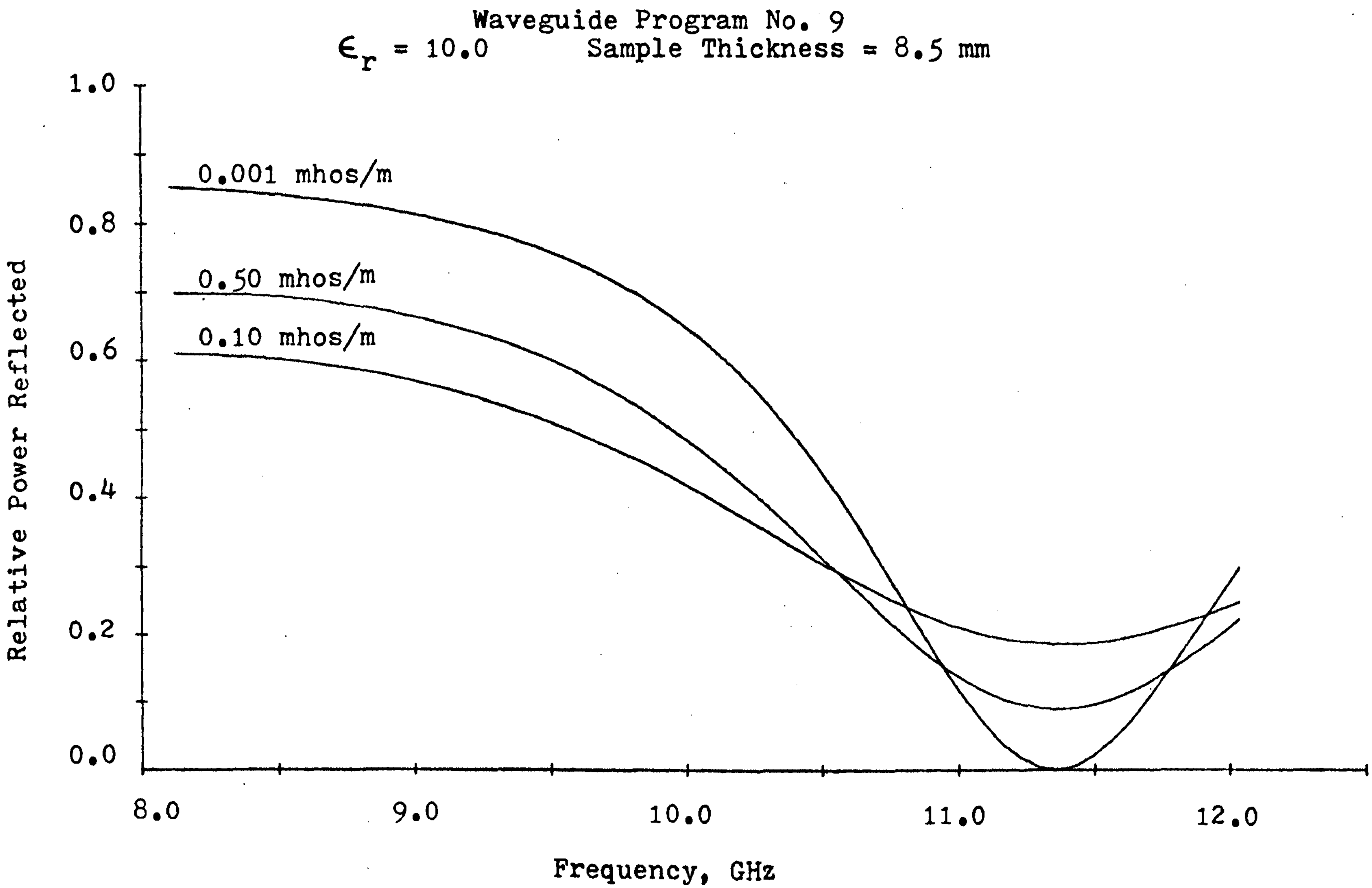

FIGURE 5.8b. Relative power reflected versus frequency for a dielectrically filled waveguide

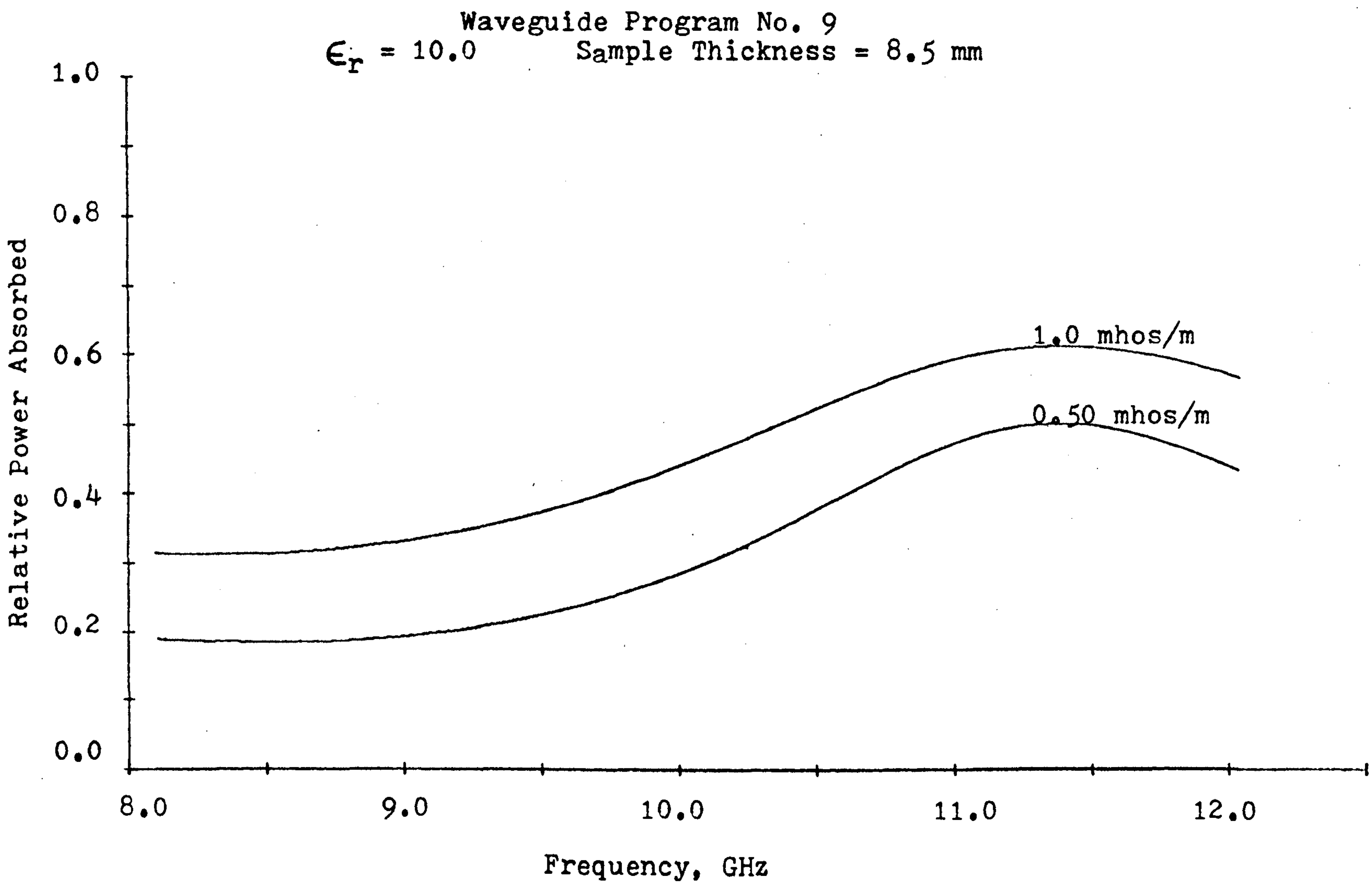

FIGURE 5.8c. Relative power absorbed versus frequency for a dielectrically filled waveguide

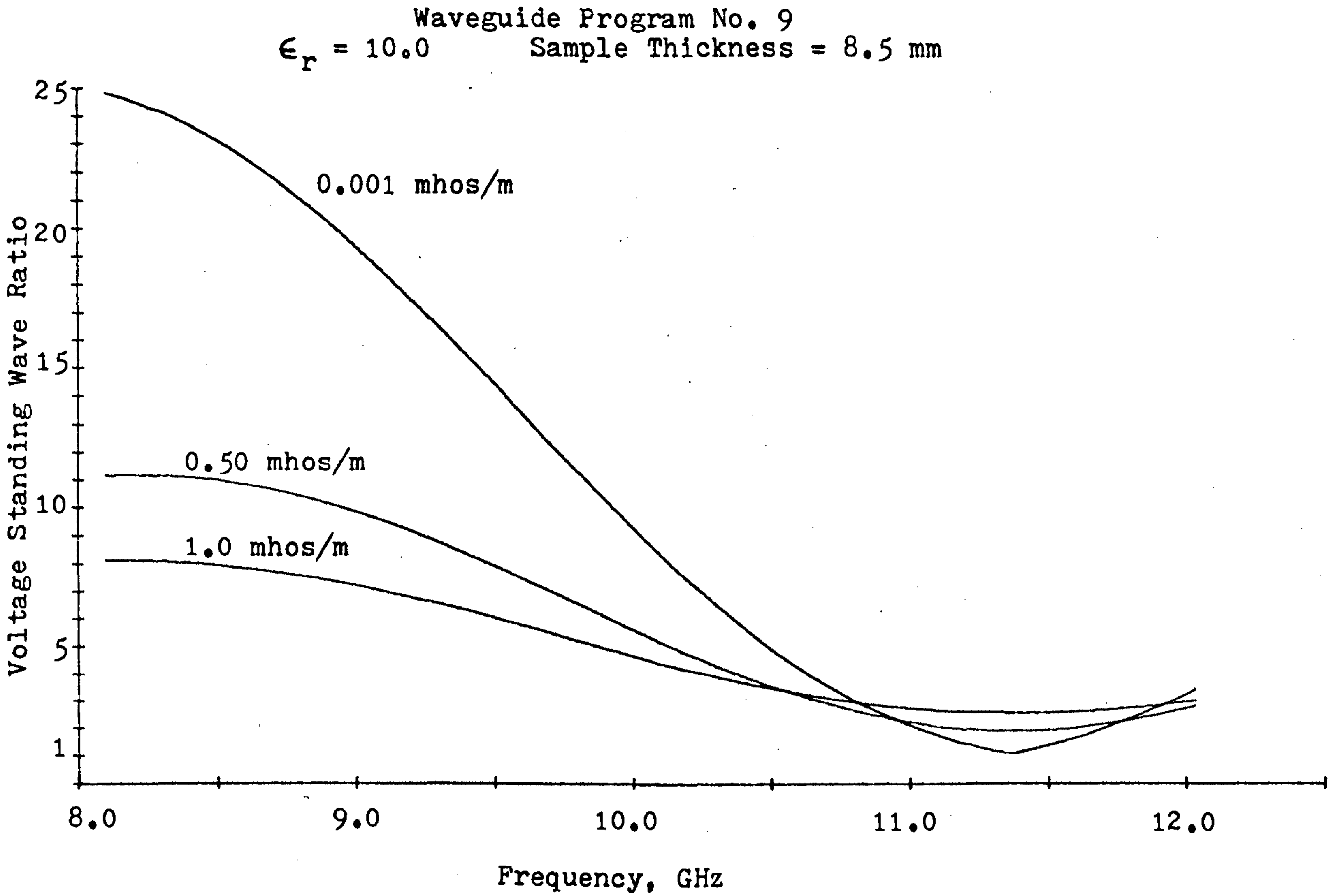

FIGURE 5.8d. Voltage standing wave ratio versus frequency for a dielectrically filled waveguide

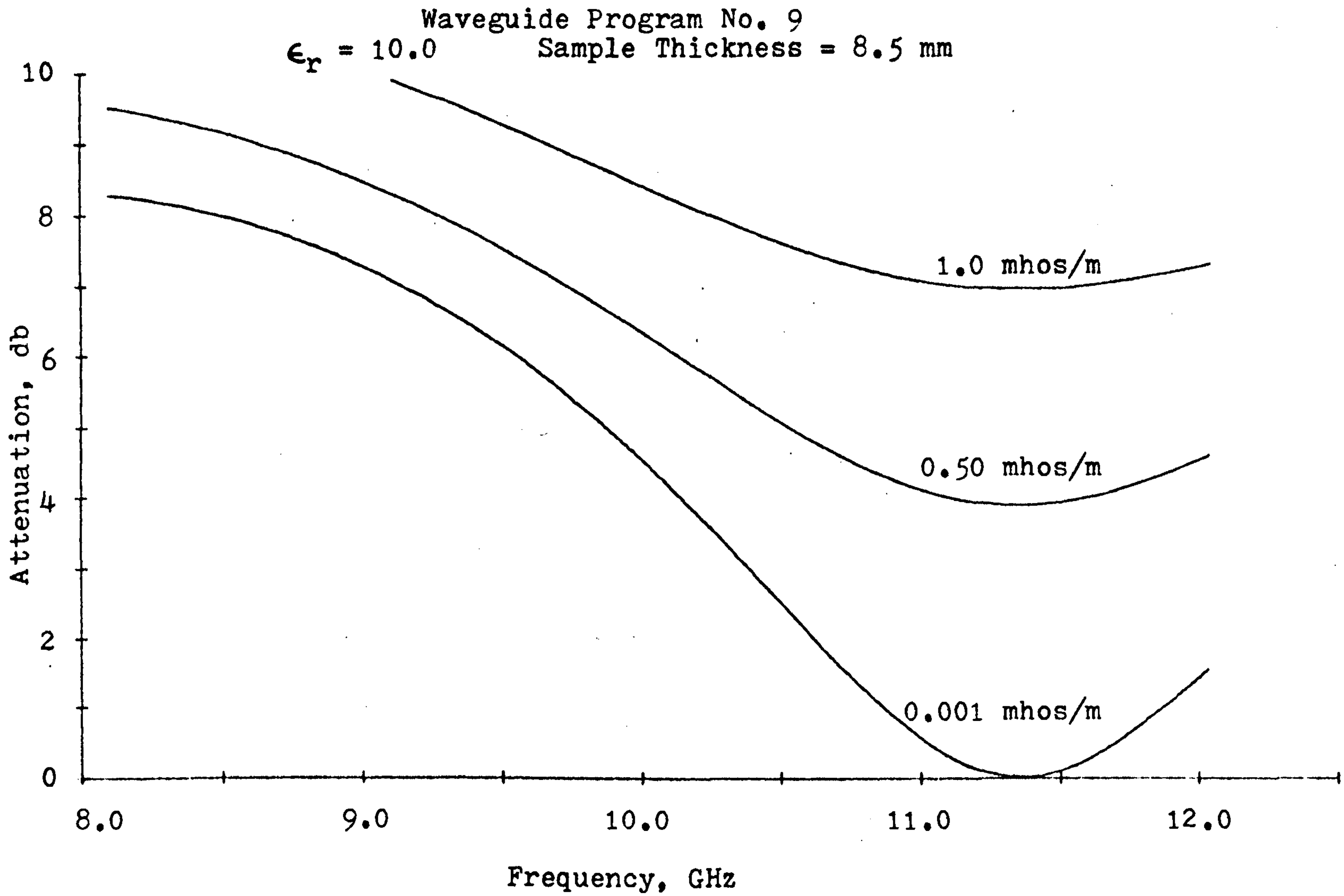

FIGURE 5.8e. Attenuation of transmitted wave versus frequency for a dielectrically filled waveguide

chapter demonstrates that additional research is required before the theoretically predicted variations with frequency agree with the observed variations. A frequency dependent complex permittivity similar to that derived in Chapter III, equation (3.47), should yield theoretical predictions in closer agreement with experiment.

C. Inhomogeneous Media

Various types of linear, parabolic, and exponential conductivity variations were considered. The results for propagation in X-band, rectangular waveguide are summarized in Table 5.1. In the table, the term "positive slope" indicates that the conductivity is increasing in the direction of propagation. Some of the important points indicated by the tabulated data are:

1) The total amount of attenuation produced by a given taper is the same for both positive and negative slopes (see examples 1 and 2, or 4 and 5, etc.). This is as expected, since for each pair of examples the networks are reciprocal. This provides an additional check on the theory and computer programming.

2) In most cases the input voltage standing wave ratio is much less for the positive slope than for the negative slope. However, this is not always true. This does indicate that in most cases illumination of the sample from a direction opposite to the direction of propagation is desirable, since the same amount of attenuation can be produced at a much lower input VSWR.

TABLE 5.1. Summary of computer results for various forms of conductivity variations

Ex. No.	General Form of Inhomogeneity	Equation For $\sigma(z)$ $(0 \leq z \leq 0.005 \text{ m})$	$\sigma(z)_{avg}$ (mhos/m)	VSWR at Input	Percent of power Absorbed	Attn. of Transmitted Power (db)
1	Linear Taper Positive Slope	$\sigma(z) = 2\text{x}10^4 z$	50	7.41	41.9	63.24
2	Linear Taper Negative Slope	$\sigma(z) = 100 - 2\text{x}10^4 z$	50	23.93	15.4	63.24
3	Constant	$\sigma(z) = 50$	50	16.99	21.0	68.84
4	Parabolic Taper Positive Slope	$\sigma(z) = 10^5 z^2$	0.834	2.27	49.3	4.50
5	Parabolic Taper Negative Slope	$\sigma(z) = 10^5 (z - 0.005)^2$	0.834	2.17	50.8	4.50
6	Constant	$\sigma(z) = 0.834$	0.834	2.00	50.4	4.15
7	Parabolic Taper Positive Slope	$\sigma(z) = 10^6 z^2$	8.34	2.96	74.8	21.03
8	Parabolic Taper Negative Slope	$\sigma(z) = 10^6 (z - 0.005)^2$	8.34	10.48	31.0	21.03
9	Exponential Taper Positive Slope	$\sigma(z) =$ $10 \exp 1500(z - 0.005)$	1.33	3.61	50.6	7.62
10	Exponential Taper Negative Slope	$\sigma(z) = 10 \exp(-1500z)$	1.33	3.60	50.8	7.62
11	Exponential Taper Positive Slope	$\sigma(z) =$ $100 \exp 1500(z - 0.005)$	13.33	5.06	54.9	26.28
12	Exponential Taper Positive Slope	$\sigma(z) = 100 \exp(-1500z)$	13.33	20.50	17.50	26.28

3) In some experiments, such as microwave lifetime measurements (Chapter VII), it is necessary that the changes in transmitted power be due primarily to power absorption by the sample rather than power reflection. The data indicates that the percent of the power absorbed is usually greater for the case of a positive slope than a negative slope. This is not always true. The situation may be reversed for values of average conductivity and sample thickness different from that used in Table 5.1. The important point is that there can be a large difference in the power absorbed for the two cases, and each specific example must be investigated to determine the best direction from which to illuminate the sample.

The data in Table 5.1 was calculated on the basis of each inhomogeneity being subdivided into 20 equal length, homogeneous sections. Other programs using only 10 equal length sections yielded data in agreement with that shown to the first decimal place. This indicates that for the inhomogeneities investigated, rather crude approximations to the actual conductivity variations can result in surprisingly accurate answers.

VI. EXPERIMENTAL MEASUREMENT OF VARIOUS MICROWAVE PROPERTIES OF CADMIUM SULFIDE

A. Introduction

The purpose of this chapter is to describe and explain the results of several microwave experiments performed on CdS. These experiments include measurement of VSWR, attenuation, and phase shift produced by photoexcited CdS at various frequencies. The microwave measurement of the free electron lifetime has been reserved for the next chapter.

B. Cadmium Sulfide

CdS is a yellow-orange, brittle, crystalline solid of hexagonal structure. Typical values for a few of the important electrical properties of CdS are shown in Table 6.1. It must be emphasized that some of the quantities may deviate considerably from the indicated value depending upon the number and type of impurities, method of preparation, surface conditions, etc. The CdS samples used in this research were kindly supplied by Mr. J. Powderly of the Eagle-Picher Company. Figure 6.1 is a photograph of a few of the samples used, and Table 6.2 indicates the manufacturers lot number and resistivity. Since CdS is also an anisotropic, piezoelectric, acoustically active material, it was expected that the isotropic theory presented in the earlier chapters would not be able to explain all of the experimental results. Even so, the experimental results agreed qualitatively with the theoretical predictions except

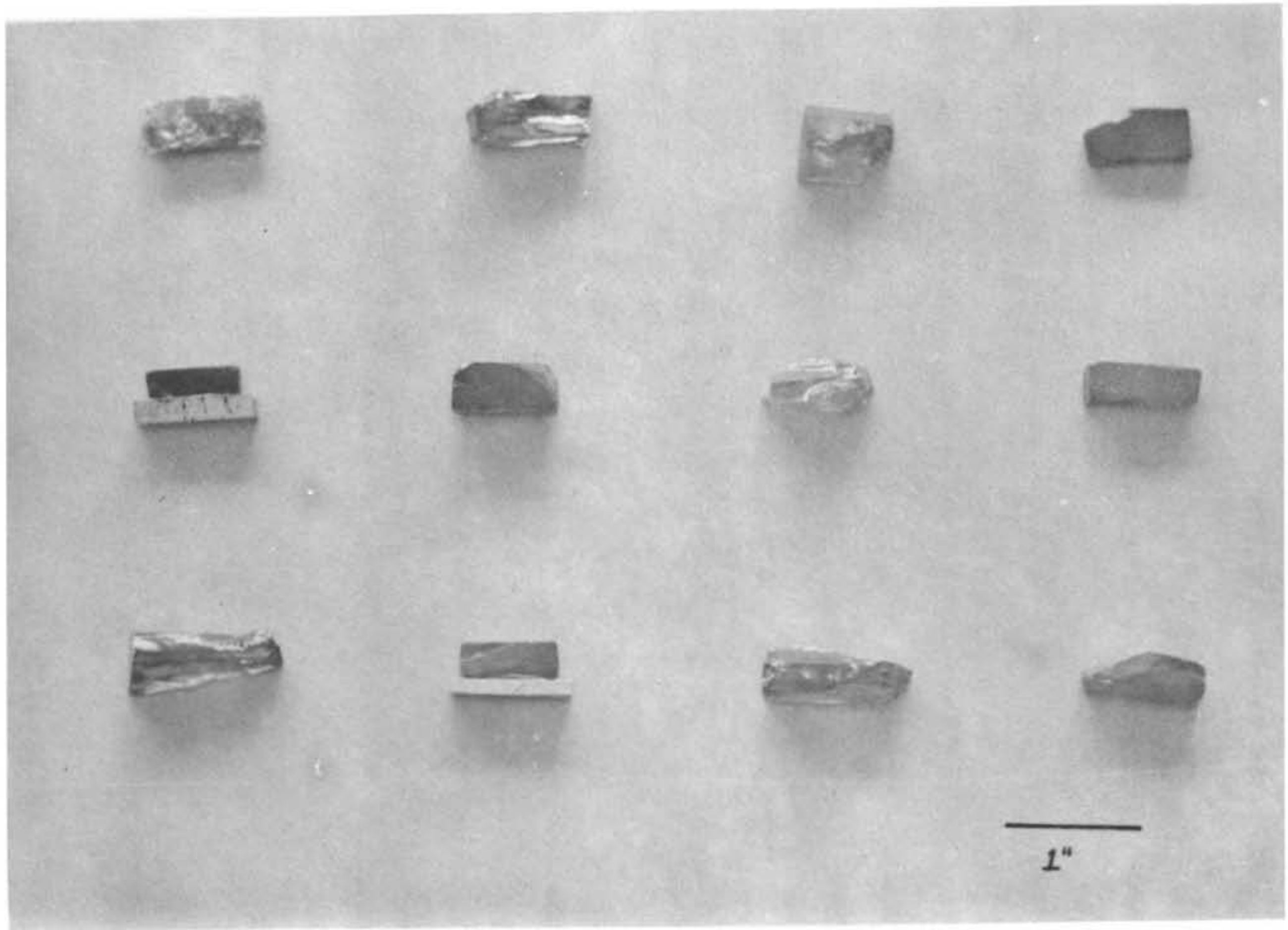

FIGURE 6.1. A few of the CdS samples used in this research

TABLE 6.1. Typical values for some important electrical properties of undoped, single-crystalline cadmium sulfide

Energy gap	2.42 ev
Electron mobility	0.30 m^2/volt-sec
Hole mobility	0.03 m^2/volt-sec
Electron lifetime	10^{-1} sec
Hole lifetime	10^{-6} sec
Relative dielectric constant	10

TABLE 6.2. Manufacturers lot number and resistivity for some of the CdS samples used in this research

CdS Sample No.	Eagle-Picher Co. Lot No.	Dark Resistivity (ohms-cm)
1	211 - 8 - P	---
2	211 - 8 - P	---
3	211 - 8 - P	---
4	211 - 8 - P	---
5	211 - 27 - S	$2.9x10^3$
6	006 - 27 - P	$5.35x10^3$
7	211 - 8 - P	---
8	B - 10	$4.8x10^3$
9	B - 12	$2.8x10^3$
10	B - 14	$2.14x10^5$
11	B - 10	$4.8x10^3$
12	010 - 25 - S	$1.0x10^2$

in the case of an unexplained resonance phenomena observed in some samples.

C. Microwave Cavity Measurements

In an attempt to observe the photodielectric effect in CdS at microwave frequencies, a small sample was placed in a hollow rectangular cavity. Sample illumination was provided through a non-radiating hole in the broadside of the cavity. The experiment was unsuccessful for two reasons:

1) The relatively high conductivity (10^{-2} mhos/m) of the CdS sample resulted in a low cavity Q. This made the cavity bandwidth approximately equal to the bandwidth of one mode of the reflex klystron which was used as the microwave source. Hence, the center frequency of the cavity could not be accurately determined.

2) The ratio of sample volume to cavity volume was so small that even if the relative dielectric constant of the sample were changed by as much as 10% the resulting shift in center frequency of the cavity would be practically immeasurable. The ratio of volumes could not be increased without further reducing the cavity Q. This failure clearly indicated some of the limitations of measuring conductivity and dielectric constant by the shift in center frequency and change in Q of a microwave cavity.

D. Attenuation Versus Light Wavelength

An experiment was conducted to determine the energy gap of CdS by means of microwave power absorption. CdS samples No. 6 and 8 were separately placed in an X-band slotted waveguide section operating at 10.0 GHz. (See the insert of Figure 6.2 for an illustration of the sample orientation.) A monochromator was used for photoexcitation, and the microwave absorption versus light wavelength was measured. A peak in microwave absorption was clearly evident in each case. From the light wavelengths corresponding to these peaks the energy gaps of samples No. 6 and 8 were determined to be 2.24 ev and 2.28 ev, respectively, by using

$$E_g = 1.24/\lambda, \qquad (6.1)$$

where E_g is the energy gap in electron volts and λ is the wavelength in microns (10^{-6} m). The typical value indicated in Table 6.1 is 2.42 ev. A visual check of the absorption edge for samples No. 6 and 8 yielded band gaps of 2.30 ev and 2.32 ev, respectively, which are in excellent agreement with the microwave photoconductivity measurements.

E. VSWR Versus Frequency

In the process of performing standard VSWR versus frequency tests on several samples, an unexpected phenomenon was observed. A block diagram and photograph of the experimental arrangement are shown in Figures 6.2 and 6.3, respectively. The results for various samples are plotted in Figures 6.4 through 6.8. Only a few samples were tested since, due to the lack of an automatic sweep oscillator, data had to be taken by a time consuming point by point method. The "resonance" phenomena appeared in four out of the five

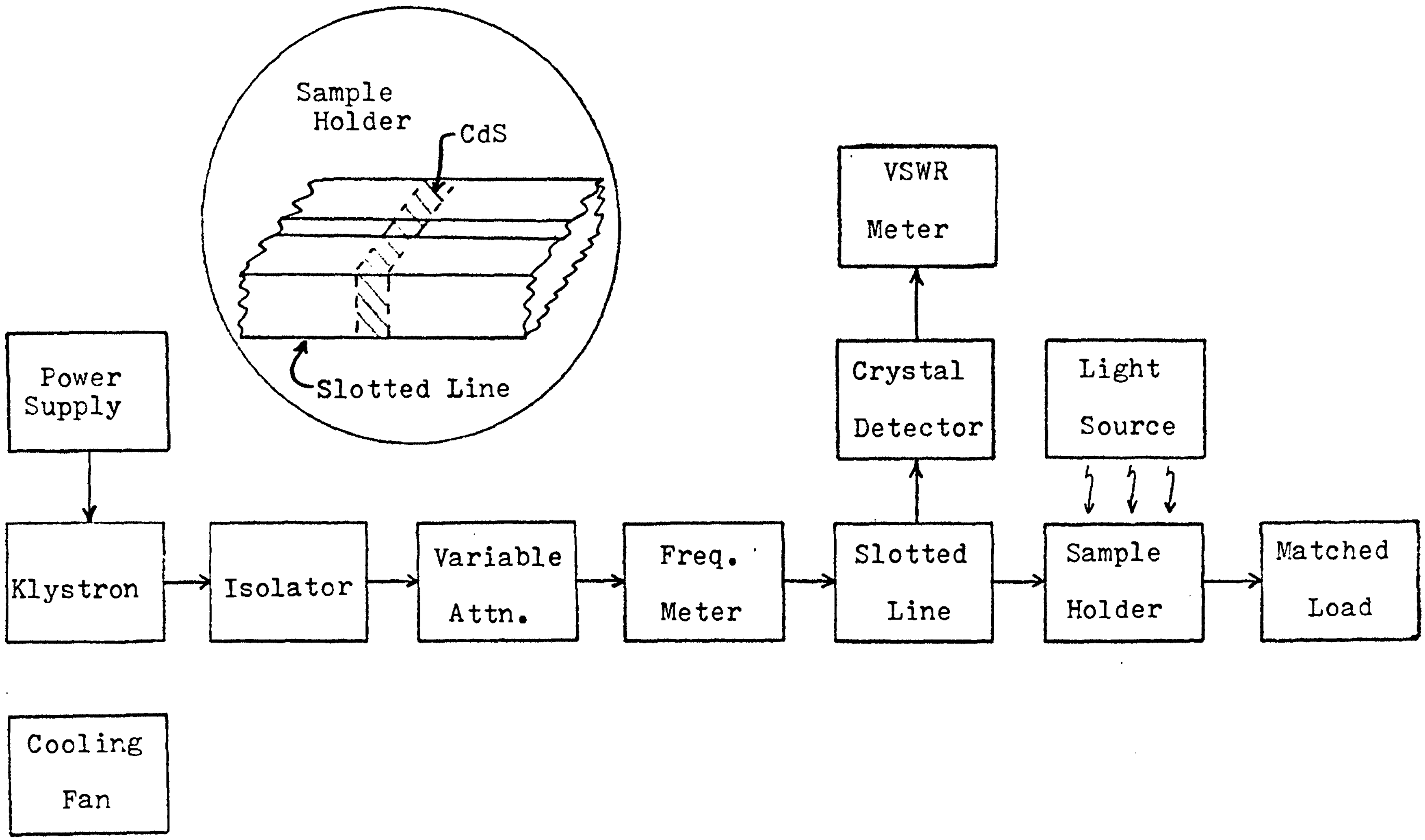

FIGURE 6.2. Block diagram of the experimental microwave arrangement used for VSWR versus frequency measurements of the CdS samples

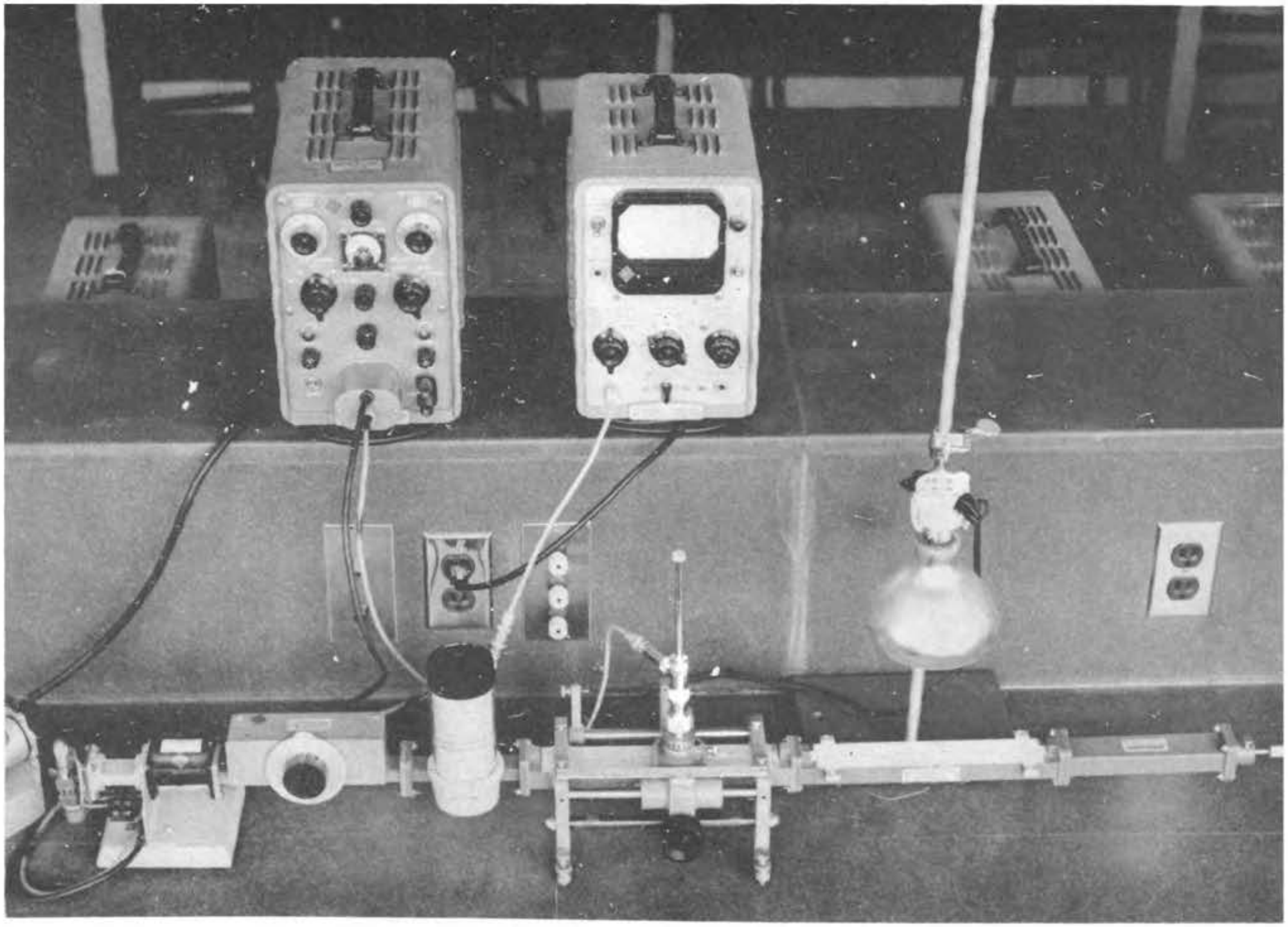

FIGURE 6.3. Apparatus used for the VSWR versus frequency measurement on CdS

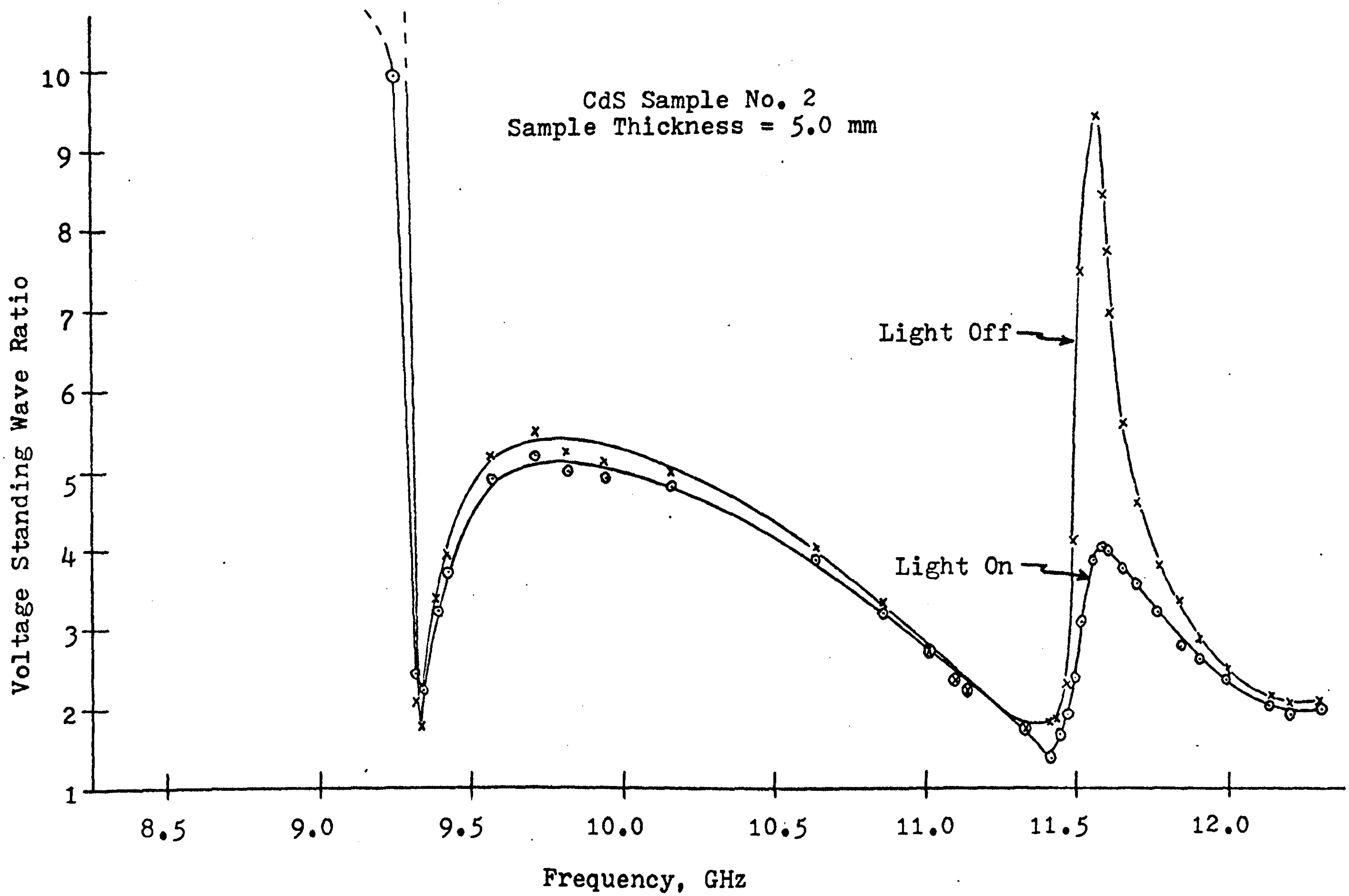

FIGURE 6.4. VSWR versus frequency for CdS sample No. 2

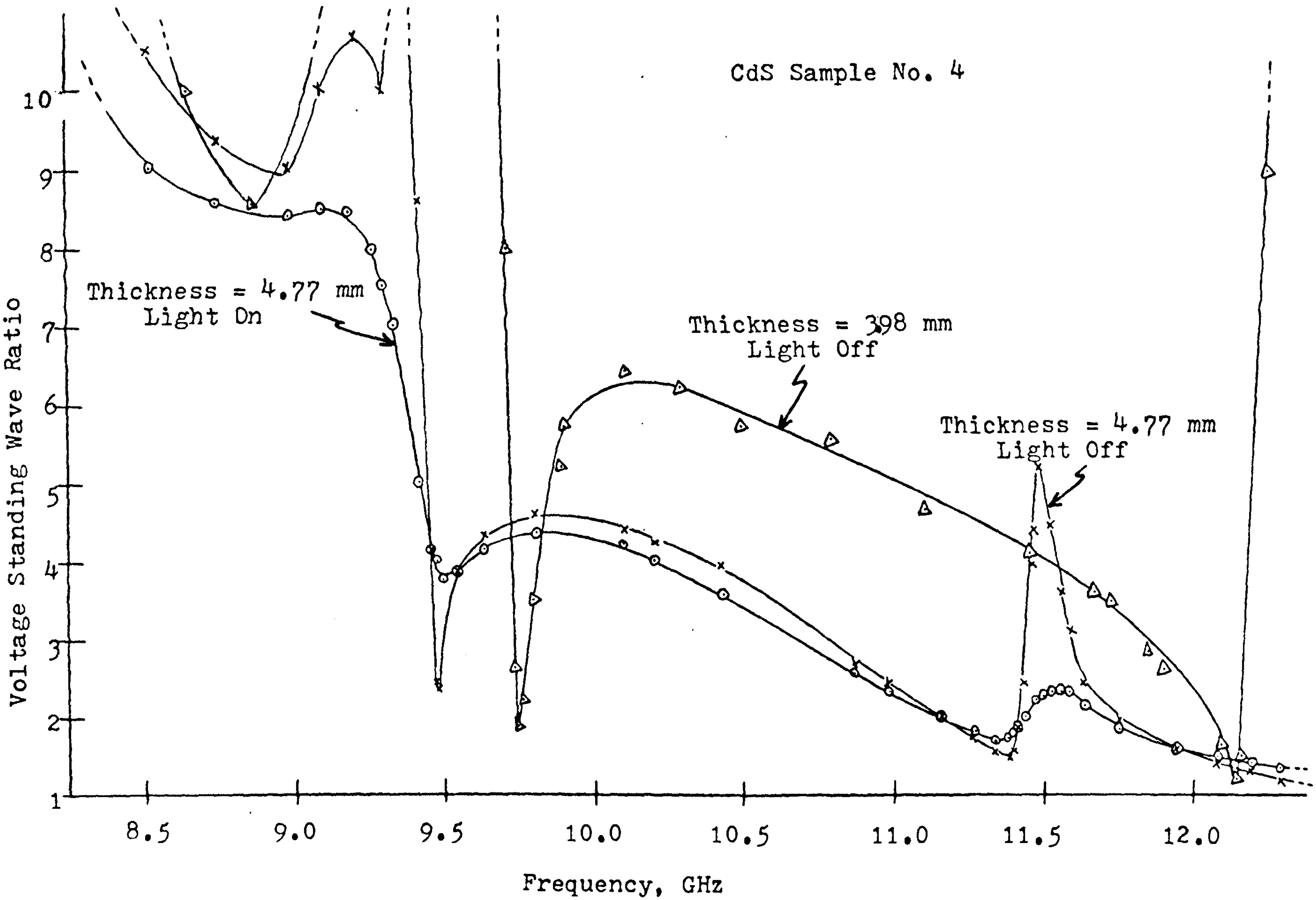

FIGURE 6.5. VSWR versus frequency for CdS sample No. 4

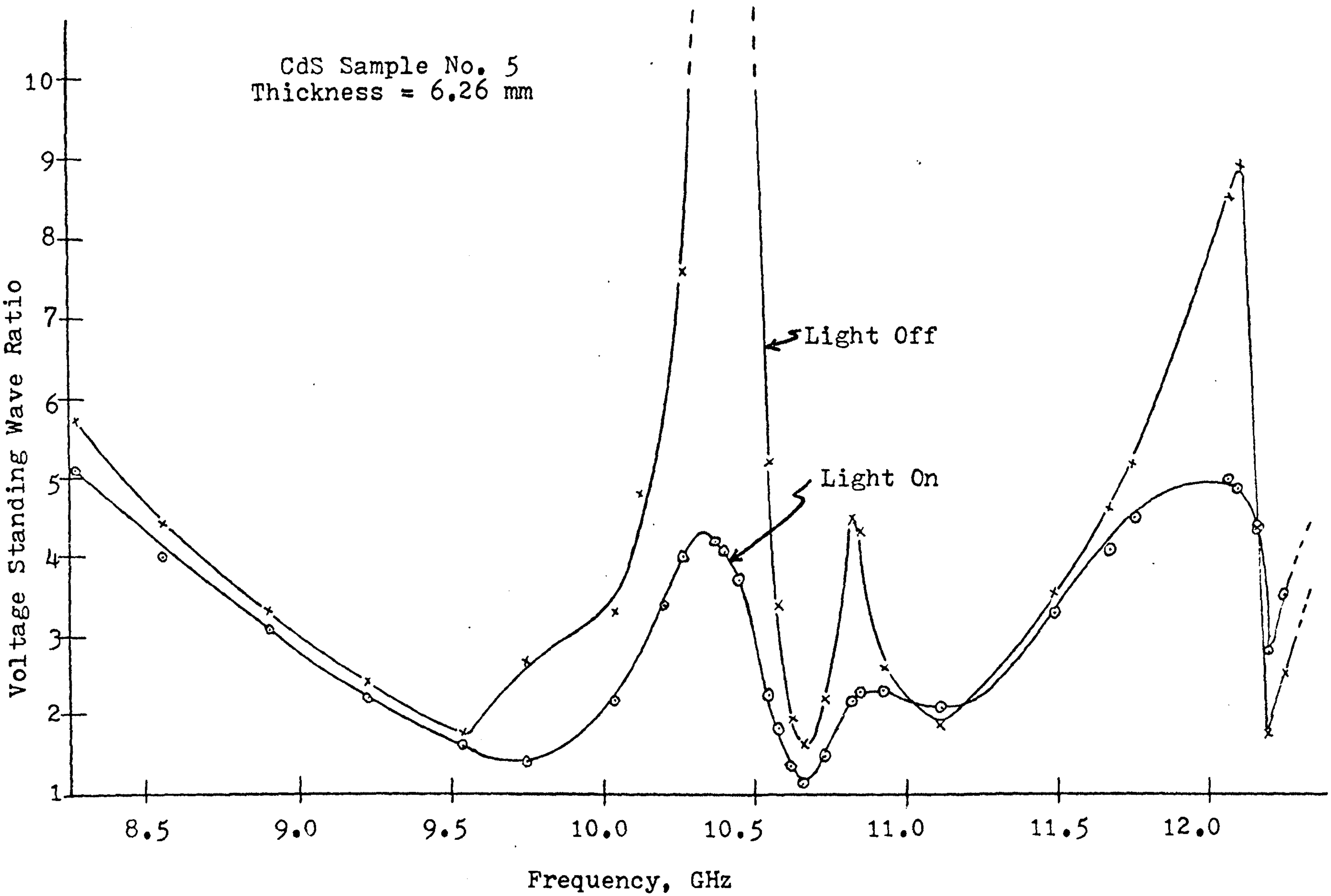

FIGURE 6.6. VSWR versus frequency for CdS sample No. 5

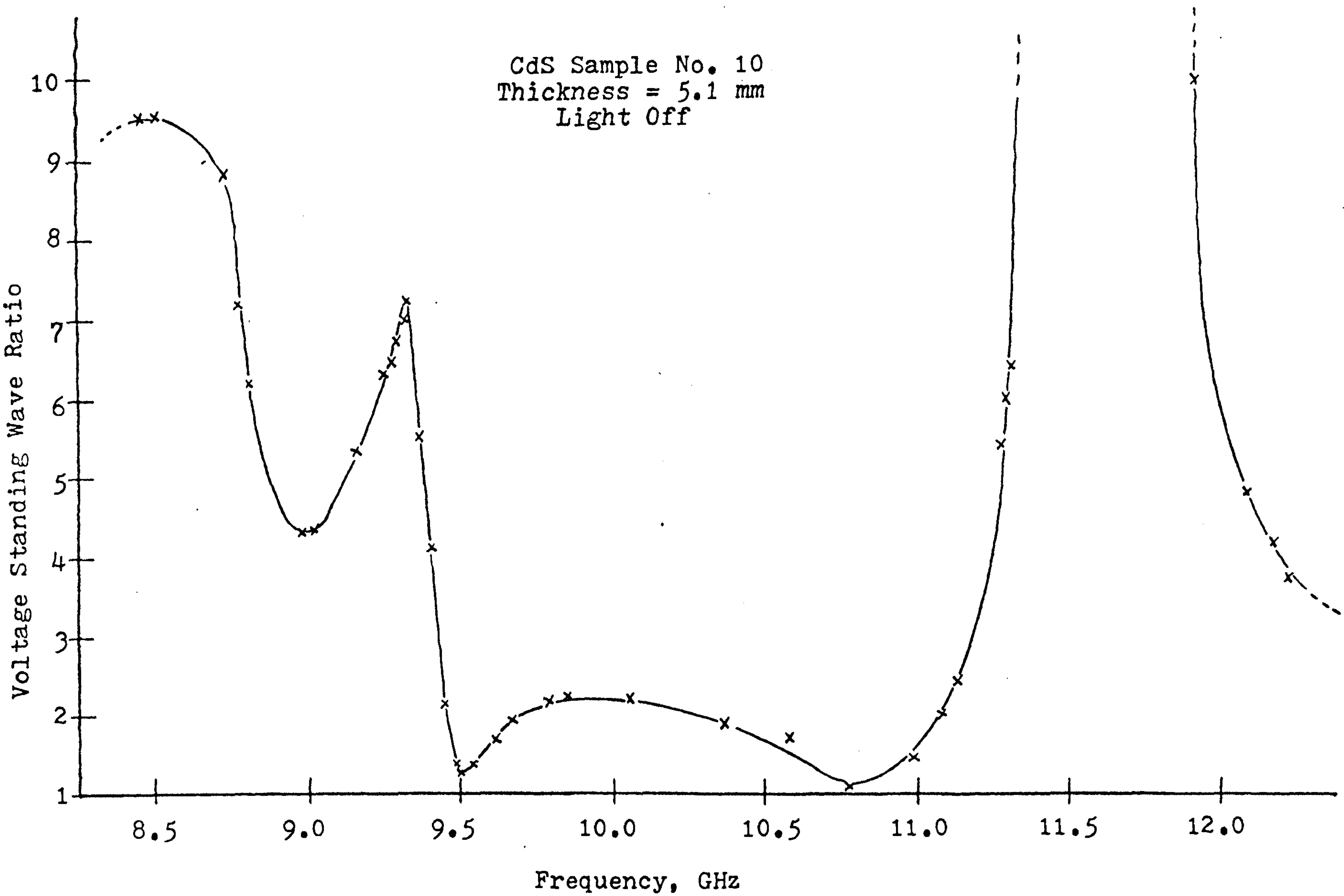

FIGURE 6.7. VSWR versus frequency for CdS sample No. 10

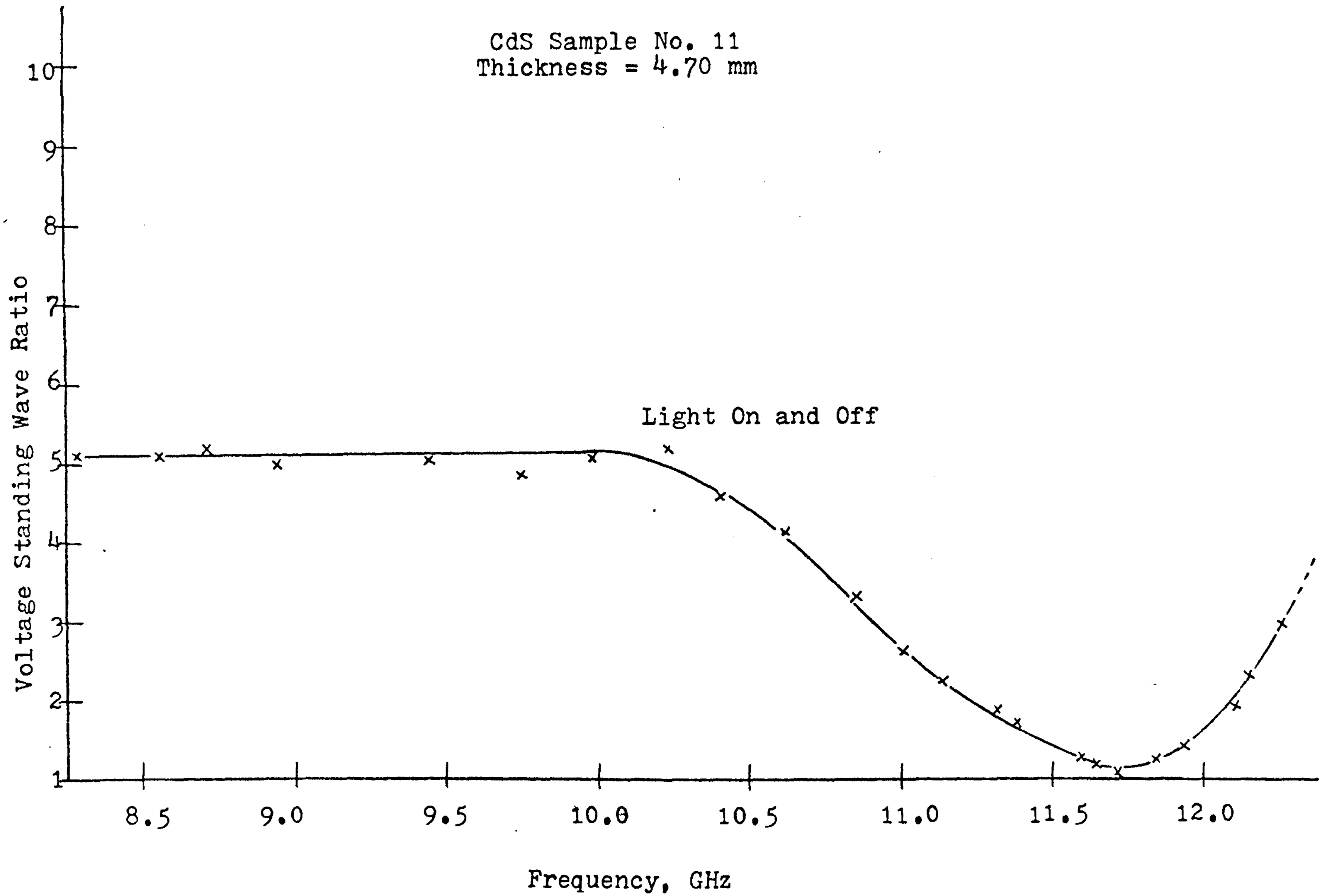

FIGURE 6.8. VSWR versus frequency for CdS sample No. 11

samples tested. Some of the possible explanations are discussed below.

1) An explanation based on the formation of a resonant dielectric cavity was eliminated because of the shape of the VSWR versus frequency curve. If a resonant cavity existed, this would produce a dip but little or no rise in the VSWR curve. Also, changes in sample thickness do not seem to be simply related to the changes produced in the resonant frequencies.

2) The best explanation at present is that the phenomena is due to the plasma resonance of the free electrons. Moss (85) gives a theoretically calculated curve of reflectivity versus frequency for plasma resonance in a semiconductor with a relative dielectric constant of 14. This curve is very similar in shape to those in Figures 6.4 through 6.7. Equations (3.36) and (3.37) indicated that the complex free carrier conductivity was given by

$$\sigma_f' = \frac{\omega^2 \omega_p^2 \epsilon_o/\tau_c}{(L\omega_p^2 - \omega^2)^2 + (\omega/\tau_c)^2} \tag{6.1}$$

$$\sigma_f'' = \frac{-\omega\,\omega_p^2 \epsilon_o(L\omega_p^2 - \omega^2)}{(L\omega_p^2 - \omega^2)^2 + (\omega/\tau_c)^2}. \tag{6.2}$$

Different values of the depolarization factor L along the three rectangular sample axes could account for the presence of more than one resonant frequency. Table 6.3 indicates remarkable agreement between the ratio of the two observed resonant frequencies for each sample and the

TABLE 6.3. Comparison of resonant frequencies and depolarization factors for several CdS samples

Sample No.	Dimension a(in.)	Dimension b(in.)	Dimension c(in.)	ω_{r1} (GHz)	ω_{r2} (GHz)	ω_{r1}/ω_{r2}	$(L_a/L_b)^{\frac{1}{2}}$
2	0.236	0.20	0.65	10.6	11.6	0.914	0.92
2	0.20	0.20	0.65	11.6	9.25	1.26	1.19
4	0.18	0.27	0.68	11.5	9.4	1.222	1.225
4	0.15	0.27	0.68	12.28	9.68	1.27	1.34
5	0.234	0.34	0.71	12.1	10.45	1.16	1.18
10	0.20	0.30	0.88	11.6	9.3	1.25	1.225

$$L_a \approx \frac{bc}{ab + bc + ca}$$

$$L_b \approx \frac{ac}{ab + bc + ca}$$

$$L_c \approx \frac{ab}{ab + bc + ca}$$

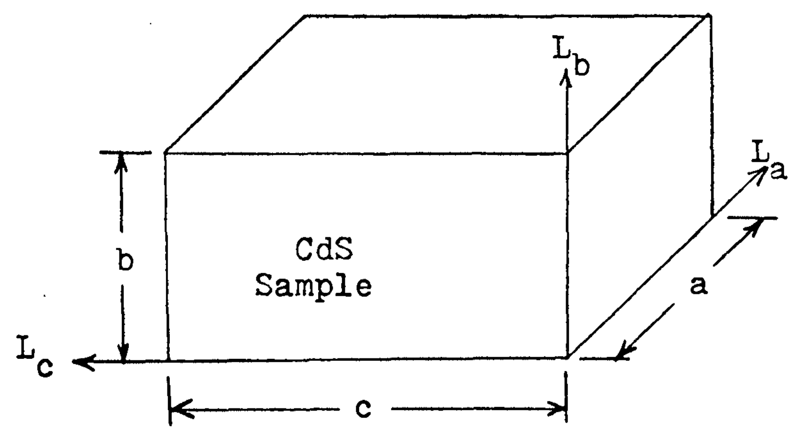

square root of the ratio of the two depolarization factors L_a and L_b. However, for sample No. 4 when the "a" dimension was reduced from 0.180 in. to 0.150 in., the theory predicted that ω_{r1} should increase and ω_{r2} should decrease. Experiment confirmed that ω_{r1} did increase by the predicted amount, however, ω_{r2} appeared to also increase. The actual variation in the lower resonant frequency ω_{r2} was difficult to determine from the experimental data because the VSWR was high over a considerable frequency range.

3) Other possible explanations are permanent dipole relaxation or excitation of a transverse optical phonon mode. The latter explanation in terms of an acoustical mode is a definite possibility since CdS is a partially ionic compound and the data in Table 6.3 indicates a relationship between the resonant frequencies and the sample dimensions. CdS is frequently used as a transducer for converting microwave photons to microwave phonons.

The only reliable conclusion that can be drawn is that there is definitely a strong resonance phenomena present but the experimental data is too limited to permit a determination of the cause. This is a very interesting problem requiring extensive additional research.

F. Attenuation and Phase Shift Measurements

The purpose of this section is to describe the experimental results of the attenuation and phase shift produced at X-band by various photoexcited CdS samples.

Figure 6.9 illustrates the increased attenuation produced by CdS sample No. 2 under moderate (40 foot-candles) illumination inside a slotted line section of X-band waveguide. The changes in power were measured directly by a thermistor and microwave power meter combination. Care was taken to repeatedly rezero the power meter. The figure indicates a small (0.2 db) average attenuation at all frequencies in the X-band range with large variations superimposed at the "resonant" frequencies. This data confirmed the resonance phenomena described in the previous section. The exact dark conductivity of this sample was unknown, however, approximate dc resistance measurements indicated that the conductivity was 10^{-5} mhos/m. The theoretical calculations from Chapter V demonstrated that the conductivity must be increased into the range of 0.1 mhos/m to 10 mhos/m in order to produce significant attenuation of a 10 GHz microwave signal. Under the illumination used, the conductivity of the sample could be increased to a maximum of approximately 10^{-2} mhos/m. This limitation coupled with the fact that the sample filled only one-third of the waveguide cross section explains the reason for the low average attenuation. This emphasizes the importance of knowing the range over which the conductivity must be varied in order to produce attenuation. The theoretical calculations in Chapter V are a necessary prerequisite to the design of any photoconductive microwave devices.

A microwave bridge arrangement (shown in Figures 6.10

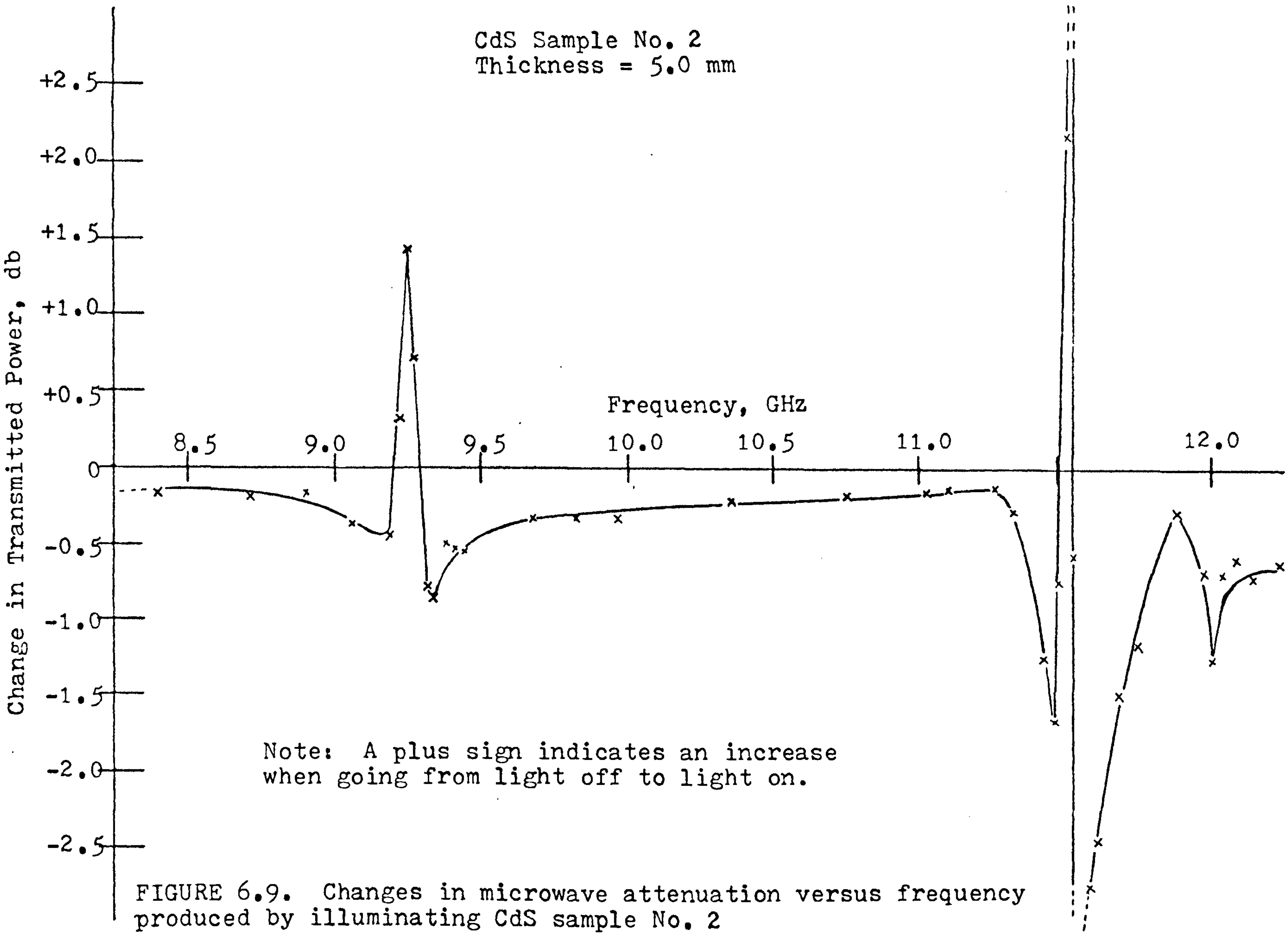

FIGURE 6.9. Changes in microwave attenuation versus frequency produced by illuminating CdS sample No. 2

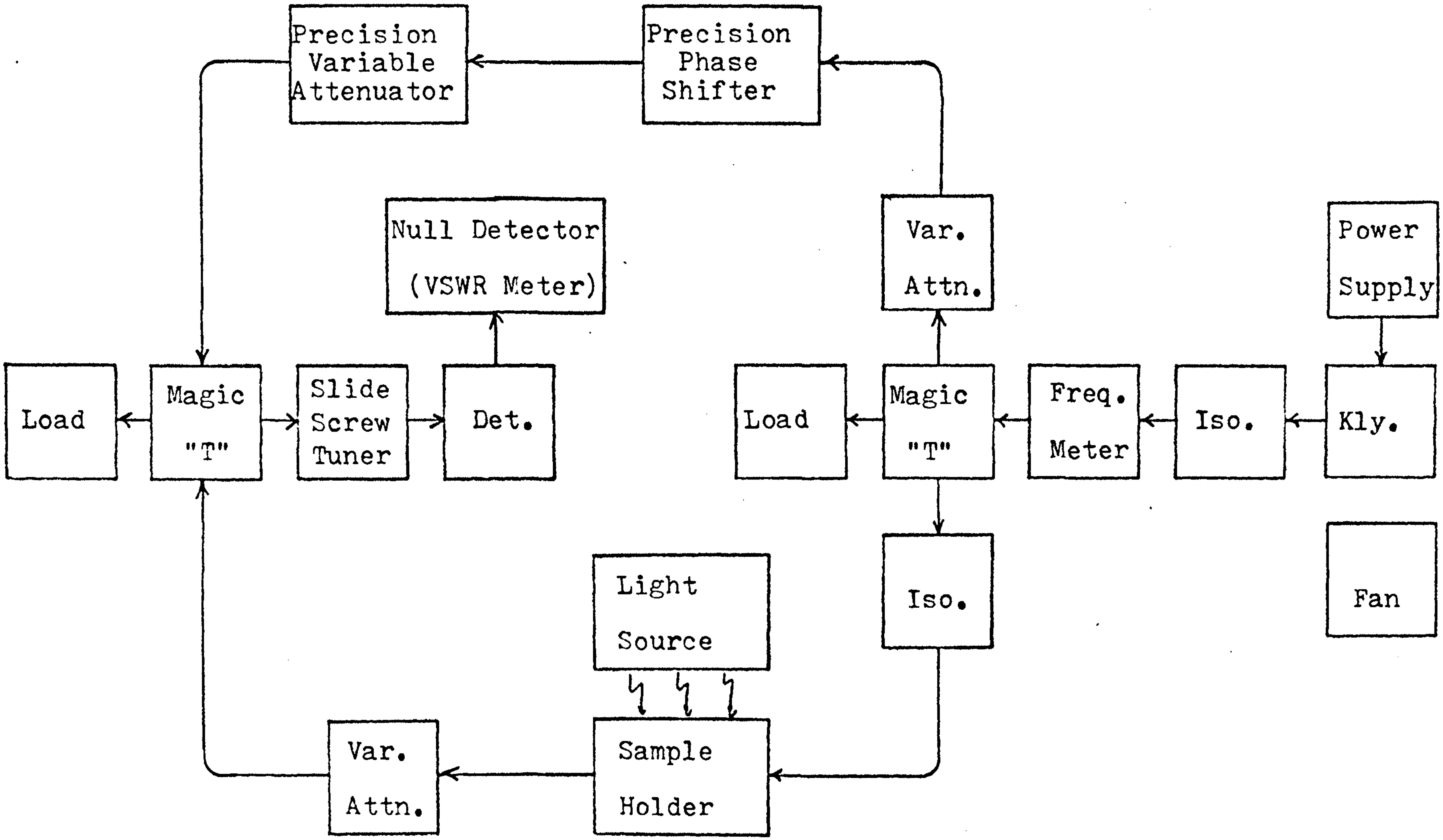

FIGURE 6.10. Block diagram of the microwave bridge arrangement used for the attenuation and phase shift measurements on CdS

and 6.11) was setup to permit simultaneous measurement of the changes in attenuation and phase shift produced by photoexcited CdS. Isolators and attenuators were inserted at critical points in the bridge to insure a low VSWR where required. The results for sample No. 2 are shown in Figure 6.12. The small average attenuation revealed by direct power measurement is not shown in Figure 6.12 because of the lower sensitivity of the bridge measurements. The shape of the attenuation and phase shift curves are similar to the results expected for resonance absorption and anomalous dispersion. The small shift in the resonant frequencies between Figures 6.9 and 6.12 could be due to any one or a combination of such factors as temperature changes, slightly different crystal orientation inside the waveguide, use of two different frequency meters, etc. Typical values for the changes in attenuation and phase shift produced by other samples at a single frequency are shown in Table 6.4. In each case, the frequency used was outside the influence of the "resonance" phenomena. Very little correlation can be expected between the change in attenuation produced by a sample and its dark conductivity, because the theoretical calculations from Chapter V indicate that the sample thickness is also a very important parameter. Correlation could be expected only if all the samples were of the same thickness and completely filled the waveguide cross section. The reasons for the small changes in attenuation shown in Table 6.4 are; too low a value of dark conductivity, non-optimum

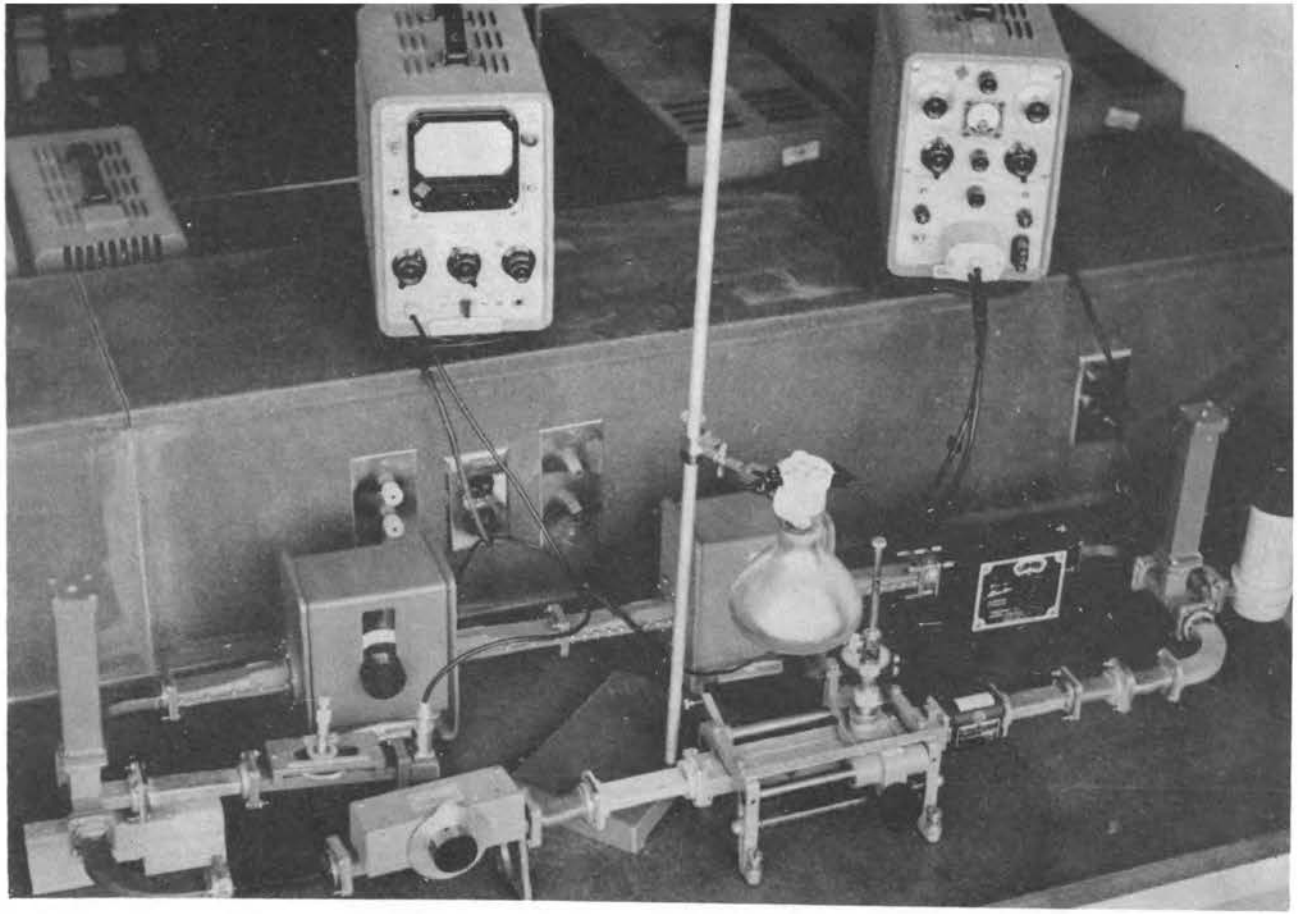

FIGURE 6.11. Microwave bridge apparatus used for the attenuation and phase shift measurements on CdS

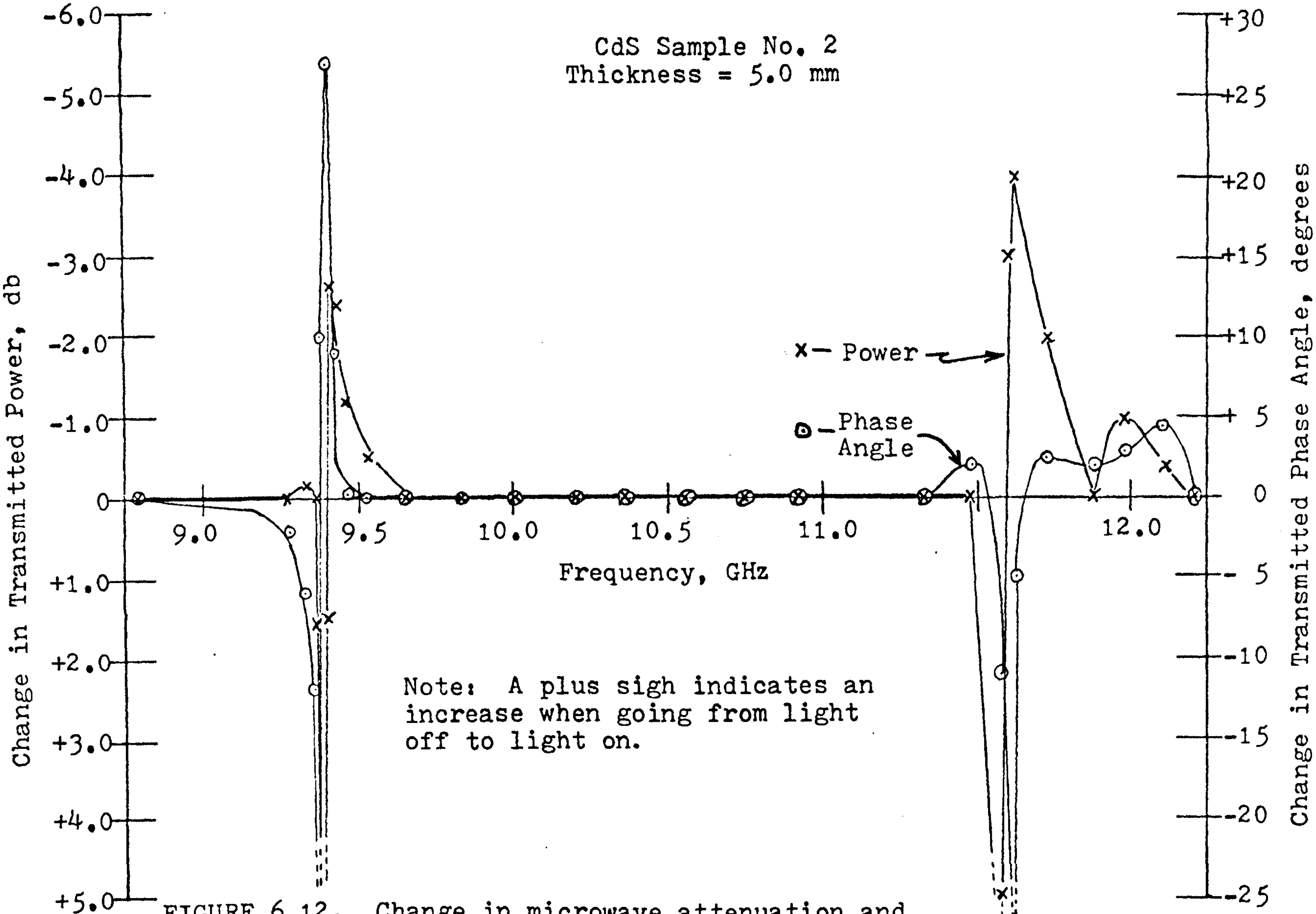

FIGURE 6.12. Change in microwave attenuation and phase shift produced by CdS sample No. 2

TABLE 6.4. Typical values for the change in microwave attenuation and phase shift produced by illuminated CdS samples

Sample No.	Attenuation Change (db)	Phase Shift Change (deg.)	Test Frequency (GHz)
2	+0.15	+0	9.98
4	+1.05	+4	8.365
6	+1.7	-6	10.013
8	-1.85	-27	10.013
9	+0.13	+2	10.013
10	0	0	10.0

Note: A + sign indicates that that quantity increased when going from the dark to the illuminated condition.

sample thickness, and, most important, insufficient filling of the waveguide cross section. The experimental measurements indicate that for the optimum conditions dictated by the theory of Chapter V it should be possible to obtain at least 10 db of microwave attenuation by photoexcitation of CdS crystals.

G. Experiments with CdS Crystalline Powder

The problems with growing large single crystals of CdS make the use of crystalline powder or sintered layers desirable. The large surface area to volume ratio for a powder usually results in a free carrier lifetime one to two orders-of-magnitude less than that for a single crystal. This produces a corresponding decrease in the light to dark conductivity ratio. Unfortunately, this means that the attenuation changes produced by the powdered form will be only 1/100 to 1/10 of that produced by the single crystal.

Figure 6.13 shows the apparatus used for compressing the powdered material. Various binders were tried. The binder most commonly used in the literature was a 3% mixture of ethyl cellulose in diacetone alchol. This resulted in an easily scratched powder possessing practically no mechanical strength. The author found that the use of a small amount of polystyrene plastic cement resulted in a strong, durable powder. With either binder the changes in attenuation due to illumination were barely detectable (typically 0.05 db at 40 foot-candles). Considerable research with powdered materials is required. It may be possible through

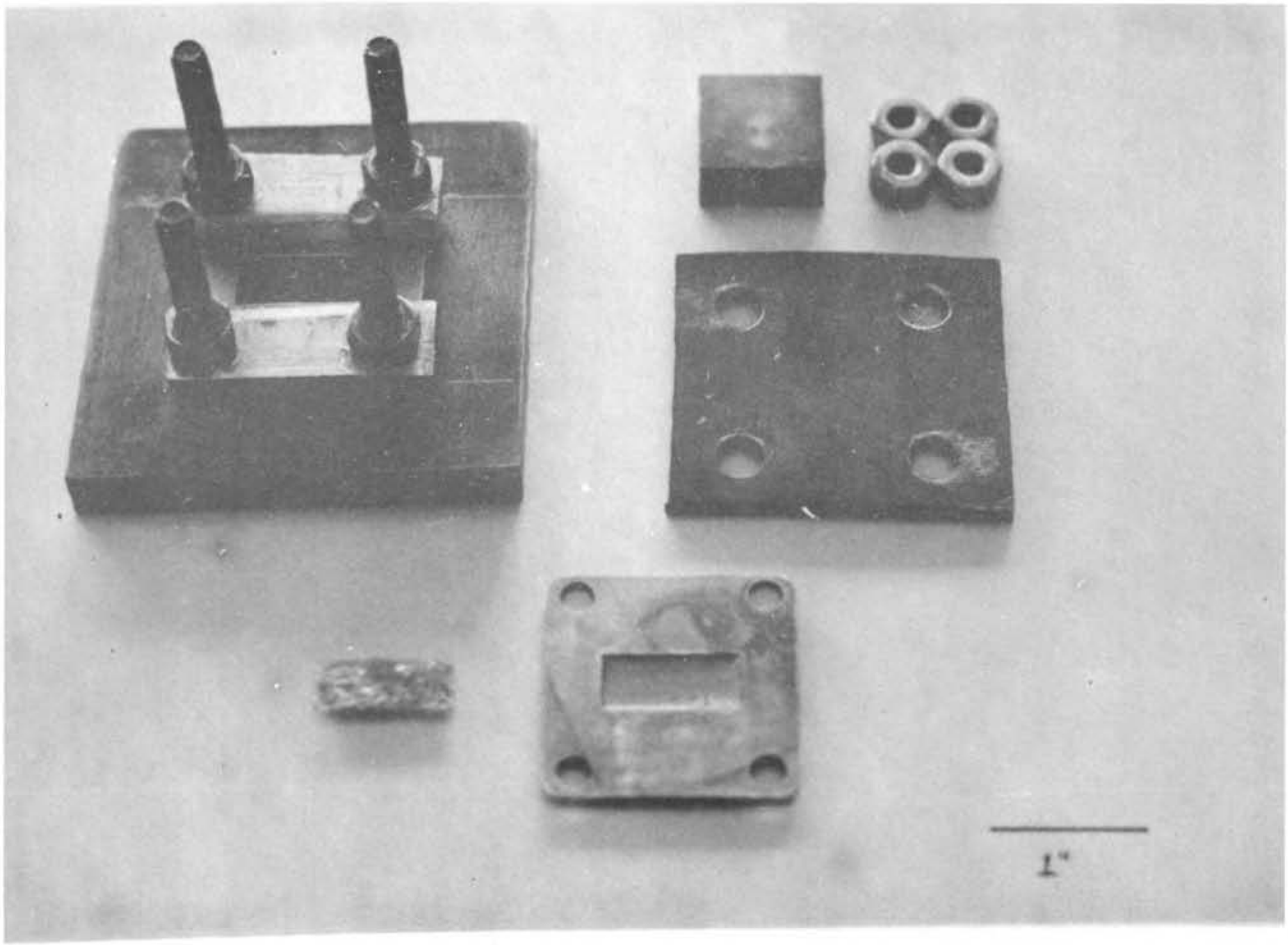

FIGURE 6.13. Device used for compressing CdS powder

the interaction of microwaves and photoexcited powders to measure the interfacial polarization and the surface lifetime.

VII. MICROWAVE MEASUREMENT OF THE FREE CARRIER LIFETIME AND COMPLEX PERMITTIVITY OF SEMICONDUCTING MATERIALS

A. Introduction

The purpose of this chapter is two-fold:

1) Develop the theory for the microwave measurement of free carrier lifetimes, and then present the experimentally measured results for dc and microwave lifetimes of electrons in CdS;

2) Discuss some of the methods used and experimental difficulties encountered in the measurement of complex permittivity, and then present experimental results for the conductivity measurements on thin silicon wafers.

Both of the topics discussed in this chapter are of extreme practical importance. The free carrier lifetime, conductivity, and dielectric constant are key parameters which determine most of the electrical properties of any material. A detailed understanding of both derived theory and experimental techniques are required in order to make accurate measurements of any one of the above three parameters.

B. Lifetime Measurement

1. dc Lifetime

The circuit used to measure the dc lifetime of the photoexcited majority carriers in CdS is presented in Figure 7.1, and a photograph of the experimental apparatus is shown in Figure 7.2. The output voltage is determined by

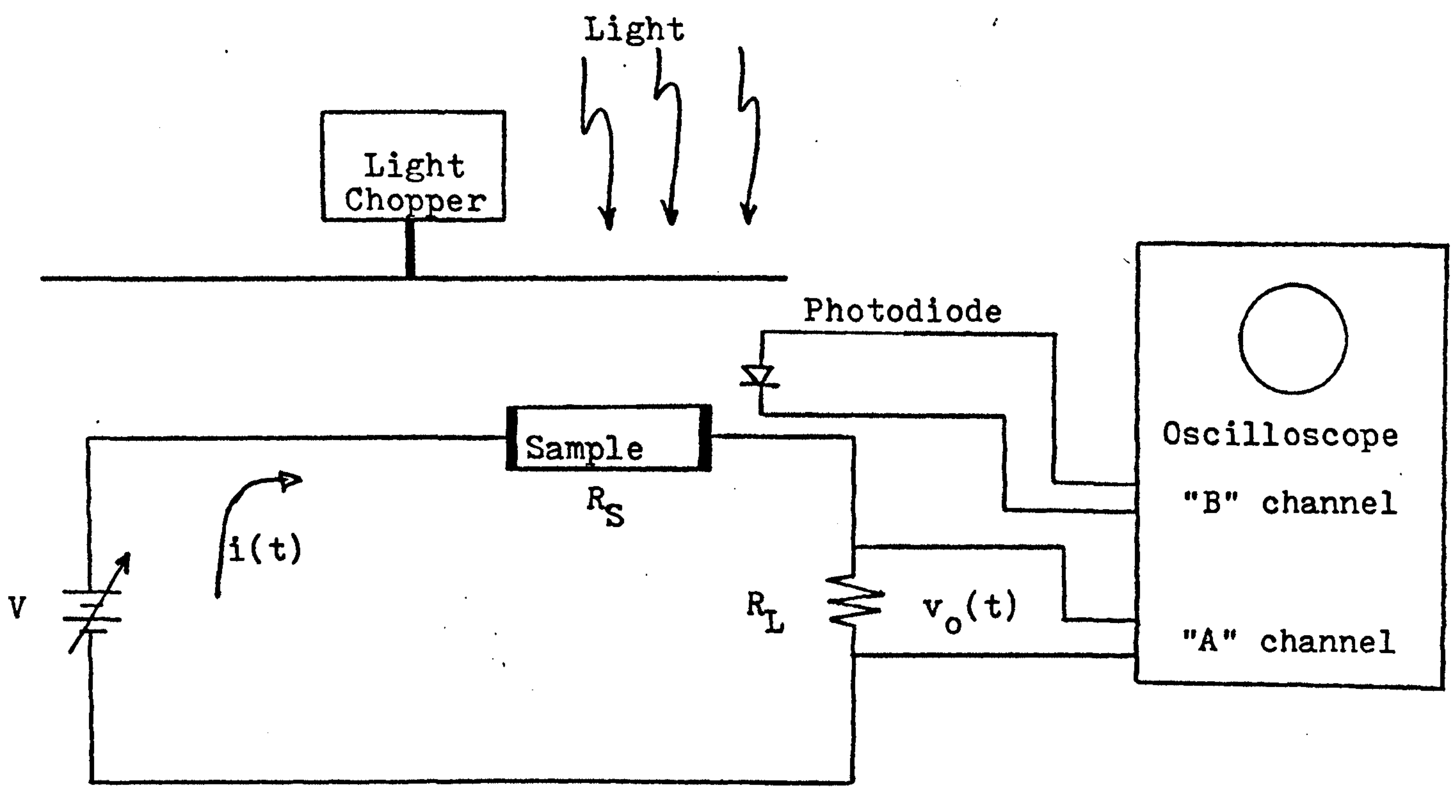

FIGURE 7.1. Circuit used to measure the dc lifetime of CdS

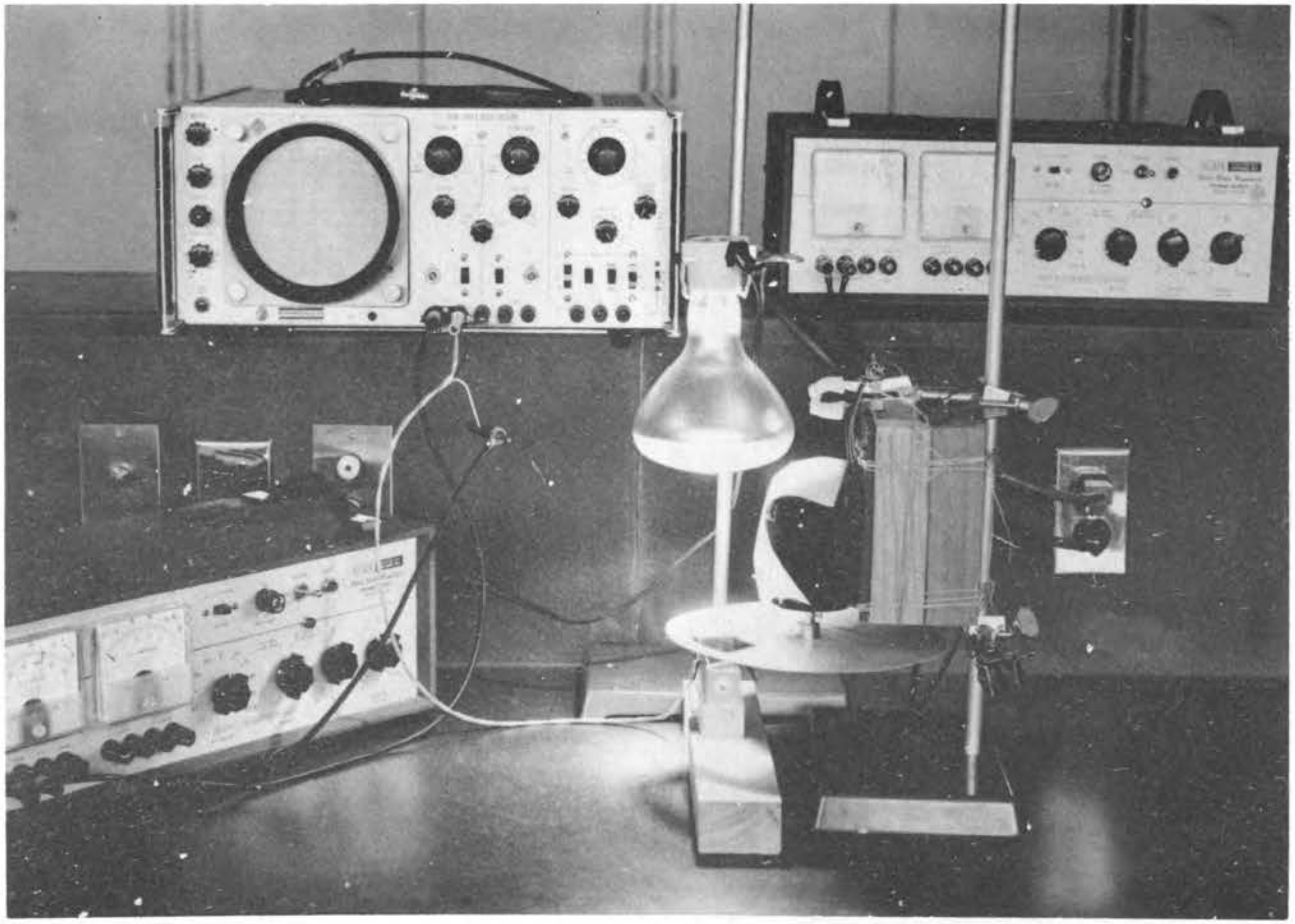

FIGURE 7.2. Experimental apparatus used to measure the dc lifetime of electrons in CdS

$$v_o(t) = \frac{VR_L}{R_s(t) + R_L} \tag{7.1}$$

Immediately after the cessation of a light pulse the time varying sample resistance is

$$R_s(t) = \frac{L}{\sigma A} = \frac{L}{q\mu_n n_o + (\Delta n)\exp(-t/\tau_n)A}, \tag{7.2}$$

where n_o and Δn represent the dark equilibrium density and photoexcited density of free electrons, respectively, L and A are the length and cross sectional area of the rectangular sample, and τ_n is the electron lifetime. For the CdS samples tested n_o was 10^{16} to 10^{17} electrons/m^3 and Δn was 10^{19} to 10^{20} electrons/m^3. Hence, $R_s(t)$ can be accurately approximated by

$$R_s(t) \approx K_1 \exp(t/\tau_n). \tag{7.3}$$

Choosing the load resistor R_L much less than $R_s(t)$ yields

$$v_o(t) \approx K_2 \exp(-t/\tau_n). \tag{7.4}$$

The electron lifetime can be measured from a photograph of the exponentially decaying voltage waveform on the oscilloscope. Typical photographs are shown in Figure 7.3. Logarithmic plots of the voltage decay data from the two photographs are presented in Figure 7.4. The initial lifetimes for samples No. 2 and 5 are 42 msec and 19.5 msec, respectively. In most cases exponential decays with two different time constants (lifetimes) were observed. These different lifetimes are easily explained in terms of trapping effects (86). The lifetime was found to decrease with increasing light intensity as indicated by Ryvkin (87). The

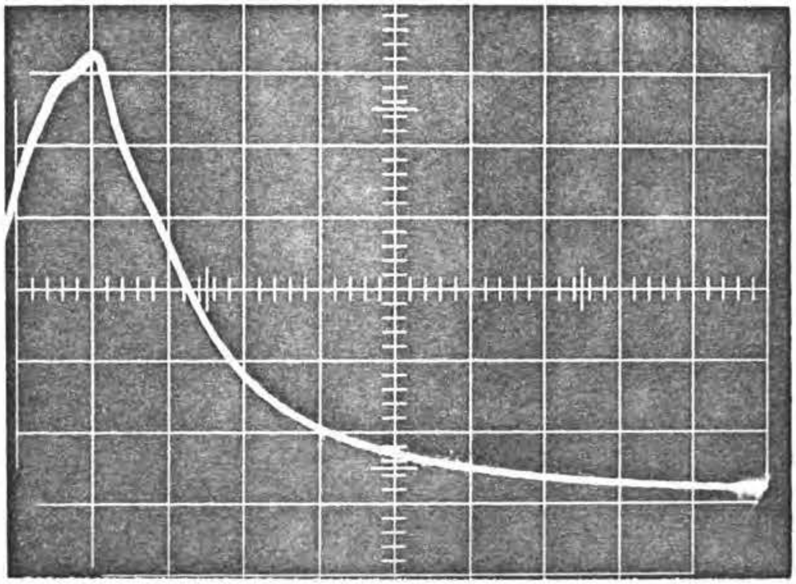

(a)

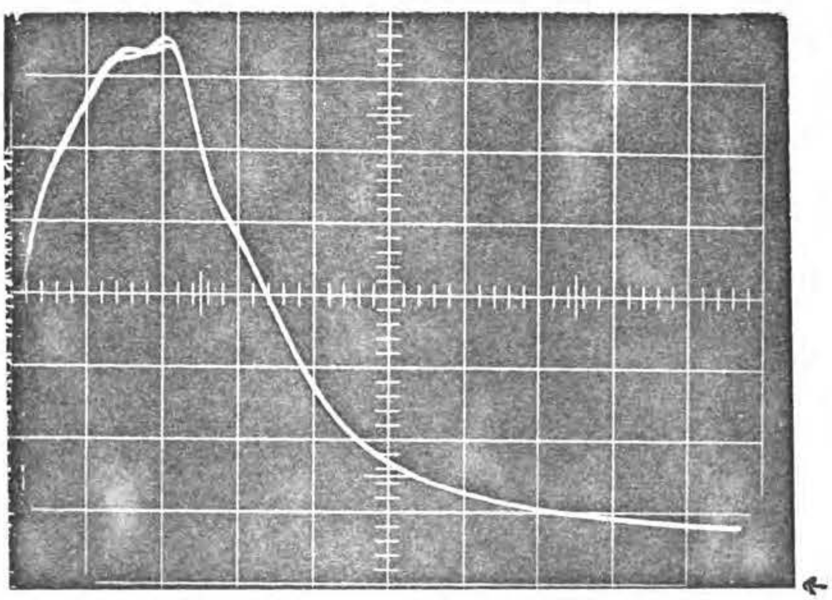

(b)

FIGURE 7.3. dc lifetime measurement of CdS. (a) Sample No. 2, Vert. = 10 mvolts/cm, Horz. = 20 msec/cm; (b) Sample No. 5, Vert. = 10 mvolts/cm, Horz. = 10 msec/cm. (Bottom line is reference.)

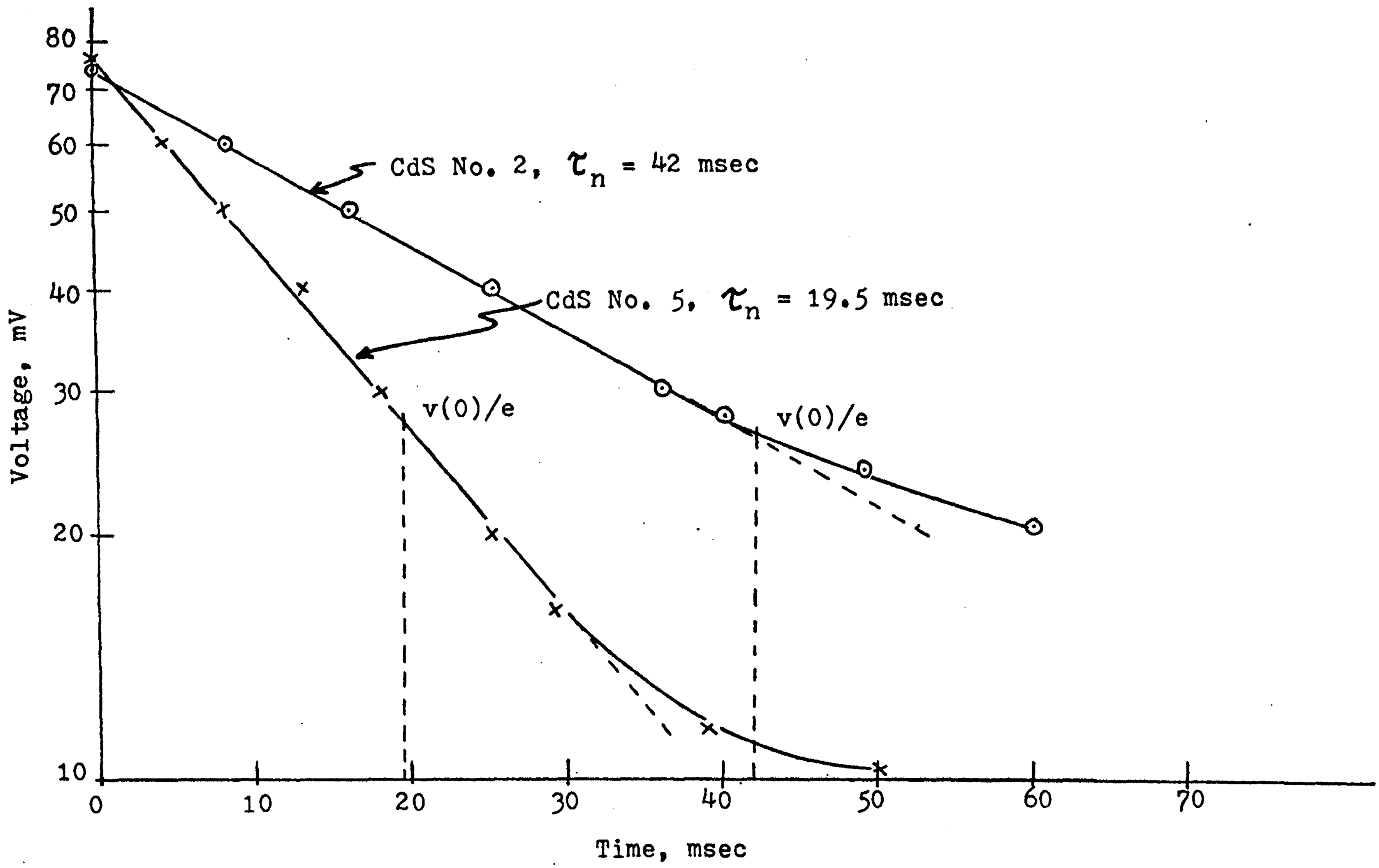

FIGURE 7.4. dc measurement of electron lifetime for CdS samples No. 2 and 5 from exponential voltage decay

extent to which surface conditions affected the lifetime was not investigated. This experimental procedure can be considered accurate only for times up to approximately two or three initial time constants. For times after this, the assumption that

$$(\Delta n)\exp(-t/\tau_n) >> n_o, \qquad (7.5)$$

used in deriving equation (7.5), may no longer be valid.

Indium contacts were formed on the CdS samples by pressing thin wafers of In on each end of the samples and then passing a large current (10 mA) at high voltage (400 V) through the illuminated sample for a few seconds. Illumination of the contacts during the lifetime measurements produced less than a 10% change in the lifetime.

2. Microwave Lifetime

A detailed derivation of the time varying microwave power transmitted through a section of rectangular waveguide filled with a linear, isotropic, homogeneous material with a time varying conductivity is presented in Appendix E. A thorough understanding of this derivation, including the assumptions, is a necessary prerequisite to making accurate experimental measurements. The resulting expression for the transmitted power is

$$P_t(t) \approx P_o\exp\left[K\exp(-t/\tau_n)\right], \qquad (7.6)$$

where P_o and K are constants defined in the Appendix. In the literature review it was pointed out that many investigators are using an oversimplified expression for $P_t(t)$ which neglects the transmission and reflection coefficients at the material boundaries. This, plus violation of the assumption that $\sigma << \omega\epsilon$, results in questionable experimental data for much of the work published to date.

The results presented in this dissertation are for low conductivity, single crystals of CdS. A block diagram and photograph of the experimental apparatus are shown in Figures 7.5 and 7.6, respectively. The power incident on the CdS crystals, P_i, was adjusted such that the change in the voltage output from the microwave detector was proportional to $\log_{10}\left[P_t(t)/P_i\right]$. Thus, the detector voltage displayed on the oscilloscope was of the form

$$v(t) = V_o + K_1 \exp(-t/\tau_n), \tag{7.7}$$

where V_o represents a time independent reference level. The free electron lifetime, τ_n, can be determined from the time constant of the exponential portion of v(t). A typical photograph is shown in Figure 7.7, and the results for CdS samples No. 2 and 5 are plotted in Figure 7.8. Both samples have brief (10 msec) initial exponential decays with time constants approximately 50% longer than their respective dc measured values, followed by long (150 msec) exponential decays each with a time constant of approximately 200 msec. All samples tested followed this same general pattern. A major reason for the difference in the initial lifetime measured at dc and that measured at microwave frequencies is the difference in illumination conditions. In order to satisfy the assumptions for each type of measurement, the illumination was strong in the dc case and weak in the

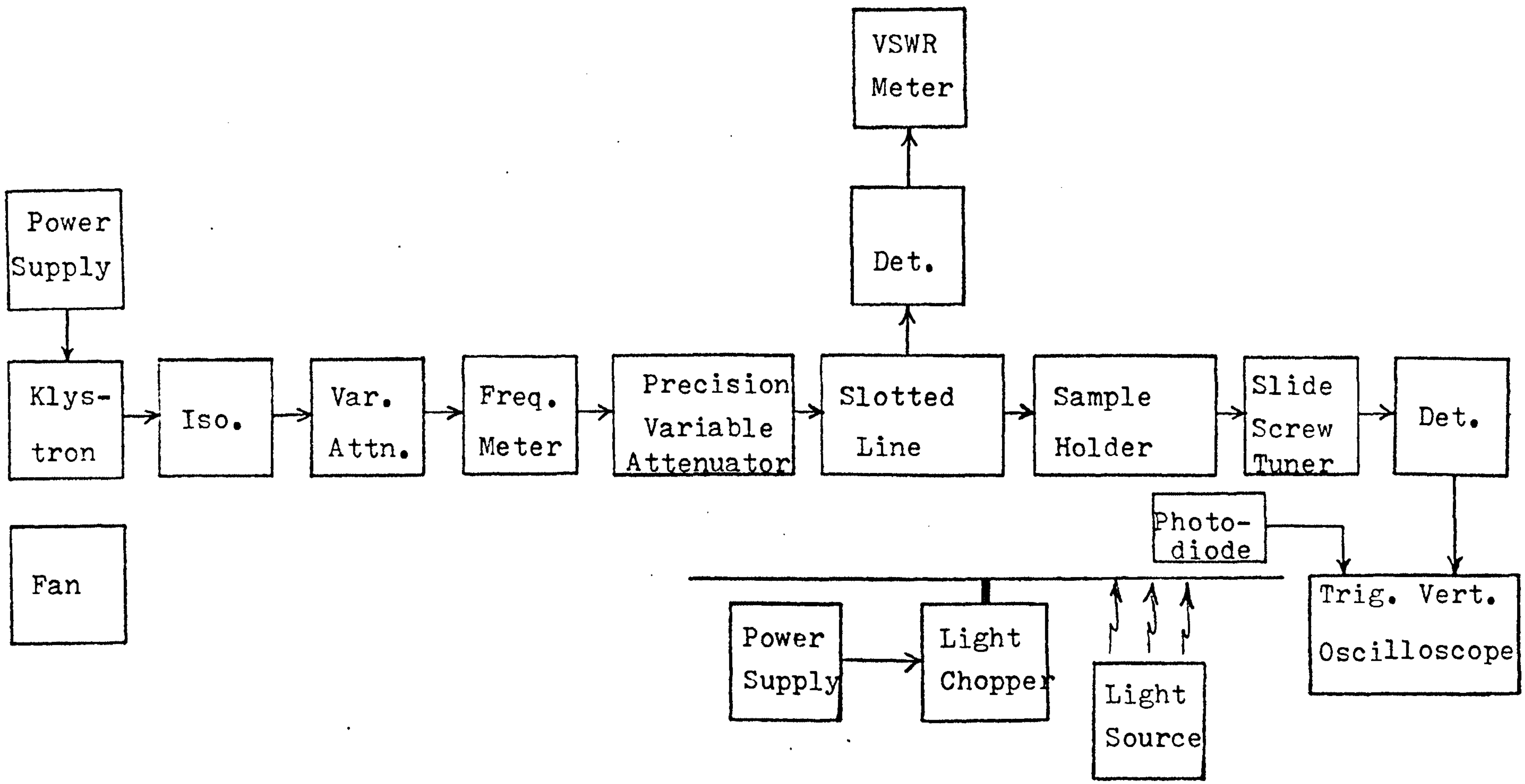

FIGURE 7.5. Block diagram of the experimental apparatus used for the microwave measurement of the free electron lifetime in CdS

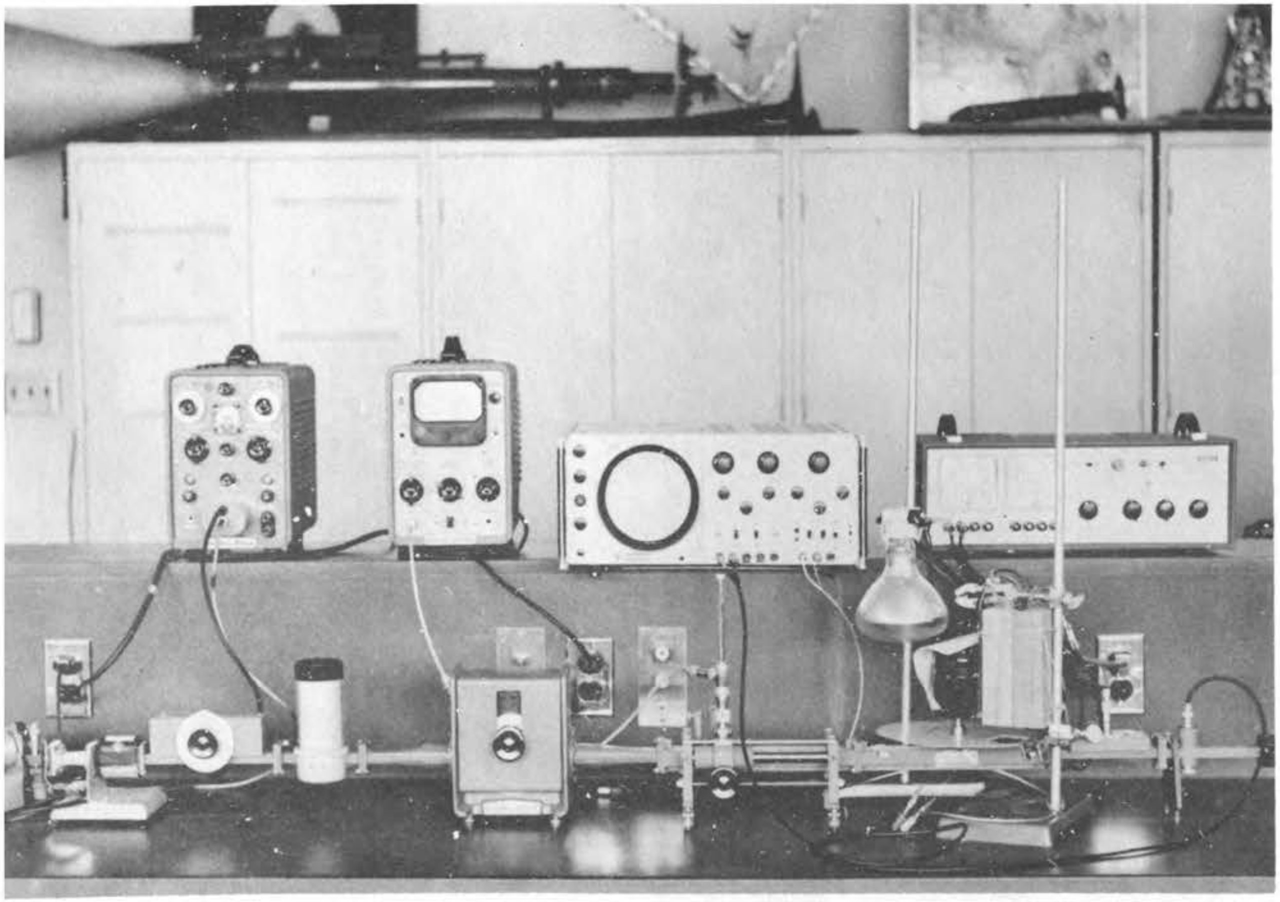

FIGURE 7.6. Experimental apparatus used for the microwave measurement of the electron lifetime in CdS

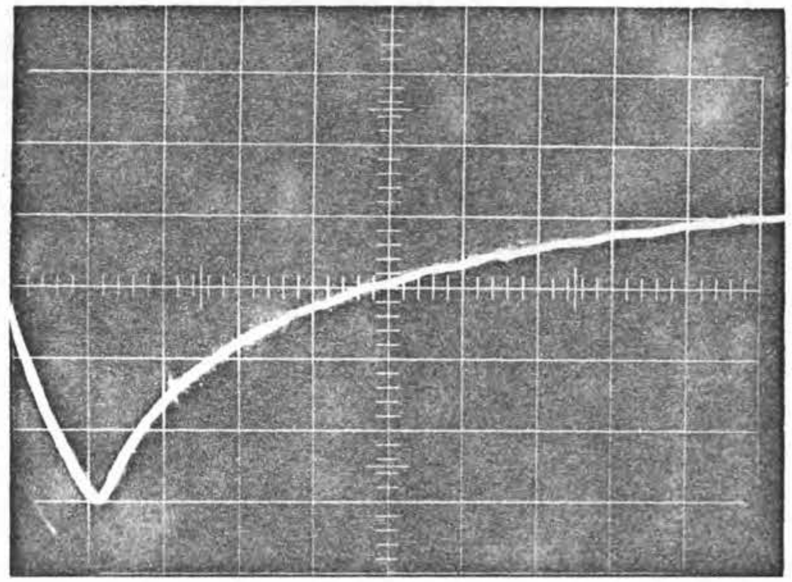

FIGURE 7.7. Microwave lifetime measurement of CdS sample No. 2. Vert. = 10 mvolts/cm, Horz. = 20 msec/cm. (Top line is reference level.)

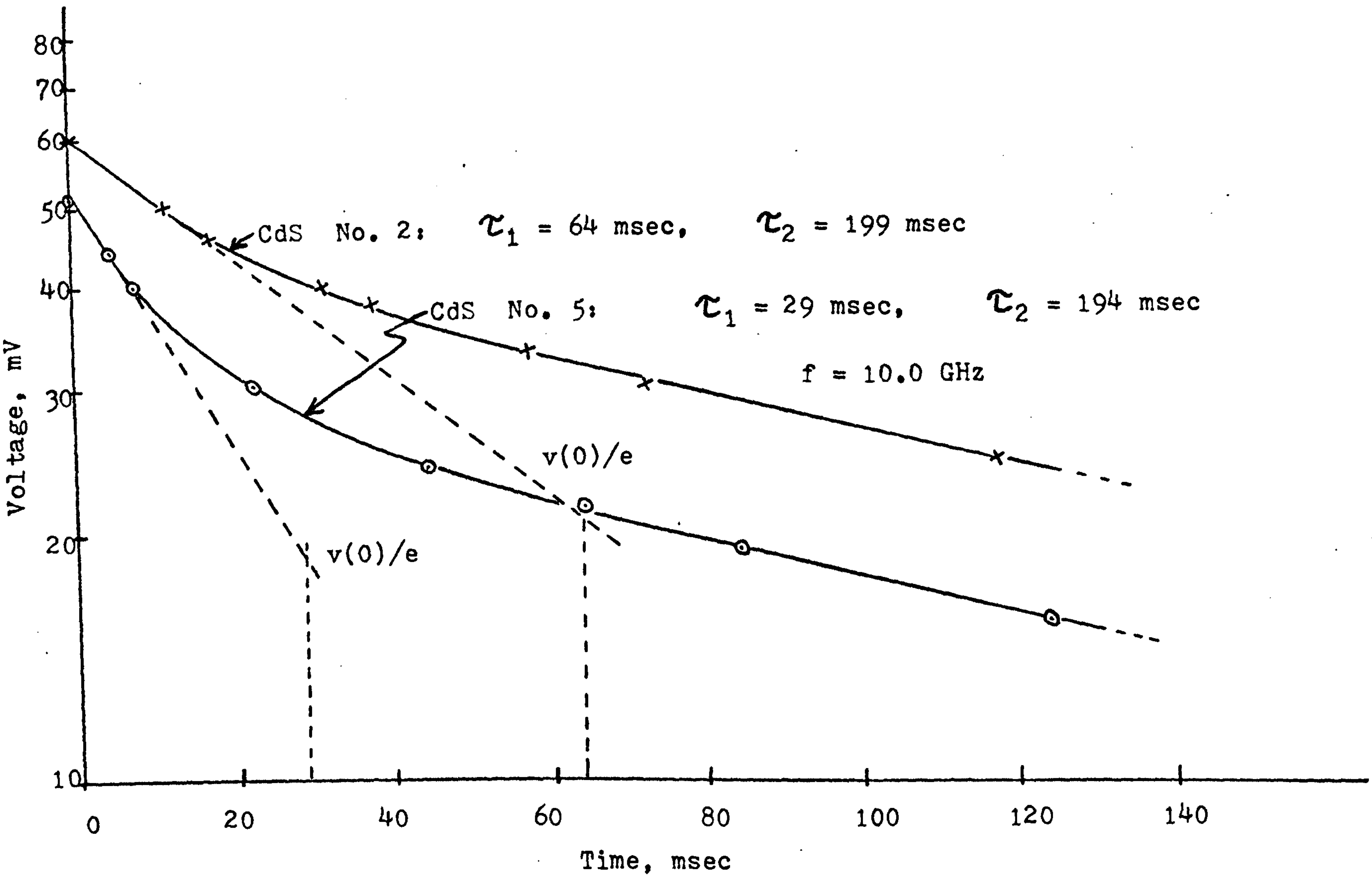

FIGURE 7.8. Microwave measurement of electron lifetime for CdS samples No. 2 and 5 from exponential detector voltage decay

microwave case. Normally, the measured lifetime decreases with increasing light intensity, and, hence it was expected that the dc lifetime would be smaller than the microwave lifetime. The time constant of the second exponential decay could not be accurately measured by the dc technique. The manufacturer's measurements of electron lifetime were not available for the specific crystals tested, however, typical values for the "average" lifetime of crystals of this type are 150 msec to 600 msec (88). There is some doubt about the true cause of the long lifetime measured at microwave frequencies. In the above discussion the cause was assumed to be the trapping and later thermal release of conduction electrons. Even though the measured value of 200 msec falls within the expected range, the author has an intuitive suspicion that such effects as dipole relaxation may have influenced the measured value. Considerable further research is required in this area.

C. Complex Permittivity Measurement

1. General Discussion

In general the determination of both the real and imaginary parts of the complex permittivity at a particular frequency requires two independent measurements. Measurement of the magnitude and phase of the reflection coefficient or magnitude and phase of the transmission coefficient are two examples. For a given sample thickness and frequency, the computer calculations of Chapter V could be expanded into a set of nomographs from which the real and imaginary parts could be easily determined from experimental data. If either the real or imaginary part is known, then only one experimental measurement is required.

The theory used in predicting the experimental results for complex permittivity measurements assumes perfect contact between the sample and the waveguide walls. This is never achieved in practice, since there are usually very small air gaps between the sample and the walls. If either $\sigma_f \gtrsim \omega \epsilon_b$ or $\epsilon_b > 20$ significant errors can result in the measured values of σ_f and ϵ_b. Champlin, et al. (89, 90) have analyzed this problem in considerable detail and proposed a unique solution. If circular waveguide, operating in a mode with the transverse electric field in the radial direction only, is used instead of rectangular waveguide, then there is no electric field across the sample-waveguide junction and potential barriers at the junction have no influence on the measured result. This particular technique could be easily used to measure the conductivity of silicon wafers since they are normally of circular cross section. This would eliminate one of the major sources of error when measuring the conductivity of highly conductive samples.

In the remainder of the chapter, computer calculated results are used in combination with experimental measurements for rectangular waveguide to determine the relative dielectric constant of some lossless dielectrics and the conductivity of several thin Si wafers.

2. Measurement of the Relative Dielectric Constant of Lossless Dielectrics

The main purpose of this section is to provide additional experimental verification of the theory and computer programs used in Chapter IV and V. Figure 7.9 shows the calculated variation in VSWR with relative dielectric constant for a rectangular waveguide filled with a homogeneous, lossless dielectric. The relative dielectric constant was determined by measuring the VSWR produced by a 5 mm thick sample and then using Figure 7.9. The excellent agreement between the measured values and the manufacturer's published values is evident from Table 7.1.

3. Measurement of the Conductivity of Thin Silicon Wafers

The purpose of this section is to demonstrate the feasability of using microwave techniques to measure the conductivity of Si wafers. The microwave method measures the average conductivity of the bulk material, whereas, the presently used four point probe technique determines the conductivity of only one small section of a wafer. Also, the probe method requires corrections when used on "thin" samples and is more influenced by surface conditions than are the microwave measurements.

Assuming the relative dielectric constant is known ($\epsilon_r = 12$), the conductivity can be determined from the re-

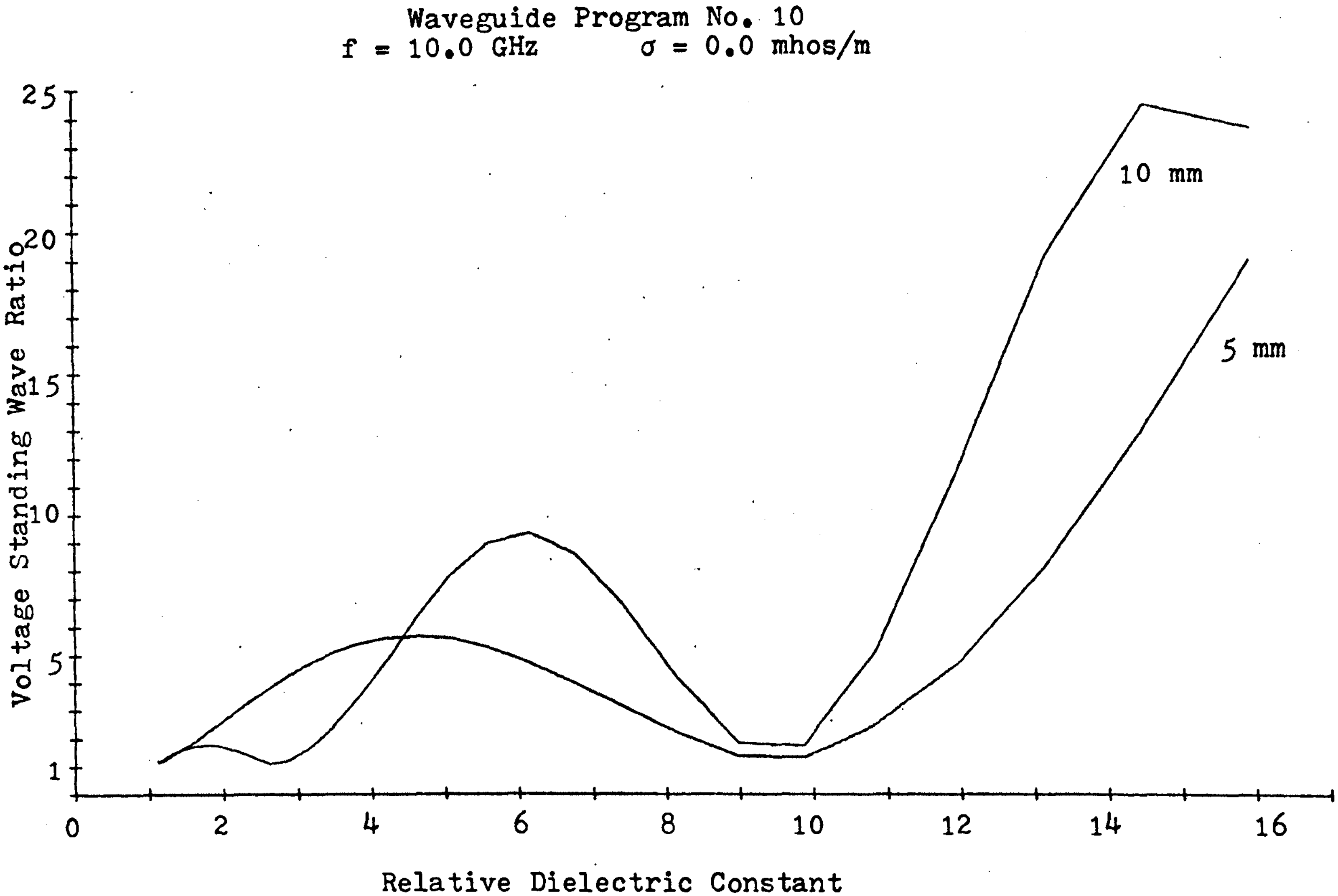

FIGURE 7.9. VSWR versus relative dielectric constant for rectangular waveguide filled with a lossless dielectric

TABLE 7.1. Comparison of experimentally measured and manufacturer specified values of the relative dielectric constant of several lossless dielectrics

Measured* VSWR	ϵ_r from Computer Data	ϵ_r from Manufacturer's Specifications
4.3	2.9	3.0
5.4	3.8	4.0
3.9	6.7	6.0
1.41	9.95	10.0

Note: Sample thickness is 5 mm in each case.

* 10.0 GHz

sults of a simple VSWR measurement. Using an arrangement similar to that shown in Figures 6.2 and 6.3 (with the light source removed), each wafer was placed transverse to the waveguide axis between the two flat flanges connecting the slotted line and the matched load. A production line process for automatic microwave conductivity measurements could be patterned after this technique. The VSWR measurements were used in combination with computer calculated data to determine the conductivity. In Table 7.2, the results of the microwave measurements for several samples are compared with the manufacturer's measured range. The microwave measurements are consistently near the smaller value of the expected range. The uncertainty in the sample thickness could account for this, since an average value was used in the computer calculation. In order to perform highly accurate microwave measurements, the tolerance on the thickness measurements would have to be reduced and the frequency should be adjusted to bring the VSWR into the 1.2 to 1.4 range. By using different frequencies in the 1 GHz to 30 GHz range, conductivities from approximately 0.01 mhos/m to 50 mhos/m could be accurately measured.

TABLE 7.2. Comparison of microwave conductivity measurements with the manufacturer's expected range for several thin Si wafers

Sample Thickness (mils)	Manufacturer's Measured Range (mhos/m)	VSWR	Microwave* Conductivity (mhos/m)
4.0 - 4.5	5 - 10	1.53	7.1
1.8 - 2.2	33 - 50	1.87	31
1.8 - 2.2	11 - 20	1.40	13
1.8 - 2.2	4 - 6.7	1.21	4.9
1.8 - 2.2	6.7 - 10	1.24	6.5
1.7 - 2.3	16.7 - 25	1.43	14
1.6 - 2.3	36 - 43	2.0	36
2.0 - 3.0	20.8 - 3.13	1.70	22
2.5 - 3.3	11.4 - 19	1.62	15
2.8 - 3.2	29.2 - 48.4	2.25	32

*9 GHz

VIII. MICROWAVE APPLICATIONS FOR PHOTOCONDUCTIVE MATERIALS

A. Introduction

The purpose of this chapter is to briefly describe three new microwave applications for photoconductive materials and to add some new ideas to one existing application. In some cases the results of limited experimental work are described. The author also investigated additional applications such as demodulation of microwave modulated light, variable frequency bandpass filters, microwave mixing, and frequency multiplication, which are not described.

B. Photocontrolled Antenna Array

By using either the photoconductive or photodielectric effect of certain materials it is possible to vary amplitude and phase of the electromagnetic energy radiated from each element in an antenna array. This can be accomplished by placing a properly shaped sample of the material in each feed line leading to the individual elements, in a manner similar to that presently used for ferrite phase shifters. The theoretical calculations of Chapter V indicate that at least 10 db of attenuation or 30 degrees of phase shift could be obtained with reasonable light intensities (< 100 foot-candles) if the sample thickness and dark conductivity are properly chosen.

Another method of forming an antenna array (91) was attempted experimentally. This consisted of covering (almost completely) the open end of an X-band waveguide terminated in an "infinite" ground plane with a thin single crystal of CdS. It was anticipated that illumination of alternate strips, parallel to the narrow wall of the waveguide, would reduce the radiation from these strips because of their increased conductivity, thus causing the resulting antenna pattern to be dependent upon the non-illuminated strips. It was further anticipated that the antenna pattern could be changed by changing the width, separation, and number of nonilluminated strips. The experiment failed because the light diffused throughout the entire crystal resulting in essentially a uniformly increased conductivity, rather than alternate highly conductive strips. Further experiments were not attempted, however, if the light diffusion problem can be eliminated (possibly by the use of individual crystals separated by light shields) the above method could result in a very unique and practical antenna array.

C. Variable Impedance Waveguide Terminations

Variable impedance waveguide terminations for impedance matching and mismatching purposes can be made if photoconductive material is used as part of the termination. Figure 8.1 shows the theoretically predicted variation in VSWR with increasing conductivity of the photoconductive material for the particular load arrangement shown in the insert of that figure. For the photoconductive section terminated with a waveguide of characteristic impedance $Z_{OL} = 1.0 + j0.5$, the

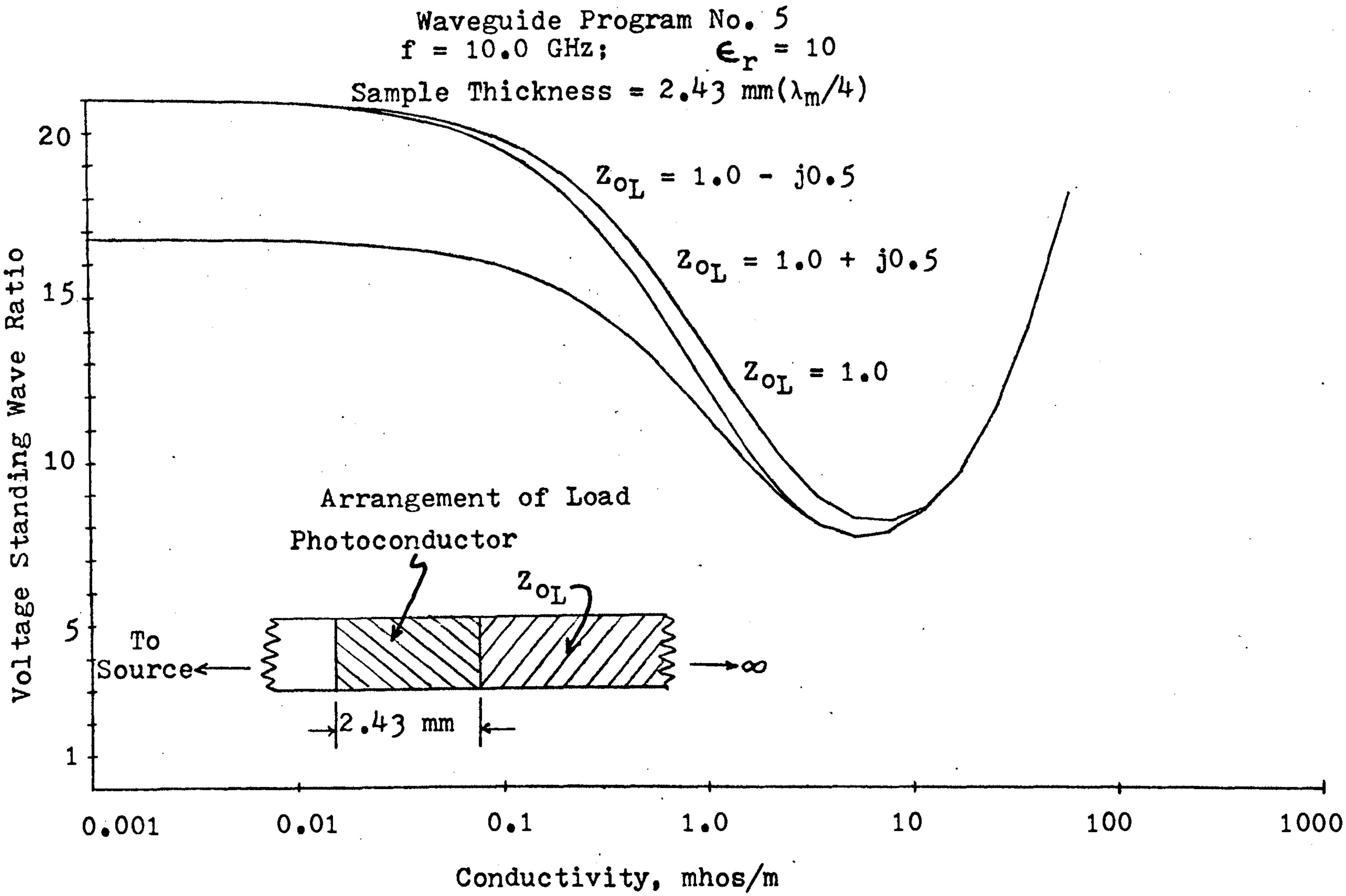

FIGURE 8.1. VSWR versus conductivity for a mismatched, photoconductive, waveguide termination

VSWR can be varied from 21 to 8 by increasing the conductivity from 0.01 mhos/m to 5.0 mhos/m. The range over which the VSWR varies can be easily changed by changing the sample thickness. Table 8.1 indicates the experimental results for the VSWR and impedance of a different load arrangement under illuminated and non-illuminated conditions. A Smith chart was used to determine the characteristic impedance from measurements of the VSWR and the shift in the first minimum point of the VSWR pattern, when the load was replaced by a "short circuit". The table indicates that the illumination increases considerably the real part of the load impedance, but has little effect on the imaginary part.

D. <u>Precision Variable Attenuator</u>

Figure 8.2 shows an artist's conception of a photo-controlled, precision variable, microwave attenuator. The attenuation is produced by the photoconductive coating on the thin dielectric strip. The attenuation is increased by mechanically increasing the width of the slit in the light shield between the source and the photoconductor. The purpose of the photodiode is to supply a voltage to the calibration meter, that is proportional to the light intensity from the source. The calibration meter indicates when recalibration is necessary because of changes in the light source intensity. Devices of this type should be capable of producing an attenuation accurate to within ± 0.05 db for at least the 0 db to 5 db range. More exotic designs using such sources as

TABLE 8.1. Variation in VSWR and impedance with illumination conditions for a photoconductive waveguide load

CdS Sample No.	Illumination Condition	Location of First Minimum	VSWR	Characteristic Impedance (ohms)
1	No light	9.32 cm	2.0	0.57 - j0.34
	40 fc	9.35 cm	1.7	0.66 - j0.30
2	No light	9.53 cm	14	0.15 - j1.02
	40 fc	9.53 cm	3.8	0.5 - j0.9
3	No light	9.05 cm	11.8	0.08 - j0.0
	40 fc	9.05 cm	4.8	0.20 - j0.0

Arrangement of load:

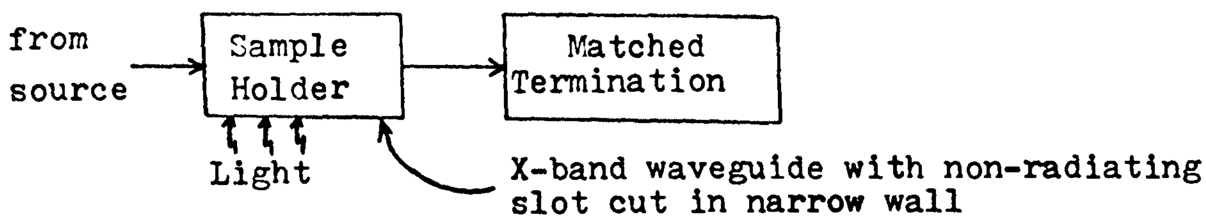

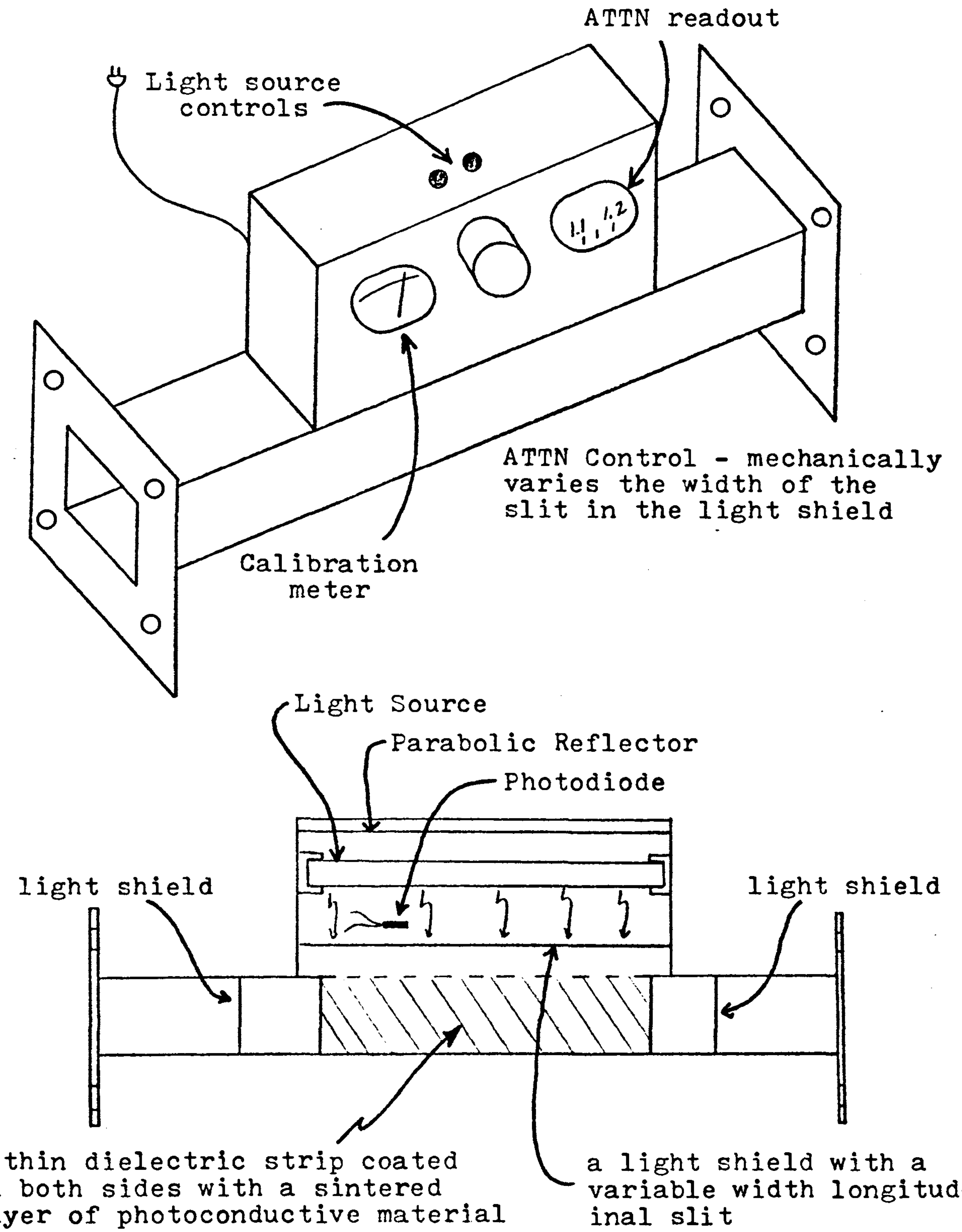

FIGURE 8.2. Artist's conception of a photocontrolled, precision variable, microwave attenuator

GaAs light emitting diodes may also prove practical. These designs would permit electronic rather than mechanical variation of the attenuation.

E. Microwave Modulation

A limited amount of work (42, 92, 93) has already been done in the area of photoconductive modulation of a microwave carrier. The long lifetime of the free carriers presently seriously limits the modulation to frequency components less than approximately 100 KHz. Both phase and amplitude modulation of either the transmitted or the reflected signal are possible, depending upon the range over which the conductivity is varied. This was illustrated in Chapter V. Figure 8.3 indicates a new and potentially useful effect. For the case of phase modulation of the reflected signal, the range of phase variation may be increased if the photoconductive section of the waveguide is terminated with a reactive load. For a matched load the phase may be varied by typically 80 degrees, however, Figure 8.3 shows that this may easily be increased to 110 degrees for a load with a characteristic impedance of (1 + j0.5) ohms.

Another very promising modulation technique is variation of the dielectric constant by photoexcitation. Very little work has been done in this area because the change produced in the room temperature dielectric constant at microwave frequencies by photoexcitation is normally considered negligible for the materials presently used. However, the experi-

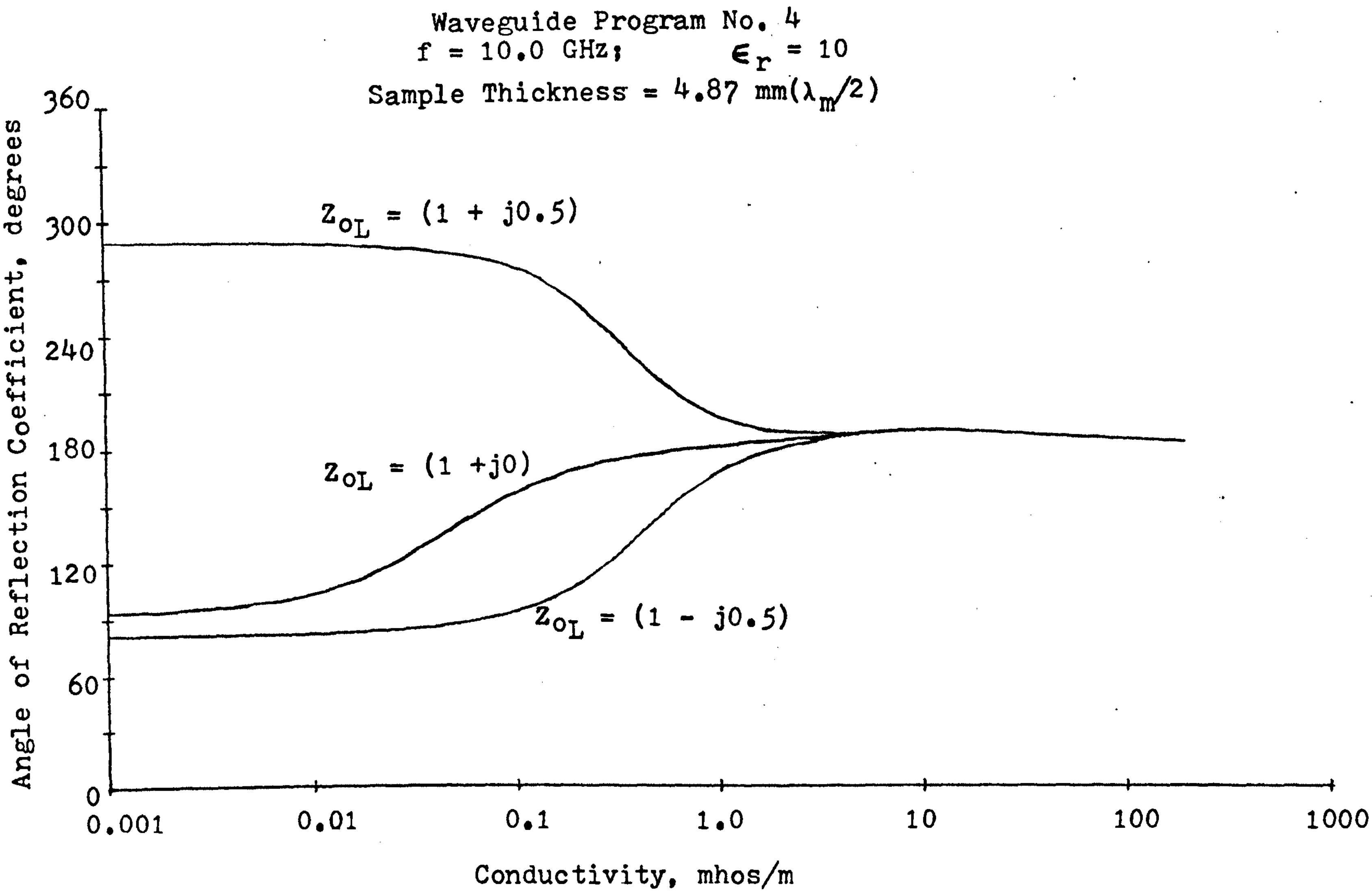

FIGURE 8.3. Variation in angle of reflection coefficient with conductivity for a section of filled waveguide terminated with loads of different characteristic impedance

ments conducted by the author on CdS (Chapter VI) gave some indications of significant changes in dielectric constant as well as conductivity. A 10% change in the dielectric constant can have as much of an effect as an order-of-magnitude change in the conductivity. Hence, only approximately a 5% change in the dielectric constant is required to make photodielectric modulation practical.

IX. SUMMARY

A. General Summary

The primary emphasis has been on the derivation and numerical solution of the electromagnetic field equations for propagation through rectangular waveguide filled with a lossy, isotropic, linear, inhomogeneous media. The theoretical effects of photoinduced conductivity and dielectric constant variations on microwave attenuation, phase shift, and voltage standing wave ratio were calculated and plotted for typical examples in the X-band frequency range. The theoretical predictions were verified qualitatively by experiment. Microwave measurements of the free electron lifetime in CdS and the conductivity of thin Si wafers were accomplished successfully. An unusually strong, room temperature resonance phenomena was observed experimentally in CdS. Some possible explanations were discussed, but no definite conclusions were drawn. Finally, several new microwave applications for photoconductive materials were described.

B. Summary of Original Contributions by the Author

The more significant original contributions presented in this dissertation are listed below in their order of importance.

1) The most important original contribution was the calculation and plotting of microwave attenuation, phase shift, and VSWR as functions of conductivity, sample thickness, and frequency. Many important practical conclusions

were drawn from these graphs. Although others have considered a few special cases, no one has published results as comprehensive as that presented in Chapter V.

2) The accurate microwave measurement of the conductivity of thin Si wafers has demonstrated the practical usefulness of this technique. Although others have performed such measurements on thick (1 cm) samples, very few have attempted measurements on the more commonly used thin wafers with thicknesses ranging from about 0.05 mm to 0.5 mm.

3) A detailed derivation of the microwave transmission through a rectangular waveguide filled with a material having a time varying conductivity was presented. The results of this derivation were used in the microwave free carrier lifetime measurements. This derivation included the effect of reflection from the sample being tested, something often ignored by others, and also clearly indicated <u>all</u> assumptions that must be met in order to make accurate lifetime measurements. The <u>method</u> used in this derivation was developed by the author.

4) Successful measurement at microwave frequencies of the free electron lifetime in CdS was reported. Techniques similar to those used by the author have been previously used by others on Si and Ge, but to date no results have been reported for CdS.

5) An unexpected resonance phenomena, which has the potential of developing into an important discovery, was observed in CdS. No such effect has been reported in the

literature. This phenomena may provide information about some property of CdS such as a microwave-acoustical interaction or a plasma resonance.

6) Several new microwave applications of photoconductors were described, and a few new ideas concerning photoconductive and photodielectric microwave modulation were presented.

C. Suggestions for Further Research

The following suggestions for additional research have been grouped according to the three general areas considered in this dissertation.

1. Microwave Interaction with Lossy Dielectric Materials

There is a definite need for more theoretical work concerning the free carrier contribution to the complex permittivity of semiconductors. One of the major problems involves the formulation of the correct relationship between the locally acting electric field and the macroscopic electric field, when depolarization and plasma resonance effects are included.

Extensive experimental work on the resonance phenomena observed in CdS is needed, and is presently being planned by the author. By narrowing down the possible causes, theoretical work can be initiated that will hopefully explain the phenomena.

Work on the photodielectric effect at microwave frequencies has scarcely begun. Both theoretical and experimental efforts are required in this area.

The microwave properties of photoconductive crystalline powders must be investigated. The present theories on the effects of potential barriers at the grain boundaries and interfacial polarization require critical review and experimental verification.

Some extremely difficult theoretical work is also required concerning electromagnetic wave propagation through a waveguide filled with a lossy, anisotropic media. Since most materials are anisotropic to some extent, such theory is required before experimental results can be satisfactorily predicted and explained.

2. Microwave Measurement of Material Properties

Considerable work remains to be done on the microwave measurement of the free carrier lifetime in many materials. Differences between dc and microwave measured values may prove useful in distinguishing photoconductivity effects from photodielectric effects. The influence of the method of excess carrier generation (photoinduced, injected, etc.) also requires further investigation.

Limited work has been done on the microwave measurement of the mobility of free carriers in Si and Ge. More accurate experimental methods plus measurements on other materials are required.

3. Microwave Applications

After the completion of some of the more basic research mentioned in Section (1), the detailed design of some practical microwave devices should be attempted. Although some possible devices have already been described, it is inevitable that more useful applications will become apparent as further research is conducted.

BIBLIOGRAPHY

1. T.S. Moss, Photoconductivity in the Elements. New York: Academic Press, 1952.

2. R.G. Breckenridge, B.R. Russell, and E.E. Hahn, Photoconductivity Conference. New York: Wiley, 1954.

3. S. Flugge, Electrical Conductivity I, Encyclopedia of Physics, vol. 12. Berlin: Springer-Verlag, 1956, pp. 316-395.

4. D.A. Wright, "Photoconductivity," British J. of Applied Physics, vol. 9, pp. 205-214, June 1958.

5. R.H. Bube and L.A. Barton, "The achievement of maximum photoconductivity performance in cadmium sulfide crystals," RCA Review, pp. 564-598, December 1959.

6. C. Herring, "Transport," J. of Physics and Chemistry of Solids, vol. 8, pp. 543-549, 1959,

7. R.H. Bube, Photoconductivity of Solids. New York: Wiley, 1960.

8. A. Rose, "Photoconductivity in perspective," J. of Physics and Chemistry of Solids, vol. 22, pp. 1-4, 1961.

9. A. Rose, Concepts in Photoconductivity and Allied Problems. New York: Interscience, 1963.

10. S.M. Ryvkin, Photoelectric Effects in Semiconductors. New York: Consultants Bureau, 1964.

11. S. Larach, Photoelectronic Materials and Devices. New Jersey: Van Nostrand, 1965.

12. S.M. Ryvkin, "Kinetics of impurity photoconductivity," J. of Physics and Chemistry of Solids, vol. 22, pp. 5-17, 1961.

13. R.H. Bube, E.L. Lind, and A.B. Dreeben, "Properties of cadmium sulfide with high impurity concentrations," Physical Review, vol. 128, pp. 532-539, October 1962.

14. B.A. Kulp, K.A. Gale, and R.G. Schulze, "Impurity conductivity in single-crystal CdS," Physical Review, vol. 140, pp. A252-A256, October 1965.

15. C.S. Kang, P. Beverley, P. Phipps, and R.H. Bube, "Photoelectronic processes in ZnS single crystals," Physical Review, vol. 156, pp. 998-1009, April 1967.

16. J. Kommandeur, "Photoconductivity in organic single crystals," J. of Physics and Chemistry of Solids, vol. 22, pp. 339-349, 1961.

17. L.N. Ionov, I.A. Akimov, and A.N. Terenin, "Photoconductivity of organic dyes at a frequency of 10^{10} Hz," Soviet Physics-Doklady, vol. 11, pp. 599-602, January 1967.

18. S.M. Thomsen and R.H. Bube, "High-sensitivity photoconductor layers," Rev. of Scientific Instruments, vol. 26, pp. 664-665, July 1955.

19. F.H. Nicoll and B. Kazan, "Large area high-current photoconductive cells using cadmium sulfide powder," J. of the Optical Society of America, vol. 45, pp. 647-650, August 1955.

20. H.B. De Vore, "Gains, response times, and trap distribution in powder photoconductors," RCA Review, vol. 20, pp. 79-91, March 1959.

21. R.H. Bube, "Mechanism of photoconductivity in microcrystalline powders," J. of Applied Physics, vol. 31, pp. 2239-2254, December 1960.

22. G.F. Garlick and A.F. Gibson, "Electron traps and dielectric changes in phosphorescent solids," Proc. of the Royal Society of London, vol. 188A, pp. 485-509, 1947.

23. G.F. Farlick and A.F. Gibson, "Dielectric changes in phosphors containing more than one activator," Proc. of the Physical Society, vol. 62A, pp. 731-736, 1949.

24. H. Kallmann, B. Kramer, and P. Mark, "Impedance measurements on CdS crystals," Physical Review, vol. 99, pp. 1328-1333, August 1955.

25. S. Kronenberg and C.A. Accardo, "Dielectric changes in inorganic phosphors," Physical Review, vol. 101, pp. 989-992, February 1956.

26. P. Mark and H.P. Kallmann, "AC impedance measurements of photoconductors containing blocking layers analyzed by the Maxwell-Wagner theory," J. of the Physics and Chemistry of Solids, vol. 23, pp. 1067-1078, 1962.

27. Y.T. Sikvonen, D.R. Boyd, and E.L. Kitts, "Analysis and performance of a light-sensitive capacitor," Proc. of IEEE, vol. 53, pp. 378-385, April 1965.

28. Y.A. Vidadi and L.D. Rozenshtein, "Photodielectric effect in phthalocyanine," Soviet Physics-Doklady, vol. 11, pp. 516-518, December 1966.

29. N.S. Kasperovich, B.M. Nikolaev, and Y.A. Oksman, "The photodielectric effect in compensated germanium," Soviet Physics-Solid State, vol. 9, pp. 343-345, August 1967.

30. E.Z. Meilikhov, "Photodielectric effect and negative photoconductivity in Ge at 10^{10} cps frequency," Soviet Physics-Solid State, vol. 8, pp. 428-430, February 1966.

31. R.S. Elliott, Electromagnetics. New York: McGraw-Hill, 1966, pp. 327-394.

32. M.A. Heald and C.B. Wharton, Plasma Diagnostics with Microwaves. New York: Wiley, 1965, pp. 392-405.

33. A.R. von Hippel, Dielectrics and Waves. New York: Wiley, 1954.

34. W.M. Schwarz, Intermediate Electromagnetic Theory. New York: Wiley, 1964, pp. 77-82.

35. V.L. Ginzburg, Propagation of Electromagnetic Waves in Plasma. New York: Gordon and Breach, 1960, pp. 27-28.

36. A.F. Gibson, "Infra-red and microwave modulation using free carriers in semiconductors," J. of Scientific Instruments, vol. 35, pp. 273-278, August 1958.

37. J.N. Bhar, "Microwave techniques in the study of semiconductors," Proc. of IEEE, vol. 51, pp. 1623-1631, November 1963.

38. K.S. Champlin, D.B. Armstrong, and P.D. Gunderson, "Charge carrier inertia in semiconductors," Proc. of IEEE, vol. 52, pp. 677-685, June 1964.

39. O. Madelung, Physics of III-V Compounds. New York: Wiley, 1964, pp. 79-82.

40. M.A. Heald and C.B. Wharton, Plasma Diagnostics with Microwaves. New York: Wiley, 1965, pp. 1-12.

41. K. Chen, "Interaction of a high-intensity EM field with a low-density plasma," IRE Trans. on Antennas and Propagation, vol. AP-10, pp. 31-42, January 1962.

42. W.H. Hartwig and G.D. Arndt, "Application of the photodielectric effect to laser communication," Southwestern IEEE Conference, 1966.

43. J.R. Wait, Electromagnetic Waves in Stratified Media. New York: Macmillan, 1962.

44. L.M. Brekhovskikh, Waves in Layered Media. New York: Academic, 1960.

45. J.R. Wait, "Reflection of electromagnetic waves obliquely from an inhomogeneous medium," J. of Applied Physics, vol. 23, pp. 1403-1404, December 1952.

46. J.H. Richmond, "Transmission through inhomogeneous plane layers," IRE Trans. on Antennas and Propagation, vol. AP-10, pp. 300-305, May 1962.

47. J. Heading, "Composition of reflection and transmission formulae," J. of Research of the National Bureau of Standards, vol. 67D, pp. 65-77, January 1963.

48. G.J. Gabriel and M.E. Brodwin, "The solution of guided waves in inhomogeneous anisotropic media by perturbation and variational methods," IEEE Trans. on Microwave Theory and Techniques, vol. MTT-13, pp. 364-370, May 1965.

49. J.H. Richmond, "The WKB solution for transmission through inhomogeneous plane layers," IRE Trans. on Antennas and Propagation, vol. AP-10, pp. 472-473, July 1962.

50. D.A. Holmes, "Propagation in rectangular waveguide containing inhomogeneous, anisotropic dielectric," IEEE Trans. on Microwave Theory and Techniques, vol. MTT-12, pp. 152-154, March 1964.

51. H. Osterberg, "Propagation of plane electromangetic waves in inhomogeneous media," J. of Optical Society of America, vol. 48, pp. 513-520, August 1958.

52. R.E. Collin, Field Theory of Guided Waves. New York: McGraw-Hill, 1960, pp. 79-96.

53. D.A. Holmes and D.L. Fencht, "Electromagnetic wave propagation in briefringent multilayers," J. of Optical Society of America, vol. 56, pp. 1763-1769, December 1966.

54. G.P. Bein, "Plane wave transmission and reflection coefficients for lossy inhomogeneous plasma," IEEE Trans. on Antennas and Propagation, vol. AP-14, pp. 511-513, July 1966.

55. L. Young, "Prediction of absorption loss in multilayer interference filters," J. of the Optical Society of America, vol. 52, pp. 753-761, July 1962.

56. B. Salzberg, "Propagation of electromagnetic waves through a stratified medium. I," J. of the Optical Society of America, vol. 40, pp. 465-470, July 1950.

57. H.W. Baeumler, "Reflection, transmission, and abrosption of plane electromagnetic waves by lossy dielectric panels," Ohio State Research Foundation, Report 777-17, August 1960.

58. H. Jacobs, F.A. Brand, J.D. Meindl, S. Weitz, and R. Benjamin, "New microwave techniques in the measurement of semiconductor phenomena," IRE International Convention Record, pp. 30-42, 1962.

59. M.W. Gunn, "Wave propagation in rectangular waveguide containing a semiconducting film," Proc. IEEE, vol. 114, pp. 207-210, February 1967.

60. H. Jacobs, G. Morris, and R.C. Hofer, "Interferometric effect with semiconductors in the millimeter-wave region," J. of the Optical Society of America, vol. 57, pp. 993-997, August 1967.

61. D.T. Stevenson and R.J. Keyes, "Measurement of carrier lifetimes in germanium and silicon," J. of Applied Physics, vol. 26, pp. 190-194, February 1955.

62. R.L. Watters and G.W. Ludwig, "Measurement of minority carrier lifetime in silicon," J. of Applied Physics, vol. 27, pp. 489-496, May 1956.

63. J.S. Blakemore, "Lifetime in p-type silicon," Physical Review, Vol. 110, pp. 1301-1308, June 1958.

64. B.R. Nag and P. Das, "Microwave propagation in semiconductors with carrier density varying in time," IRE Trans. on Microwave Theory and Techniques, vol. MTT-10, pp. 564-567, November 1962.

65. H.A. Atwater, "Microwave measurement of semiconductor carrier lifetimes," J. of Applied Physics, vol. 31, pp. 938-939, June 1960.

66. A.P. Ramsa, H. Jacobs, and F.A. Brand, "Microwave techniques in measurement of lifetime in germanium," J. of Applied Physics, vol. 30, pp. 1054-1060, July 1959,

67. H. Jacobs, A.P. Ramsa, and F.A. Brand, "Further consideration of bulk lifetime measurement with a microwave electrodeless technique," Proc. of IEEE, vol. 48, pp. 229-233, February 1960.

68. S. Deb and B.R. Nag, "Measurement of lifetime of carriers in semiconductors through microwave reflection," J. of Applied Physics, vol. 33, p. 1604, April 1962.

69. H. Jacobs, F.A. Brand, J.D. Meindl, M. Benanti, and R. Benjamin, "Electrodeless measurement of semiconductor resistivity at microwave frequencies," Proc. of IRE, vol. 49, pp. 928-932, May 1961.

70. H. Jacobs, F.A. Brand, and J.D. Meindl, "Multiple reflections of microwaves propagating through a semiconductor medium," Proc. IRE, vol. 49, pp. 1683-1684, November 1961.

71. B.R. Nag and S.K. Roy, "Microwave measurement of conductivity and dielectric constant of semiconductors," Proc. of IEEE, vol. 50, pp. 2515-2516, Decmeber 1962.

72. B.R. Nag, S.K. Roy, and C.K. Chatterji, "Microwave measurement of conductivity and dielectric constant of semiconductors," Proc. IEEE, vol. 51, p. 962, June 1963.

73. B.R. Nag, S.K. Roy, and C.K. Chatterji, "Correction to 'Microwave measurement of conductivity and dielectric constant of semiconductors'," Proc IEEE, vol. 52, p. 185, February 1964.

74. D.A. Holmes and D.L. Feucht, "Microwave measurement of conductivity and dielectric constant of semiconductors," Proc. IEEE, vol. 52, p. 100, January 1964.

75. K.S. Champlin, "Comment on 'Microwave measurement of conductivity and dielectric constant of semiconductors'," Proc. IEEE, vol. 52, pp. 1061-1062, September 1964.

76. L. Lindmayer and M. Kutsko, "Reflection of microwaves from semiconductors," Solid-State Electronics, vol. 6, pp. 377-381, 1963.

77. R.H. Sheikh and M.W. Gunn, "Wave propagation in a rectangular waveguide inhomogeneously filled with semiconductors," IEEE Trans. on Microwave Theory and Techniques, vol. MTT-16, pp. 117-121, February 1968.

78. J.J. Brandstatter, An Introduction to Waves, Rays and Radiation in Plasma Media. New York: McGraw-Hill, 1963, pp. 39-52.

79. C. Kittel, Introduction to Solid State Physics. New York: Wiley, 1967, pp. 375-395.

80. G.C. Jain, Properties of Electrical Engineering Materials. New York: Harper and Row, 1967, pp. 211-231.

81. S. Flugge, Dielectrics. Berlin: Springer-Verlag, 1956, pp. 34-138.

82. A.F. Gibson, J.W. Granville, and E.G. Paige, "A study of energy-loss processes in germanium at high electric fields using microwave techniques," J. of Physics and Chemistry of Solids, vol. 19, pp. 198-217, 1961.

83. I.M. Dykman and E.I. Tolpygo, "Microwave conductivity of semiconductors with carriers heated by a dc field," Soviet Physics-Solid State, vol. 7, pp. 332-338, August 1965.

84. M. Boren and E. Wolf, Principles of Optics. New York: Pergamon Press, 1965, pp. 51-70.

85. T.S. Moss, Optical Properties of Semi-conductors. London: Butterworths Scientific Publications, 1959, p. 23.

86. R.H. Bube, Photoconductivity of Solids. New York: Wiley, 1967, p. 276.

87. S.M. Ryvkin, Photoelectric Effects in Semiconductors. New York: Consultants Bureau, 1964, p. 120.

88. J. Powderly, private communication.

89. K.S. Champlin and G.H. Glover, "Influence of waveguide contact on measured complex permittivity of semiconductors," J. of Applied Physics, vol. 37, pp. 2355-2360, May 1966.

90. K.S. Champlin, J.D. Holm, and G.H. Glover, "Electrodeless determination of semiconductor conductivity from TE_{01}^{o} - mode reflectivity," J. of Applied Physics, vol. 38, pp. 96-98.

91. G.G. Skitek, private communication.

92. H. Jacobs, R.W. Benjamin, and D.A. Holmes, "Semiconductor reflection type microwave modulation," Solid-State Electronics, vol. 8, pp. 699-708, 1965.

93. H.S. Sommers, Jr. and W.B. Teutsch, "Demodulation of low-level broad-band optical signals with semiconductors: Part II - Analysis of the photoconductive detector," Proc. IEEE, vol. 52, pp. 144-153, February 1964.

APPENDIX A

DEFINITION OF ELECTRIC FIELDS INTERNAL AND EXTERNAL TO A DIELECTRIC

When discussing an electric field in conjunction with a dielectric media it is mandatory that the particular field under consideration be clearly defined. Frequently in the literature the symbol $\bar{E}$ is used without a clear definition of its meaning and much confusion and incorrect interpretation results. The purpose of this Appendix is to define and explain the notation used for electric field intensity in this dissertation.

The electric fields associated with a dielectric (A15) may be subdivided as indicated in Figure A.1. The fields are defined as follows:

$\bar{E}_{app}$ - the applied field outside the dielectric.

$\bar{E}_{ext}$ - the resulting field external to the dielectric. This is the field used in Maxwell's equations applied external to the dielectric.

$\bar{E}_{dep}$ - the depolarizing field produced by the surface charge on the dielectric.

$\bar{E}_{int}$ - the resulting macroscopic field inside the dielectric. This is the field used in Maxwell's equation applied internal to the dielectric.

$\bar{P}$ - the resulting polarization vector field inside the dielectric.

$\bar{E}_{bd}$ - the field inside the cavity due to the surface charge on the cavity wall.

$\bar{E}_{cav}$ - the field produced by the dipoles which fill the cavity with the exception of the dipole located at the center of the cavity (point C).

$\bar{E}_{loc}$ - the resulting field (local field) at point C excluding the field of the dipole at that point.

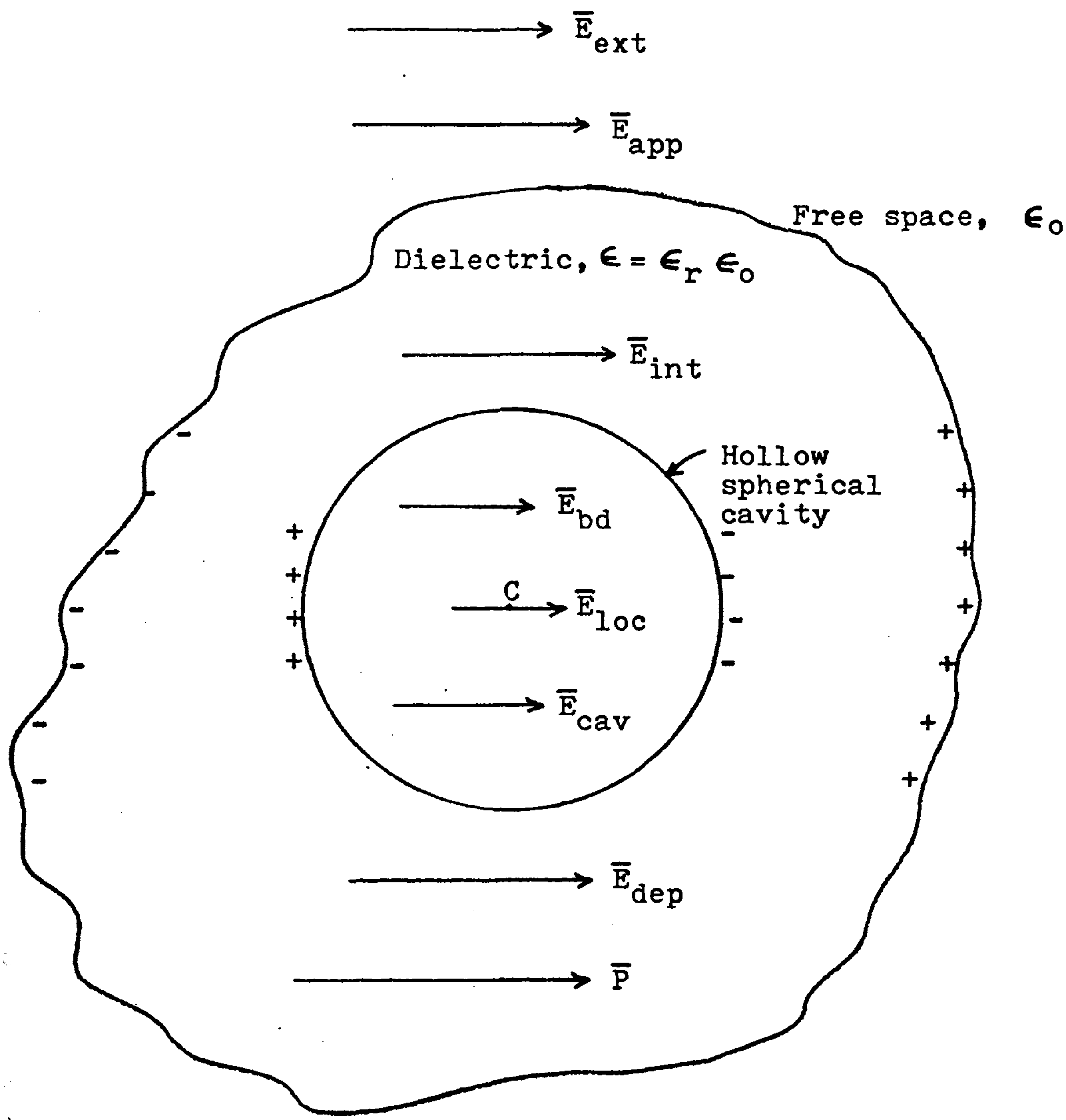

FIGURE A.1. Various electric fields associated with a dielectric medium

Hence,

$$\bar{E}_{int} = \bar{E}_{ext} + \bar{E}_{dep} = \bar{E}_{ext} - L\,\bar{P}/\epsilon_o \tag{A.1}$$

where L is the depolarizing factor. L is determined only by the geometry of the dielectric and is used to relate the resultant internal and external fields. The local field at point C is

$$\bar{E}_{loc} = \bar{E}_{ext} + \bar{E}_{dep} + \bar{E}_{bd} + \bar{E}_{cav} \tag{A.2}$$

where

$$\bar{E}_{bd} = \bar{P}/(3\epsilon_o), \tag{A.3}$$

and

$$\bar{E}_{cav} = 0 \tag{A.4}$$

for homogeneous materials with a high degree of crystal symmetry.

Hence,

$$\bar{E}_{loc} = \bar{E}_{int} + \bar{P}/(3\epsilon_o) = \bar{E}_{ext} - L\,\bar{P}/\epsilon_o + \bar{P}/(3\epsilon_o). \tag{A.5}$$

Note that the internal field is reduced in comparison to the external field, and that the local field is increased in comparison to the internal field. Since L ranges between 0 and 1, the local field can be either greater than or less than the external field. In the text the symbol $\bar{E}$ is used to represent the resultant macroscopic field in the medium under consideration. Hence, at one point $\bar{E}$ may represent $\bar{E}_{ext}$ and at another point $\bar{E}$ may represent $\bar{E}_{int}$. The specific meaning of $\bar{E}$ is indicated if it is not obvious from the context.

APPENDIX B

FREE CARRIER GENERATION RATE PRODUCED BY PHOTON ABSORPTION

Consider a semi-infinite photoconductive layer (Figure B.1) with light of intensity I_i incident at $z = 0^-$.

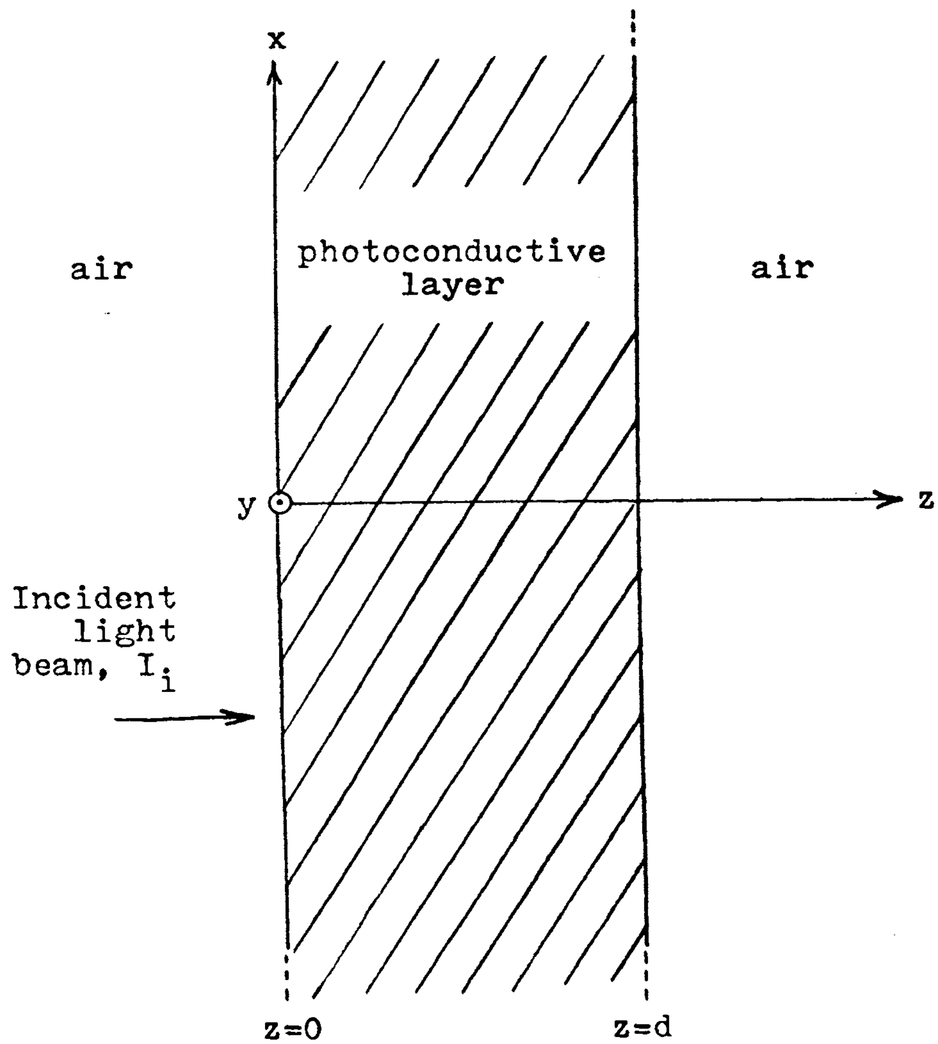

FIGURE B.1. Light beam incident on photoconductive layer

$$I_i = Q_i hf = Q_i hc/\lambda \tag{B.1}$$

$$Q_i = \lambda I_i/hc = (5.035 \times 10^{24})\lambda I_i, \tag{B.2}$$

where Q_i is the rate at which photons are incident on each square meter of the plane $z = 0^-$, h is Plank's constant, c is the speed of light in free space, and λ is the wave-length of the incident light in free space.

Let R equal the reflection coefficient at $z = 0$. Then $(1-R^2)$ equals that portion of the incident energy transmitted into the material. Let β equal the quantum efficiency and δ equal the coefficient of absorption. Then, assuming that δ is large enough so that reflection from the $z = d$ plane may be neglected, the expression for the light intensity as a function of z is

$$I(z) = (1 - R^2)I_i \exp(-\delta z); \qquad 0 \leq z \leq d. \tag{B.3}$$

The rate at which photons are incident on each square meter of an arbitrary plane z is

$$Q(z) = (5.035 \times 10^{24})\lambda(1 - R^2)I_i \exp(-\delta z); \quad 0 \leq z \leq d. \tag{B.4}$$

The free hole-electron generation rate, f(z), is given by β times the negative of the rate at which photons are being absorbed.

$$f(z) = \beta\left[-dQ(z)/dz\right]. \tag{B.5}$$

$$f(z) = (5.035 \times 10^{24})(1 - R^2)\beta\lambda\delta I_i \exp(-\delta z); \quad 0 \leq z \leq d \tag{B.6}$$

Let

$$I_o = (5.035 \times 10^{24})(1 - R^2)\beta\lambda\delta I_i \tag{B.7}$$

Then,

$$f(z) = I_o \exp(-\delta z); \qquad 0 \leq z \leq d. \tag{B.8}$$

Note that the units of I_i are watts/m^2 and the units of I_o and $f(z)$ are (hole-electron pairs)/m^3-sec.

<u>Example Problem</u> - For a CdS sample arranged as shown in Figure B.1, determine the light intensity, I_i, required at $z = 0$ in order to produce a conductivity of 1 mho/m at the front face ($z = 0^+$). Assume $\sigma_o = 0$.

In simplest terms

$$\Delta n(z) = f(z)\tau_n. \tag{B.9}$$

$$\sigma = 1 \text{ mho/m} = q\mu_n \Delta n(0^+) \tag{B.10}$$

Using $\mu_n = 10^{-2} m^2/\text{V-sec}$,

$$\Delta n(0^+) = \frac{1 \text{ mho/m}}{1.6 \times 10^{-19} \text{coul})(10^{-2} m^2/\text{V-sec})}$$

$$\Delta n(0^+) = 6.3 \times 10^{20} \text{elec}/m^3. \tag{B.11}$$

For $\tau_n = 10^{-3}$sec,

$$f(0^+) = \Delta n(0^+)/\tau_n = 6.3 \times 10^{20} \text{elec}/m^3/10^{-3}\text{sec}$$

$$= 6.3 \times 10^{23} \text{elec}/m^3\text{-sec} \tag{B.12}$$

Using the following typical values,

$\beta = 0.5$

$\delta = 1500/\text{m}$

$\lambda = 5200\text{Å}$

$(1 - R^2) = 0.6$

$$I_i = f(0^+)/[(5.035 \times 10^{24})\beta\delta\lambda(1 - R^2)] \tag{B.13}$$

$$I_i = \frac{6.3 \times 10^{23} \text{elec}/m^3\text{-sec}}{(5.035 \times 10^{24}/\text{joule-m})(0.5)(1500/\text{m})(5.2 \times 10^{-7}\text{m})(0.6)}$$

$$I_i = 534 \text{ watts}/m^2$$

Using 1 lumen = 1.46×10^{-3} watt,

$$I_i = 3.66 \times 10^5 \text{ lumen/m}^2 = 36.6 \text{ lumens/cm}^2.$$

The total luminous output of a typical 300 watt, narrow beam spotlight is 3800 lumens. Such a light source could produce the required conductivity over approximately a 100 cm^2 area.

APPENDIX C

DERIVATION OF EQUATIONS RELATING $\Delta n(z)$ AND $\Delta p(z)$ FOR AN INHOMOGENEOUSLY ILLUMINATED PHOTOCONDUCTIVE LAYER

The equations describing the operation of a photoconductor with a single trapping level (A11) are summarized below:

$$\partial p/\partial t = -\Delta p/\tau_p + g_{vt} - r_{tv} + f - \nabla\cdot\overline{J}_p/q \tag{C.1}$$

$$\partial n/\partial t = -\Delta n/\tau_n + g_{tc} - r_{ct} + f + \nabla\cdot\overline{J}_n/q \tag{C.2}$$

$$\partial n_t/\partial t = r_{ct} - g_{tc} + g_{vt} - r_{tv} \tag{C.3}$$

$$\overline{J}_p = q\mu_p p\overline{E} - qD_p \quad p \tag{C.4}$$

$$\overline{J}_n = q\mu_n n\overline{E} + qD_n \quad n \tag{C.5}$$

$$\overline{J} = \overline{J}_p + \overline{J}_n \tag{C.6}$$

$$\nabla\cdot\epsilon_b\overline{E} = \rho \tag{C.7}$$

Since steady-state conditions will be assumed, the terms involving the capture and release of carriers by traps will all equal zero. Further, assuming no external electric fields are applied the previous set of equations reduce to:

$$0 = -\Delta p(z)/\tau_p + f(z) - \nabla\cdot\overline{J}_p/q \tag{C.8}$$

$$0 = -\Delta n(z)/\tau_n + f(z) + \nabla\cdot\overline{J}_n/q \tag{C.9}$$

$$\overline{J}_p = q\mu_p(p_o + \Delta p(z))\,\overline{E} - qD_p\nabla(\Delta p(z)) \tag{C.10}$$

$$\overline{J}_n = q\mu_n(n_o + \Delta n(z))\,\overline{E} + qD_n\nabla(\Delta n(z)) \tag{C.11}$$

$$\overline{J} = \overline{J}_p + \overline{J}_n = 0 \tag{C.12}$$

$$\nabla\cdot\epsilon_b\overline{E} = q(\Delta p(z) - \Delta n(z)). \tag{C.13}$$

D_n and D_p are the diffusion coefficients for electrons and holes, respectively. Under most conditions the diffusion coefficient and mobility for a particular type of carrier are related by

$$D/\mu = kT/q. \tag{C.14}$$

If grain boundaries or other potential barriers are present, such as in a crystalline powder material, then the dc value of D and μ may be an order-of-magnitude smaller than the corresponding high frequency ac values. For the equations presently being discussed dc values should be used.

Substituting equations (C.10) and (C.11) into equations (C.8) and (C.9), respectively, yields:

$$\begin{aligned} D_p d^2(\Delta p(z))/dz^2 &- \mu_p E d(\Delta p(z))/dz \\ &- q\mu_p p_o \Delta p(z)/\epsilon_b - q\mu_p \Delta p(z)^2/\epsilon_b \\ &+ q\mu_p \Delta n(z)(p_o + \Delta p(z))/\epsilon_b - \Delta p(z)/\tau_p \\ &+ f(z) = 0 \end{aligned} \tag{C.15}$$

$$\begin{aligned} D_n d^2(\Delta n(z))/dz^2 &+ \mu_n E d(\Delta n(z))/dz \\ &- q\mu_n n_o \Delta n(z)/\epsilon_b - q\mu_n \Delta n(z)^2/\epsilon_b \\ &+ q\mu_n \Delta p(z)(n_o + \Delta n(z))/\epsilon_b - \Delta n(z)/\tau_n \\ &+ f(z) = 0 \end{aligned} \tag{C.16}$$

$$\nabla \cdot \epsilon_b \bar{E} = q(\Delta p(z) - \Delta n(z)). \tag{C.17}$$

The above three, coupled partial differential equations must be solved for $\Delta n(z)$, $\Delta p(z)$ and E. $\bar{E}$ represents the Dember field produced when $D_p \neq D_n$.

APPENDIX D

COMPUTER PROGRAMS FOR NUMERICAL SOLUTION OF THE ELECTROMAGNETIC FIELD EQUATIONS

The purpose of this Appendix is to present the two major computer programs used in this dissertation. Each program is written in the Fortran IV computer language. The first program, a listing of which begins on page 156, was designed to calculate the electromagnetic energy transmitted through a lossy, homogeneous, semi-infinite slab located in free space. The second program, a listing of which begins on page 162, was designed to calculate the electromagnetic energy transmitted through a lossy, inhomogeneous material in a rectangular waveguide. In both programs such parameters as frequency, dielectric constant, conductivity, and sample thickness may be easily varied. Typical output variables which may be both printed and plotted are frequency, dielectric constant, conductivity, sample thickness, power reflected, power absorbed, power transmitted, angle of reflection coefficient, angle of transmission coefficient, VSWR, and attenuation. A different plot routine is illustrated with each program. The Fortran symbols used for the input and output variables are defined in Table D.1.

TABLE D.1. Definition of some of the variables used in the computer programs

Fortran Symbol	Text Symbol	Definition
RELDC	ϵ_r	Relative dielectric constant
WIDTH		Sample thickness (meters)
FREQ	f	Cyclic frequency (Hz)
SIGMAO	σ_o	Dark conductivity of a homogeneous sample (mhos/m)
SIGMAI, SIG	σ_i	Conductivity of the i^{th} layer (mhos/m)
SIGMAZ		Conductivity of the homogeneous slab in free space (mhos/m)
XLIGHT	I_i	Intensity of incident light (watts/m^2)
ATTN	δ	Absorption coefficient of light (m^{-1})
XMUPDC		dc hole mobility (m^2/V-sec)
XMUPAC	μ_p	ac hole mobility (m^2/V-sec)
TAUP	τ_p	Hole lifetime (sec)
XMUNDC		dc electron mobility (m^2/V-sec)
XMUNAC	μ_n	ac electron mobility (m^2/V-sec)
TAUN	τ_n	Electron lifetime (sec)
PHI1		Incident angle of electromagnetic wave for slab in free space (rad.)
RSQRD, RR		Relative power reflected
SSQRD, SS		Relative power absorbed
TSQRD, TT		Relative power transmitted
VSWR, SWR		Voltage standing wave ratio
RPHASE, PPH		Angle of reflection coefficient (deg.)

TABLE D.1. Continued

Fortran Symbol	Text Symbol	Definition
TPHASE, TPH		Angle of transmission coefficient (deg.)
DBB, DB		Attenuation of transmitted wave (db)

Computer program for the calculation of the electromagnetic energy transmitted through a lossy, homogeneous, semi-infinite slab located in free space:

```
FORTRAN IV G LEVEL 1, MOD 2            MAIN                 DATE = 69009

                  C  VANDOREN              SINGLE LAYER**FREE SPACE
                  C
                  C
                  C WAVE PROPAGATION THROUGH A THIN, LOSSY, ISOTROPIC LAYER
                  C
                  C
0001                    DIMENSION SIG(500),RR(500),TT(500),SS(500),PHI(500)
0002                    DIMENSION SWR(500),RPH(500),TPH(500),DB(500)
0003                    DIMENSION FRE(500),WID(500),REL(500)
0004                    DIMENSION CON(6)
0005                    COMPLEX X1,Y1,K2,XSIN2,X2,XCOS2,ETA2D2,ARGPJ,ARGMJ,Z2,T3,R3,T2
0006                    COMPLEX R2,M3(2,1),M2(2,2),M1(2,2),M23(2,1),M123(2,1)
0007                    COMPLEX R,T,CSQRT,CEXP,CONJG,CMPLX,Z3,ZX
0008                 50 FORMAT(///T6,'SIGMA',T16,'RSQRD',T26,'TSQRD',T36,'SSQRD',
                       XT46,'VSWR',T55,'RPHASE',T65,'TPHASE',T77,'DB',T88,'FREQ',
                       XT99,'WIDTH',T109,'RELDC',T119,'PHI1'//)
0009                    READ(1,100)FREQ,DFREQ,JFREQ
0010                100 FORMAT(2E20.3,I20)
0011                    READ(1,150)RELDC,DRELDC,JRELDC
0012                150 FORMAT(2F20.5,I20)
0013                    READ(1,200)WIDTH,DWIDTH,JWIDTH
0014                200 FORMAT(2F20.5,I20)
0015                    READ(1,250)SIGMA,DSIGMA, JSIGMA
0016                250 FORMAT(2F20.5,I20)
0017                    READ(1,300)PHI1,DPHI1,JPHI1
0018                300 FORMAT(2F20.5,I20)
0019                    WRITE(3,100)FREQ,DFREQ,JFREQ
0020                    WRITE(3,150)RELDC,DRELDC,JRELDC
0021                    WRITE(3,200)WIDTH,DWIDTH,JWIDTH
0022                    WRITE(3,250)SIGMA2,DSIGMA,JSIGMA
0023                    WRITE(3,300)PHI1,DPHI1,JPHI1
```

```
      RFREQ=FREQ
      RRELDC=RELDC
      RWIDTH=WIDTH
      RSIGMA=SIGMA2
      RPHI1=PHI1
      I=0
      J=0
      ZX=(1.0,0.0)
   41 J=J+1
      WRITE(3,43)ZX
   43 FORMAT(///2F10.3//)
      IPHI1=0
    9 IPHI1=IPHI1+1
      IRELDC=0
    7 IRELDC=IRELDC+1
      IFREQ=0
    5 IFREQ=IFREQ+1
      WRITE(3,50)
      IWIDTH=0
    3 IWIDTH=IWIDTH+1
      ISIGMA=0
    1 ISIGMA=ISIGMA+1
      I=I+1
C     PROP CONST FOR MEDIA 2 (PHOTOCONDUCTIVE LAYER)
      OMEGA=6.28*FREQ
      SIGOM=SIGMA2/OMEGA
      DIEL=RELDC*8.85E-12
      X1=CMPLX(DIEL,-SIGOM)
      Y1=CSQRT(X1)
      OMPER=OMEGA*1.121E-03
      K2=OMPER*Y1
C     PROP CONST FOR MEDIA 1 (AIR)
      K1=OMEGA/3.0E+08
C     COSINE OF ANGLE OF REFRACTION IN MEDIA 2
      XSIN1=SIN(PHI1)
      XSIN2=(K1*XSIN1)/K2
```

```
      X2=1.0+XSIN2*XSIN2
      XCOS2=CSQRT(X2)
      ETA2D2=K2*XCOS2*WIDTH
      ARGPJ=(0.0,1.0)*ETA2D2
      ARGMJ=(0.0,-1.0)*ETA2D2
      Z1=377
      Z3=377.0*ZX
      Z2=(OMEGA*1.257E-06)/(K2*XCOS2)
      T3=(2*Z3)/(Z3+Z2)
      R3=(Z3-Z2)/(Z3+Z2)
      T2=(2*Z2)/(Z2+Z1)
      R2=(Z2-Z1)/(Z2+Z1)
C     CALCULATION OF MATRIX ELEMENTS
      M3(1,1)=(1.0,0.0)
      M3(2,1)=(0.0,0.0)
      M2(1,1)=CEXP(ARGPJ)/T3
      M2(2,2)=CEXP(ARGMJ)/T3
      M2(1,2)=R3*M2(1,1)
      M2(2,1)=R3*M2(2,2)
      M1(1,1)=1.0/T2
      M1(1,2)=R2/T2
      M1(2,1)=M1(1,2)
      M1(2,2)=M1(1,1)
      M23(1,1)=M2(1,1)*M3(1,1)+M2(1,2)*M3(2,1)
      M23(2,1)=M2(2,1)*M3(1,1)+M2(2,2)*M3(2,1)
      M123(1,1)=M1(1,1)*M23(1,1)+M1(1,2)*M23(2,1)
      M123(2,1)=M1(2,1)*M23(1,1)+M1(2,2)*M23(2,1)
C     TOTAL REFLECTION AND TRANSMISSION COEFFICIENTS
      R=M123(2,1)/M123(1,1)
      RSQRD=R*CONJG(R)
      T=M3(1,1)/M123(1,1)
      TSQRD=T*CONJG(T)*REAL(1.0/ZX)
      SSQRD=1.0-RSQRD-TSQRD
C     CALC OF INCIDENT AND REFLECTED AMPLITUDES
      EISQRD=M123(1,1)*CONJG(M123(1,1))
      EIMAG=SQRT(EISQRD)
      DBB=-10.0*ALOG10(EIMAG*EIMAG/REAL(1.0/ZX))
```

```
      ERSQRD=M123(2,1)*CONJG(M123(2,1))
      ERMAG=SQRT(ERSQRD)
      VSWR=(EIMAG+ERMAG)/(EIMAG-ERMAG)
      TPHASE=(-57.3)*ATAN2(AIMAG(T),REAL(T))
      RPHASE=(-57.3)*ATAN2(AIMAG(R),REAL(R))
      IF(RPHASE-0.0)20,21,21
   20 RPHASE=360.0+RPHASE
   21 CONTINUE
      IF(TPHASE-0.0)22,23,23
   22 TPHASE=360.0+TPHASE
   23 CONTINUE
      RR(I)=RSQRD
      TT(I)=TSQRD
      SS(I)=SSQRD
      PHI(I)=PHI1
      SWR(I)=VSWR
      RPH(I)=RPHASE
      TPH(I)=TPHASE
      DB(I)=-DBB
      FRE(I)=FREQ
      WID(I)=WIDTH
      REL(I)=RELDC
      WRITE(3,400)SIGMA2,RSQRD,TSQRD,SSQRD,VSWR,RPHASE,TPHASE,DBB
     XFREQ,WIDTH,RELDC,PHI1
  400 FORMAT(8F10.4,E13.3,F10.5,2F10.4)
      SIGMA2=SIGMA2*DSIGMA
      IF(ISIGMA-JSIGMA)1,2,2
    2 SIGMA2=RSIGMA
      WIDTH=WIDTH+DWIDTH
      IF(IWIDTH-JWIDTH)3,4,4
    4 WIDTH=RWIDTH
      FREQ=FREQ+DFREQ
      IF(IFREQ-JFREQ)5,6,6
    6 FREQ=RFREQ
      RELDC=RELDC+DRELDC
      IF(IRELDC-JRELDC)7,8,8
    8 RELDC=RRELDC
      PHI1=PHI1+DPHI1
```

```
      IF(IPHI1-JPHI1)9,10,10
   10 CONTINUE
      ZX=ZX+(0.0,0.0)
      IF(J-1)41,42,42
   42 CONTINUE
      CALL PENPOS ('VANDOREN',8,0)
      CALL NEWPLT (2,25,2.25,9.75)
      CALL ORIGIN (0.0,0.0)
      CALL XSCALE (0.0,0.015,7.5)
      CALL YSCALE (0.0,1.01,4.0)
      CALL XAXIS (0.001)
      CALL YAXIS (0.1)
      DO 70 I=1,180,60
   70 CALL XYPLT (WID(I),TT(I),60,1,-1)
      CALL ENDPLT
      CALL NEWPLT (2.25,2.25,9.75)
      CALL ORIGIN (0.0,0.0)
      CALL XSCALE (0.0,0.015,7.5)
      CALL YSCALE (0.0,1.0,4.0)
      CALL XAXIS (0.001)
      CALL YAXIS (0.1)
      DO 71 I=1,180,60
   71 CALL XYPLT (WID(I),RR(I),60,1,-1)
      CALL ENDPLT
      CALL NEWPLT (2.25,2.25,9.75)
      CALL ORIGIN (0.0,0.0)
      CALL XSCALE (0.0,0.015,7.5)
      CALL YSCALE (0.0,360.0,4.0)
      CALL XAXIS (0.001)
      CALL YAXIS (30.0)
      DO 73 I=1,180,60
   73 CALL XYPLT (WID(I),RPH(I),60,1,-1)
      CALL ENDPLT
      CALL NEWPLT (2.25,2.25,9.75)
      CALL ORIGIN (0.0,0.0)
      CALL XSCALE (0.0,0.015,7.5)
      CALL YSCALE (0.0,360.0,4.0)
```

```
      CALL XAXIS (0.001)
      CALL YAXIS (30.0)
      DO 74 I=1,180,60
   74 CALL XYPLT (WID(I),TPH(I),60,1,-1)
      CALL ENDPLT
      CALL NEWPLT (2.25,2.25,9.75)
      CALL ORIGIN (0.0,0.0)
      CALL XSCALE (0.0,0.015,7.5)
      CALL YSCALE (-0.01,10.0,4.0)
      CALL XAXIS (0.001)
      CALL YAXIS (1.0)
      DO 75 I=1,180,60
   75 CALL XYPLT (WID(I),DB(I),60,1,-1)
      CALL ENDPLT
      CALL NEWPLT (2.25,2.25,9.75)
      CALL ORIGIN (0.0,0.0)
      CALL XSCALE (0.0,0.015,7.5)
      CALL YSCALE (0.0,15.0,4.0)
      CALL XAXIS (0.001)
      CALL YAXIS (1.0)
      DO 76 I=1,180,60
   76 CALL XYPLT (WID(I),SWR(I),60,1,-1)
      CALL ENDPLT
      CALL LSTPLT
      CALL EXIT
      END
```

Computer program for the calculation of the electromagnetic energy transmitted through a lossy, inhomogeneous material in a rectangular waveguide:

```
FORTRAN IV G LEVEL 1, MOD 2            MAIN                DATE = 69048

                C  VANDOREN         MULTIPLE LAYER**WAVEGUIDE
                C
                C
                C  WAVE PROPAGATION THROUGH MEDIA INSIDE WAVEGUIDE
                C
                C
                      DIMENSION SIG(500),RR(500),TT(500),SS(500)
                      DIMENSION SWR(500),RPH(500),TPH(500),DB(500)
                      DIMENSION REL(500),WID(500),FRE(500),XLT(500),ATT(500)
                      COMPLEX X3,X4,GAMMA,GAMWID,ARGPJ,ARGMJ,Z0,Z1,Z2,Z3,T3,R3
                      COMPLEX T2,R2,M3(2,1),M2(2,2),M1(2,2),M23(2,1),M123(2,1)
                      COMPLEX R,T,CMPLX,CSQRT,CEXP,CONJG,ZX
                      READ(1,100)RELDC,DRELDC,JRELDC
                  100 FORMAT(2F20.5,I20)
                      READ(1,200)WIDTH,DWIDTH,JWIDTH,LAYERS
                  200 FORMAT(2F20.7,I20,I5)
                      READ(1,300)FREQ,DFREQ,JFREQ
                  300 FORMAT(2E20.5,I20)
                      READ(1,400)SIGMA1,DSIGMA,JSIGMA
                  400 FORMAT(2F20.5,I20)
                      READ(1,500)SIGMA0
                  500 FORMAT(F20.5)
                      READ(1,600)XLIGHT,DLIGHT,JLIGHT
                  600 FORMAT(2E20.5,I20)
                      READ(1,700)ATTN,DATTN,JATTN
                  700 FORMAT(2F20.5,I20)
                      READ(1,800)XMUPDC,DMUPDC,JMUPDC
                  800 FORMAT(2E20.5,I20)
                      READ(1,800)XMUPAC,DMUPAC,JMUPAC
                      READ(1,800)TAUP,DTAUP,JTAUP
                      READ(1,800)XMUNDC,DMUNDC,JMUNDC
```

```
      READ(1,800)XMUNAC,DMUNAC,JMUNAC
      READ(1,800)TAUN,DTAUN,JTAUN
      RLIGHT=XLIGHT
      RATTN=ATTN
      RMUPDC=XMUPDC
      RMUPAC=XMUPAC
      RTAUP=TAUP
      RMUNDC=XMUNDC
      RMUNAC=XMUNAC
      RTAUN=TAUN
      RWIDTH=WIDTH
      RFREQ=FREQ
      RSIGMA=SIGMAI
      RRELDC=RELDC
      WRITE(3,1500)RELDC,DRELDC,JRELDC
 1500 FORMAT(///2F20.5,I20)
      WRITE(3,1600)WIDTH,DWIDTH,JWIDTH,LAYERS
 1600 FORMAT(/2F20.8,2I20)
      WRITE(3,1700)FREQ,DFREQ,JFREQ
 1700 FORMAT(/2E20.5,I20)
      WRITE(3,1800)SIGMAO
      WRITE(3,1600)SIGMAI,DSIGMA,JSIGMA
 1800 FORMAT(//F20.5)
      WRITE(3,1700)XLIGHT,DLIGHT,JLIGHT
      WRITE(3,1600)ATTN,DATTN,JATTN
      WRITE(3,1700)XMUPDC,DMUPDC,JMUPDC
      WRITE(3,1700)XMUPAC,DMUPAC,JMUPAC
      WRITE(3,1700)TAUP,DTAUP,JTAUP
      WRITE(3,1700)XMUNDC,DMUNDC,JMUNDC
      WRITE(3,1700)XMUNAC,DMUNAC,JMUNAC
      WRITE(3,1700)TAUN,DTAUN,JTAUN
      I=0
      J=0
      ZX=(1.0,0.0)
   91 J=J+1
      WRITE(3,93)ZX
   93 FORMAT(///2F10.3//)
```

```
      IWIDTH=0
    1 IWIDTH=IWIDTH+1
      IFREQ=0
    3 IFREQ=IFREQ+1
      IRELDC=0
    5 IRELDC=IRELDC+1
      OMEGA=6.28*FREQ
C       TRANSMITTED ENERGY FOR DARK CONDUCTIVITY
      DIEL=RELDC*8.85E-12
      X1=(3.14/2.286E-02)**2-OMEGA*OMEGA*1.257E-06*DIEL
      X2=OMEGA*1.257E-06*SIGMAO
      X3=CMPLX(X1,+X2)
      GAMMA=CSQRT(X3)
      GAMWID=GAMMA*WIDTH
      ARGPJ=GAMWID
      ARGMJ=-GAMWID
      Z2=((0.0,1.0)*OMEGA*1.257E-06)/GAMMA
      X1A=(3.14/2.286E-02)**2-OMEGA*OMEGA*1.257E-06*8.85E-12
      X4=CMPLX(X1A,0.0)
      Z1=((0.0,1.0)*OMEGA*1.257E-06)/CSQRT(X4)
      Z3=Z1
      Z0=Z3
      T3=(2*Z3)/(Z3+Z2)
      R3=(Z3-Z2)/(Z3+Z2)
      T2=(2*Z2)/(Z2+Z1)
      R2=(Z2-Z1)/(Z2+Z1)
      M3(1,1)=(1.0,0.0)
      M3(2,1)=(0.0,0.0)
      M2(1,1)=CEXP(ARGPJ)/T3
      M2(2,2)=CEXP(ARGMJ)/T3
      M2(1,2)=R3*M2(1,1)
      M2(2,1)=R3*M2(2,2)
      M1(1,1)=1.0/T2
      M1(1,2)=R2/T2
      M1(2,1)=M1(1,2)
      M1(2,2)=M1(1,1)
```

```
      M23(1,1)=M2(1,1)*M3(1,1)+M2(1,2)*M3(2,1)
      M23(2,1)=M2(2,1)*M3(1,1)+M2(2,2)*M3(2,1)
      M123(1,1)=M1(1,1)*M23(1,1)+M1(1,2)*M23(2,1)
      M123(2,1)=M1(2,1)*M23(1,1)+M1(2,2)*M23(2,1)
      R=M123(2,1)/M123(1,1)
      RSQRD=R*CONJG(R)
      T=M3(1,1)/M123(1,1)
      TSQRD=T*CONJG(T)
      SSQRD=1.0-RSQRD-TSQRD
      EISQRD=M123(1,1)*CONJG(M123(1,1))
      EIMAG=SQRT(EISQRD)
      ERSQRD=M123(2,1)*CONJG(M123(2,1))
      ERMAG=SQRT(ERSQRD)
      VSWR=(EIMAG+ERMAG)/(EIMAG-ERMAG)
      TPHASE=-57.3*ATAN2(AIMAG(T),REAL(T)
      RPHASE=-57.3*ATAN2(AIMAG(R),REAL(R)
      IF(RPHASE-0.0)40,41,41
   40 RPHASE=360.0+RPHASE
   41 CONTINUE
      IF(TPHASE-0.0)42,43,43
   42 TPHASE=360.0+TPHASE
   43 CONTINUE
      OUTPUT=EIMAG
      DBA=(-20.0)*ALOG10(EIMAG)
      WRITE(3,50)
   50 FORMAT(///T5,'SIGMA',T15,'RSQRD',T25,'TSQRD',T35,'SSQRD',
     XT45,'VSWR',T55,'RPHASE',T65,'TPHASE',T75,'DB',T85,'RELDC',
     XT95,'WIDTH',T105,'FREQ'/)
      WRITE(3,900)SIGMAO,RSQRD,TSQRD,SSQRD,VSWR,RPHASE,TPHASE,DBA,
     XRELDC,WIDTH,FREQ
  900 FORMAT(9F10.4,F10.5,E10.2)
      IMUNDC=0
   21 IMUNDC=IMUNDC+1
      IMUPDC=0
   19 IMUPDC=IMUPDC+1
      ITAUN=0
   17 ITAUN=ITAUN+1
```

```
      ITAUP=0
   15 ITAUP=ITAUP+1
      IMUNAC=0
   13 IMUNAC=IMUNAC+1
      IMUPAC=0
   11 IMUPAC=IMUPAC+1
      IATTN=0
    9 IATTN=IATTN+1
      ILIGHT=0
    7 ILIGHT=ILIGHT+1
      WRITE(3,51)
   51 FORMAT(///T5,'SIGMA',T15,'RSQRD',T25,'TSQRD',T35,'SSQRD',
     XT45,'VSWR',T55,'RPHASE',T65,'TPHASE',T75,'DB',T85,'RELDC',
     XT95,'WIDTH',T105,'FREQ',T115,'XLIGHT',T125,'ATTN'//)
      DELTAZ=WIDTH/LAYERS
      ISIGMA=0
   29 ISIGMA=ISIGMA+1
      I=I+1
      Z3=Z0*ZX
      M3(1,1)=(1.0,0.0)
      M3(2,1)=(0.0,0.0)
      Z=WIDTH-DELTAZ/2.0
      ILAYER=0
   23 ILAYER=ILAYER+1
C       CONDUCTIVITY VARIATION ACROSS PHOTOCONDUCTIVE SLAB
C       TRANSMITTED ENERGY FOR LIGHT CONDUCTIVITY
C       MATRIX FOR ITH LAYER
      OMEGA=6.28*FREQ
      DIEL=RELDC*8.85E-12
      X1=(3.14/2.286E-02)**2-OMEGA*OMEGA*1.257E-06*DIEL
      X2=OMEGA*1.257E-06*SIGMAI
      X3=CMPLX(X1,+X2)
      GAMMA=CSQRT(X3)
      GAMWID=GAMMA*DELTAZ
      ARGPJ=GAMWID
      ARGMJ=-GAMWID
      Z2=((0.0,1.0)*OMEGA*1.257E-06)/GAMMA
```

```
      T3=(2*Z3)/(Z3+Z2)
      R3=(Z3-Z2)/(Z3+Z2)
      M2(1,1)=CEXP(ARGPJ)/T3
      M2(2,2)=CEXP(ARGMJ)/T3
      M2(1,2)=R3*M2(1,1)
      M2(2,1)=R3*M2(2,2)
      M23(1,1)=M2(1,1)*M3(1,1)+M2(1,2)*M3(2,1)
      M23(2,1)=M2(2,1)*M3(1,1)+M2(2,2)*M3(2,1)
      M3(1,1)=M23(1,1)
      M3(2,1)=M23(2,1)
      Z3=Z2
      Z=Z-DELTAZ
      IF(ILAYER-LAYERS)23,24,24
   24 T2=(2*Z2)/(Z2+Z1)
      R2=(Z2-Z1)/(Z2+Z1)
      M1(1,1)=1.0/T2
      M1(1,2)=R2/T2
      M1(2,1)=M1(1,2)
      M1(2,2)=M1(1,1)
      M123(1,1)=M1(1,1)*M23(1,1)+M1(1,2)*M23(2,1)
      M123(2,1)=M1(2,1)*M23(1,1)+M1(2,2)*M23(2,1)
      R=M123(2,1)/M123(1,1)
      RSQRD=R*CONJG(R)
      T=(1.0,0.0)/M123(1,1)
      TSQRD=T*CONJG(T)*REAL(1.0/ZX)
      SSQRD=1.0-RSQRD-TSQRD
      EISQRD=M123(1,1)*CONJG(M123(1,1))
      EIMAG=SQRT(EISQRD)
      ERSQRD=M123(2,1)*CONJG(M123(2,1))
      ERMAG=SQRT(ERSQRD)
      VSWR=(EIMAG+ERMAG)/(EIMAG-ERMAG)
      TPHASE=-57.3*ATAN2(AIMAG(T),REAL(T))
      RPHASE=-57.3*ATAN2(AIMAG(R),REAL(R))
      IF(RPHASE-0.0)44,45,45
   44 RPHASE=360.0+RPHASE
   45 CONTINUE
      IF(TPHASE-0.0)46,47,47
```

```
   46 TPHASE=360.0+TPHASE
   47 CONTINUE
      DBB=-10.0*ALOG10(EIMAG*EIMAG/REAL(1.0/ZX))
      SIG(I)=ALOG10(1001.0*SIGMAI)
      RR(I)=RSQRD
      TT(I)=TSQRD
      SS(I)=SSQRD
      SWR(I)=VSWR
      RPH(I)=RPHASE
      TPH(I)=TPHASE
      DB(I)=-DBB
      REL(I)=RELDC
      WID(I)=WIDTH
      FRE(I)=FREQ*1.0E-09
      XLI(I)=XLIGHT
      ATT(I)=ATTN
      WRITE(3,1000)SIGMAI,RSQRD,TSQRD,SSQRD,VSWR,RPHASE,TPHASE,DBB,
     XRELDC,WIDTH,FREQ,XLIGHT,ATTN
 1000 FORMAT(9F10.4,F10.5,3E10.2)
      SIGMAI=SIGMAI*DSIGMA
      IF(ISIGMA-JSIGMA)29,30,30
   30 SIGMAI=RSIGMA
      XLIGHT=DLIGHT*XLIGHT
      IF(ILIGHT-JLIGHT)7,8,8
    8 XLIGHT=RLIGHT
      ATTN=ATTN+DATTN
      IF(IATTN-JATTN)9,10,10
   10 ATTN=RATTN
      XMUPAC=DMUPAC*XMUPAC
      IF(IMUPAC-JMUPAC)11,12,12
   12 XMUPAC=RMUPAC
      XMUNAC=DMUNAC*XMUNAC
      IF(IMUNAC-JMUNAC)13,14,14
   14 XMUNAC=RMUNAC
      TAUP=DTAUP*TAUP
      IF(ITAUP-JTAUP)15,16,16
   16 TAUP=RTAUP
```

```
      TAUN=DTAUN*TAUN
      IF(ITAUN-JTAUN)17,18,18
   18 TAUN=RTAUN
      XMUPDC=DMUPDC*XMUPDC
      IF(IMUPDC-JMUPDC)19,20,20
   20 XMUPDC=RMUPDC
      XMUNDC=DMUNDC*XMUNDC
      IF(IMUNDC-JMUNDC)21,22,22
   22 XMUNDC=RMUNDC
      WIDTH=WIDTH*DWIDTH
      FREQ=FREQ*DFREQ
      IF(IFREQ-JFREQ)3,4,4
    4 FREQ=RFREQ
      RELDC=RELDC+DRELDC
      IF(IRELDC-JRELDC)5,6,6
    6 RELDC=RRELDC
      WIDTH=WIDTH+DWIDTH
      IF(IWIDTH-JWIDTH)1,2,2
    2 WIDTH=RWIDTH
      ZX=ZX+(0.0,0.0)
      IF(J-1)91,92,92
   92 CONTINUE
C PLOT PROGRAM RR, TT, SS, RPH, TPH, SWR, AND DB VS SIGMA
      CALL PENPOS ('VANDOREN',8,0)
      CALL NEWPLT (2.25,2.25,9.75)
      CALL ORIGIN (0.0,0.0)
      CALL XSCALE (0.0,6.0,7.5)
      CALL YSCALE (0.0,1.0,4.0)
      CALL XAXIS (1.0)
      CALL YAXIS (0.1)
      DO 60 I=1,93,31
   60 CALL XYPLT (SIG(I),RR(I),31,1,-1)
      CALL ENDPLT
      CALL NEWPLT (2.25,2.25,9.75)
      CALL ORIGIN (0.0,0.0)
      CALL XSCALE (0.0,6.0,7.5)
      CALL YSCALE (0.0,1.0,4.0)
```

```
      CALL XAXIS (1.0)
      CALL YAXIS (0.1)
      DO 61 I=1,93,31
   61 CALL XYPLT (SIG(I),TT(I),31,1,-1)
      CALL ENDPLT
      CALL NEWPLT (2.25,2.25,9.75)
      CALL ORIGIN (0.0,0.0)
      CALL XSCALE (0.0,6.0,7.5)
      CALL YSCALE (0.0,1.0,4.0)
      CALL XAXIS (1.0)
      CALL YAXIS (0.1)
      DO 62 I=1,93,31
   62 CALL XYPLT (SIG(I),SS(I),31,1,-1)
      CALL ENDPLT
      CALL NEWPLT (2.25,2.25,9.75)
      CALL ORIGIN (0.0,0.0)
      CALL XSCALE (0.0,6.0,7.5)
      CALL YSCALE (0.0,1.0,4.0)
      CALL XAXIS (1.0)
      CALL YAXIS (0.1)
      DO 63 I=1,93,31
      CALL XYPLT (SIG(I),RR(I),31,1,-1)
      CALL XYPLT (SIG(I),TT(I),31,1,-1)
   63 CALL XYPLT (SIG(I),SS(I),31,1,±1)
      CALL ENDPLT
      CALL NEWPLT (2.25,2.25,9.75)
      CALL ORIGIN (0.0,0.0)
      CALL XSCALE (0.0,6.0,7.5)
      CALL YSCALE (0.0,10.0,4.0)
      CALL XAXIS (1.0)
      CALL YAXIS (1.0)
      DO 64 I=1,93,31
   64 CALL XYPLT (SIG(I),SWR(I),31,1,-1)
      CALL ENDPLT
      CALL NEWPLT (2.25,2.25,9.75)
      CALL ORIGIN (0.0,0.0)
      CALL XSCALE (0.0,6.0,7.5)
```

```
      CALL YSCALE (0.0,360.0,4.0)
      CALL XAXIS (1.0)
      CALL YAXIS (30.0)
      DO 65 I=1,93,31
   65 CALL SYPLT (SIG(I),RPH(I),31,1,-1)
      CALL ENDPLT
      CALL NEWPLT (2.25,2.25,9.75)
      CALL ORIGIN (0.0,0.0)
      CALL XSCALE (0.0,6.0,7.5)
      CALL YSCALE (0.0,360.0,4.0)
      CALL XAXIS (1.0)
      CALL YAXIS (30.0)
      DO 66 I=1,93,31
   66 CALL XYPLT (SIG(I),TPH(I),31,1,-1)
      CALL ENDPLT
      CALL NEWPLT (2.25,2.25,9.75)
      CALL ORIGIN (0.0,0.0)
      CALL XSCALE (0.0,6.0,7.5)
      CALL YSCALE (0.0,99.0,4.0)
      CALL XAXIS (1.0)
      CALL YAXIS (5.0)
      DO 67 I=1,93,31
   67 CALL XYPLT (SIG(I),DB(I),29,1,-1)
      CALL ENDPLT
      CALL LSTPLT
      CALL EXIT
      END
```

APPENDIX E

MICROWAVE TRANSMISSION THROUGH A MATERIAL WITH TIME VARYING CONDUCTIVITY

The purpose of this Appendix is to derive the expression for the time varying microwave power transmitted through a section of rectangular waveguide completely filled with an isotropic, homogeneous material with a slowly time varying conductivity. The waveguide section is shown in Figure E.1. "Slowly time varying" implies that $E(\partial\sigma/\partial t) \ll \sigma(\partial E/\partial t)$.

Assuming only a TE_{10} mode, the incident electric field intensity is given by

$$\overline{E}_i = E_o\left[\exp j(\omega t - \beta_o z)\right] \sin(\pi y/y_o)\overline{a}_x. \qquad (E.1)$$

The transverse component of the incident magnetic field intensity can be determined from $\overline{E}_i$ by

$$\overline{H}_{iy} = \frac{\partial E_i/\partial z}{-j\omega\mu_o}\,\overline{a}_y. \qquad (E.2)$$

Hence,

$$\overline{H}_{iy} = (\beta_o E_o/\omega\mu_o)\left[\exp j(\omega t - \beta_o z)\right] \sin(\pi y/y_o)\overline{a}_y. \qquad (E.3)$$

The real power incident is

$$P_i = \int_0^{x_o}\int_0^{y_o} (\overline{E}_i x \overline{H}_i^*)\cdot d\overline{s}/2. \qquad (E.4)$$

Inserting the expressions for $\overline{E}_i$ and $\overline{H}_i^*$, and integrating over the waveguide cross section yields

$$P_i = \frac{|E_o|^2\beta_o x_o y_o}{4\,\omega\mu_o}. \qquad (E.5)$$

Similarily the real power transmitted at z=d is

$$P_t = \frac{|E_t|^2\beta_o x_o y_o}{4\,\omega\mu_o} = \frac{|T|^2\,|E_o|^2\beta_o x_o y_o}{4\,\omega\mu_o} = |T|^2 P_i. \qquad (E.6)$$

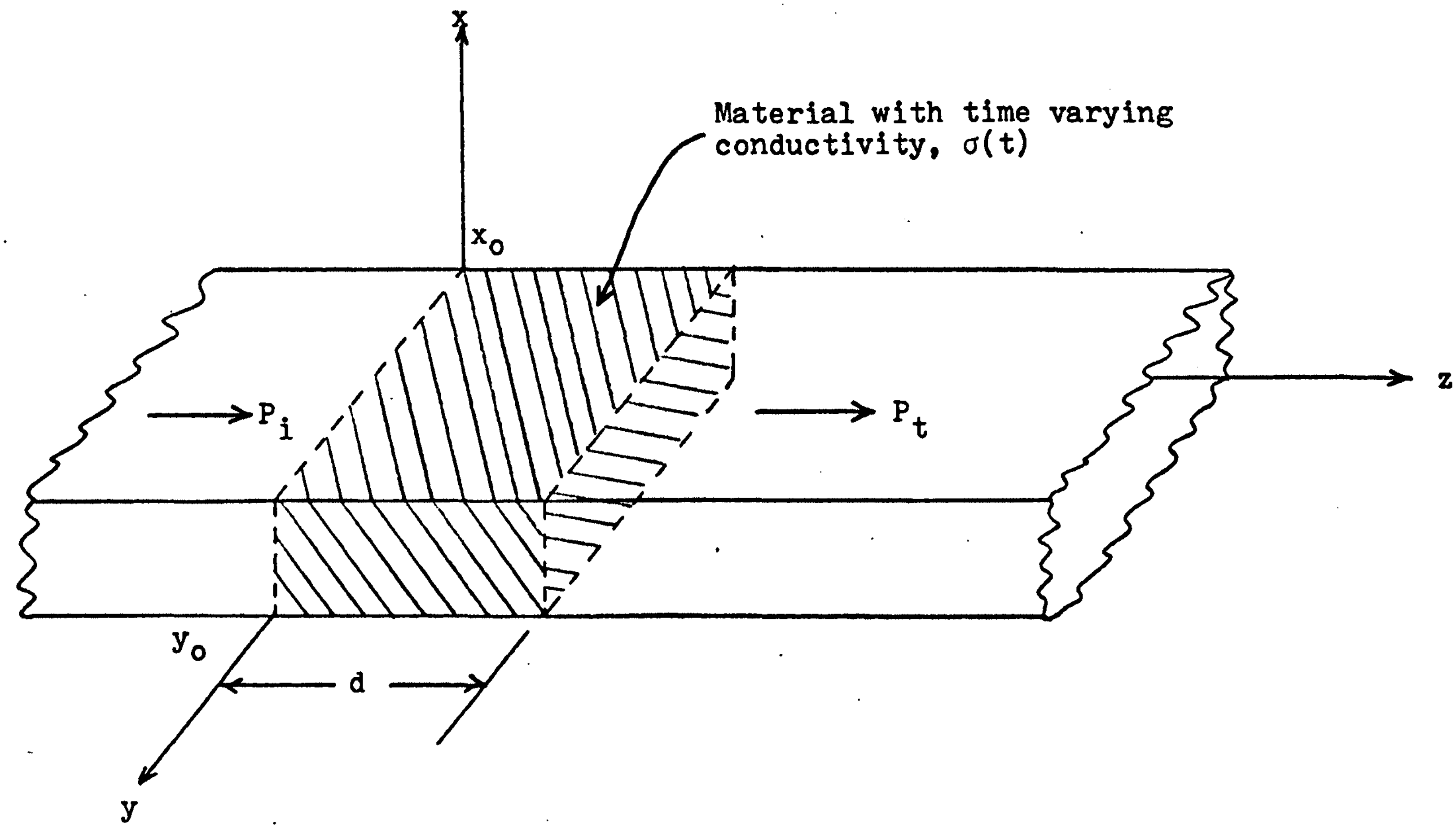

FIGURE E.1. Microwave transmission through a rectangular waveguide containing a slab of material with a time varying conductivity where T is the time varying total transmission coefficient for the layer. For a single layer the matrix equation (4.35) reduces to

$$\begin{bmatrix} E_i \\ E_r \end{bmatrix} = \begin{bmatrix} 1/T_2 & R_2/T_2 \\ R_2/T_2 & 1/T_2 \end{bmatrix} \begin{bmatrix} \exp(\gamma d)/T_3 & R_3\exp(\gamma d)/T_3 \\ R_3\exp(-\gamma d)/T_3 & \exp(-\gamma d)/T_3 \end{bmatrix} \begin{bmatrix} E_t \\ 0 \end{bmatrix} \quad (E.7)$$

where

$$R_2 = (Z - Z_o)/(Z + Z_o) = - R_3 \quad (E.8)$$

$$T_2 = (2Z)/(Z + Z_o) \quad (E.9)$$

$$T_3 = (2Z_o)/(Z + Z_o). \quad (E.10)$$

Z_o and Z are the transverse impedances of the air filled and material filled waveguides, respectively. From equation (E.7)

$$E_i = \left\{\left[\exp(\gamma d) + R_2R_3 \exp(-\gamma d)\right]/(T_2T_3)\right\}E_t, \quad (E.11)$$

and the transmission coefficient is found to be

$$T = \frac{T_2T_3\exp(\gamma d)}{R_2R_3 + \exp(2\gamma d)}. \quad (E.12)$$

Forming the product (TT*) and simplifying yields

$$|T|^2 = \frac{|T_2|^2 |T_3|^2\exp(2\alpha d)}{|R_2|^4 + 2\mathrm{Re}\left[(R_2^*)^2\exp(2\gamma d)\right] + \exp(4\alpha d)}. \quad (E.13)$$

Since usually $|R_2| < 1$, all terms in the denominator can be neglected except $\exp(4\alpha d)$. (For the low conductivity CdS samples used in this research $R_2 \approx 0.3$). Hence,

$$|T|^2 \approx |T_2|^2 |T_3|^2\exp(-2\alpha d), \quad (E.14)$$

where

$$|T_2|^2|T_3|^2 = \frac{4|Z|^2|Z_o|^2}{|Z + Z_o|^4} . \qquad \text{(E.15)}$$

The impedance may be written as

$$Z_o = j\,\omega\mu_o/\gamma_o = \omega\mu_o/\beta_o \qquad \text{(E.16)}$$

$$Z = \frac{j\,\omega\mu_o}{\gamma} = \frac{\omega\mu_o}{\beta_o}\left[\frac{\beta\beta_o + j\alpha\beta_o}{\alpha^2 + \beta^2}\right] \qquad \text{(E.17)}$$

Inserting equations (E.16) and (E.17) into equation (E.15) and simplifying considerably, yields

$$|T_2|^2|T_3|^2 = \frac{4\beta_o^{\,2}(\alpha^2 + \beta^2)}{\alpha^2 + (\beta + \beta_o)^2} . \qquad \text{(E.18)}$$

For the TE_{10} mode in the material media

$$\gamma = \left[(\pi/y_1)^2 - \omega^2\mu_o\epsilon + j\omega\mu_o\sigma\right]^{\frac{1}{2}}. \qquad \text{(E.19)}$$

For frequencies above cutoff γ may be approximated by

$$\gamma \approx \omega(\mu_o\epsilon)^{\frac{1}{2}}\left[-1 + j(\sigma/\omega\epsilon)\right]^{\frac{1}{2}}. \qquad \text{(E.20)}$$

Assuming $\sigma << \omega\epsilon$, γ may be further approximated by

$$\gamma = \alpha + j\beta = (\sigma/2)(\mu_o/\epsilon)^{\frac{1}{2}} + j\omega(\mu_o\epsilon)^{\frac{1}{2}}\left[1 + \sigma^2/(8\omega^2\epsilon^2)\right]. \qquad \text{(E.21)}$$

The phase constant in the filled guide is approximately related to the phase constant of the unfilled guide by

$$\beta \approx \beta_o\,\epsilon_r^{\frac{1}{2}}. \qquad \text{(E.22)}$$

Using the above results equation (E.6) can be simplifyied to

$$P_t \approx \frac{4\,\epsilon_r}{(1 + \epsilon_r^{\frac{1}{2}})^4}\left\{\exp\left[-\sigma(\mu_o/\epsilon)^{\frac{1}{2}}d\right]\right\} P_i. \qquad \text{(E.23)}$$

Assuming n-type material,

$$\sigma = q\mu_n\left[n_o + (\Delta n)\exp(-t/\tau_n)\right]. \tag{E.24}$$

Inserting equation (E.24) into equation (E.23) and simplifying yields

$$P_t(t) \approx P_o\exp\left[K\exp(-t/\tau_n)\right], \tag{E.25}$$

where

$$P_o = \frac{4\epsilon_r P_i}{(1 + \epsilon_r^{\frac{1}{2}})^4}\exp\left[-q\mu_n n_o(\mu_o/\epsilon)^{\frac{1}{2}}d\right] \tag{E.26}$$

$$K = -q\mu_n\Delta n(\mu_o/\epsilon)^{\frac{1}{2}}d. \tag{E.27}$$

If all the assumptions used in this derivation are satisfied, then P_o and K remain constant for weak illumination and equation (E.25) may be used to determine the free carrier lifetime. If the real part of the dielectric constant, ϵ, changes slightly (<40%) with illumination intensity, the above results may still be used provided the sample thickness is properly selected as indicated in Chapter V.

VITA

Thomas Paul Van Doren was born in Perryville, Missouri, on November 23, 1940. He was graduated from St. Joseph's High School in Farmington, Missouri, in May 1958. He entered the University of Missouri - Rolla and was graduated with a Bachelor of Science Degree in Electrical Engineering in May 1962 and a Master of Science Degree in Electrical Engineering in May 1963.

From September 1963 until September 1965 the author served as an officer with the U.S. Army Security Agency. He was employed by Collins Radio Company of Dallas, Texas, as a Microwave Systems Engineer from September 1965 until January 1967. Since January 1967 he has held the position of Instructor in Electrical Engineering at the University of Missouri - Rolla.

He is married to the former Lana Seiberling of Bonne Terre, Missouri, and they have two sons, Michael and Scott.